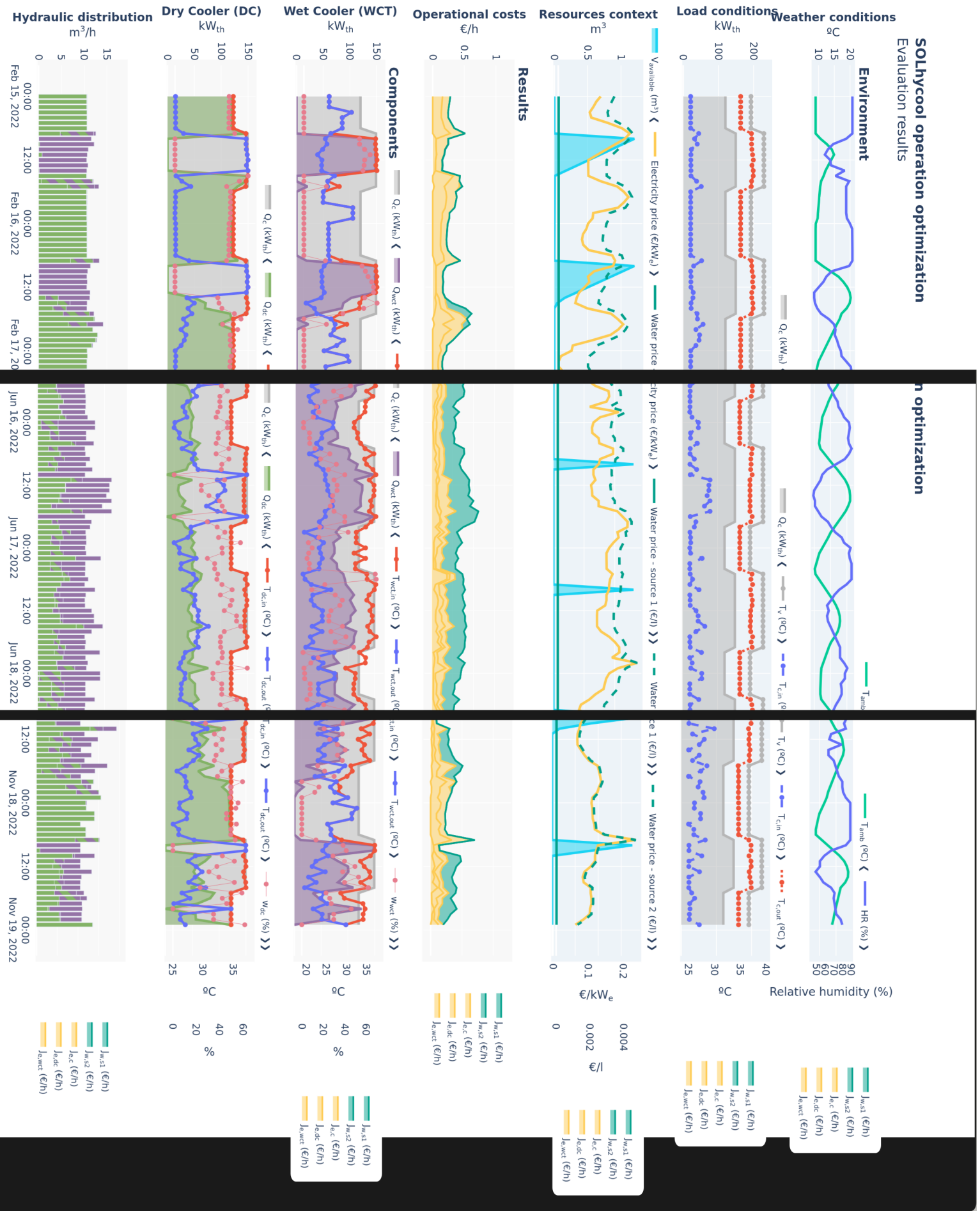




Esta sección no está terminada. Siquieres puedes echarle un ojo para ver la estructura y cómo encaja con el resto pero no merece la pena revisarla en detalle en el estado actual.

SOHycool operation optimization

## Evaluation results



### Model 0.1: Test

$T_{cc,out}, C_e, C_w, T_{c,out} = \text{combined cooler model}(q_c, R_p, R_s, \omega_{dc}, \omega_{wct}, T_{amb}, HR_i, T_v, \dot{m}_v)$   
 $T_{cc,in} = T_{c,out}$   
 $T_{dc,in} = T_{cc,in}$   
 $q_{dc} = q_c \cdot (1 - R_p)$   
 $q_{wct,p} = q_c \cdot R_p$   
 $q_{wct,s} = q_{dc} \cdot R_s$   
 $T_{dc,out}, C_{e,dc} = \text{dc model}(q_{dc}, \omega_{dc}, T_{amb}, T_{dc,in})$   
 $q_{wct}, T_{wct,in} = \text{mixer model}(q_{wct,p}, T_{cc,in}, q_{wct,s}, T_{dc,out})$   
 $T_{wct,out}, C_{e,wct}, C_{w,wct} = \text{wct model}(q_{wct}, \omega_{wct}, T_{amb}, HR, T_{wct,in})$   
 $T_{c,in}, T_{c,out} = \text{condenser model}(q_c, \dot{m}_v, T_v)$   
 $q_{cc}, T_{cc,out} = \text{mixer model}(q_{wct}, T_{wct,out}, q_{dc}, T_{dc,out})$   
 $C_e = C_{e,dc} + C_{e,wct} + C_{e,c}$   
 $C_w = C_{w,wct}$

As can be seen in Model 0.1, the counter is working.

### Problem .1: Test

Hello, here is some text without a meaning. This text should show what a printed text will look like at this place. If you read this text, you will get no information. Really? Is there no information? Is there a difference between this text and some nonsense like "Huardest gefburn"? Kjift – not at all! A blind text like this gives you information about the selected font, how the letters are written and an impression of the look. This text should contain all letters of the alphabet and it should be written in of the original language. There is no need for special content, but the length of words should match the language.

$$\min_{\mathbf{x}, \mathbf{e}; \theta} J = f(\mathbf{x}, \mathbf{e}; \theta) = f(x)$$

with:

- Model name model

$$out_1, out_2 = f(in_1, in_2, \dots, in_N)$$

- Decision variables

$$\mathbf{x} = [x_1, x_2]$$

- Environment variables

$$\mathbf{e} = [e_1, e_2, \dots, e_3]$$

- Fixed parameters

$$\theta = [\theta_1 = X, \theta_2 = Y]$$

subject to:

- Box-bounds

$$\cdot x_1 \in [\underline{x}_1, \bar{x}_1]$$

- $x_2 \in [\underline{x}_2, \bar{x}_2]$
- Constraints
  - $|out_X - out_Y| \leq \epsilon_1$
  - $out_X \leq out_Z - \Delta Z$

As can be seen in Problem .1, the counter is working.

### TL;DR

test test

### Problem: Test

$$\min_{\mathbf{x}, \mathbf{e}; \theta} J = f(\mathbf{x}, \mathbf{e}; \theta) = f(x)$$

with:

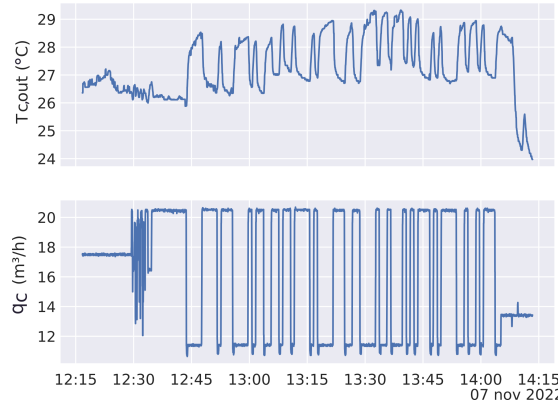
- Model name model
  - $out_1, out_2 = f(in_1, in_2, \dots, in_N)$
- Decision variables
  - $\mathbf{x} = [x_1, x_2]$
- Environment variables
  - $\mathbf{e} = [e_1, e_2, \dots, e_3]$
- Fixed parameters
  - $\theta = [\theta_1 = X, \theta_2 = Y]$

subject to:

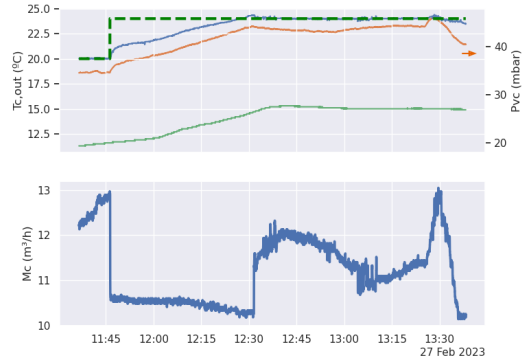
- Box-bounds
  - $x_1 \in [\underline{x}_1, \bar{x}_1]$
  - $x_2 \in [\underline{x}_2, \bar{x}_2]$
- Constraints
  - $|out_X - out_Y| \leq \epsilon_1$
  - $out_X \leq out_Z - \Delta Z$

### the heat definition of efficiency

In process heat driven system, plants that produce the same final product, the most efficient one that uses the least amount of heat. While given two plants that produce the same amount of waste heat, the one is the one that produces given that heat.



(a) Dynamic identification by means of PRBS signal



(b) Controller application results

**Figure 2:** Condenser outlet temperature control implementation. To tune the controller, the system was excited with a PRBS signal. An ARX model ( $n_a = 20$ ,  $n_b = 4$ ) was identified in MATLAB, which allowed to extract the first-order dynamic with which the controller.



The kaobook class

PhD Thesis

**Towards optimal resource management in solar thermal applications:  
desalination and CSP**

Juan Miguel Serrano Rodríguez

July 13, 2025

University of Almería

## The kaobook class

### Disclaimer

You can edit this page to suit your needs. For instance, here we have a no copyright statement, a colophon and some other information. This page is based on the corresponding page of Ken Arroyo Ohori's thesis, with minimal changes.

### No copyright

 This book is released into the public domain using the CC0 code. To the extent possible under law, I waive all copyright and related or neighbouring rights to this work.

To view a copy of the CC0 code, visit:

<http://creativecommons.org/publicdomain/zero/1.0/>

### Colophon

This document was typeset with the help of KOMA-Script and  $\text{\LaTeX}$  using the kaobook class.

The source code of this book is available at:

<https://github.com/fmarotta/kaobook>

(You are welcome to contribute!)

### Publisher

First printed in May 2019 by University of Almería

The harmony of the world is made manifest in Form and Number, and the heart and soul and all the poetry of Natural Philosophy are embodied in the concept of mathematical beauty.

– D'Arcy Wentworth Thompson



## Acknowledgements

Test test test

*Federico Marotta*



## Summary

I am of the opinion that every  $\text{\LaTeX}$  geek, at least once during his life, feels the need to create his or her own class: this is what happened to me and here is the result, which, however, should be seen as a work still in progress. Actually, this class is not completely original, but it is a blend of all the best ideas that I have found in a number of guides, tutorials, blogs and tex.stackexchange.com posts. In particular, the main ideas come from two sources:

- ▶ [Ken Arroyo Ohori's Doctoral Thesis](#), which served, with the author's permission, as a backbone for the implementation of this class;
- ▶ The [Tufte-Latex Class](#), which was a model for the style.

The first chapter of this book is introductory and covers the most essential features of the class. Next, there is a bunch of chapters devoted to all the commands and environments that you may use in writing a book; in particular, it will be explained how to add notes, figures and tables, and references. The second part deals with the page layout and design, as well as additional features like coloured boxes and theorem environments.

I started writing this class as an experiment, and as such it should be regarded. Since it has always been intended for my personal use, it may not be perfect but I find it quite satisfactory for the use I want to make of it. I share this work in the hope that someone might find here the inspiration for writing his or her own class.



## Resumen



# Contents

Acknowledgements	v
Summary	vii
Resumen	ix
Contents	xi
How to read this thesis	1
About the author	3
<b>INTRODUCTION</b>	<b>5</b>
1 Context and motivation	7
2 Modelling overview	9
2.1 Performance metrics . . . . .	9
2.2 First principle modelling . . . . .	9
2.3 Data-driven modelling . . . . .	9
2.3.1 Gaussian Process Regression . . . . .	10
2.3.2 Artificial Neural networks . . . . .	10
2.3.3 Random Forest . . . . .	12
2.3.4 Gradient Boosting . . . . .	12
2.4 Hybrid modelling . . . . .	12
2.5 Data-driven from first-principles models. Sample generation . . . . .	12
2.6 Hybrid modelling by means of Finite-State Machines (FSMs) . . . . .	12
3 Sensitivity analysis	15
4 Control overview	17
4.1 PID controllers . . . . .	17
4.2 Hierarchical control . . . . .	17
5 Optimization overview	19
5.1 NLP problems . . . . .	19
5.2 MINLP problems . . . . .	19
5.3 A discussion on constraint handling . . . . .	19
5.4 Multi-objective optimization . . . . .	20
5.5 Optimization algorithms . . . . .	20
6 Research plan	21
6.1 Hypothesis . . . . .	21
6.2 Objectives . . . . .	21
7 Contributions	23
8 Modelling of a combined cooling system	25
8.1 Wet cooler . . . . .	25
8.1.1 Poppe model . . . . .	26
8.1.2 Samples generation for first-principles to data-driven models . . . . .	28
8.1.3 Model interface . . . . .	28
8.2 Dry cooler . . . . .	29
8.2.1 Physical model . . . . .	29
8.2.2 Samples generation for first-principles to data-driven models . . . . .	29
8.2.3 Model interface . . . . .	29
8.3 Other components . . . . .	30
8.3.1 Electrical consumption . . . . .	30

8.3.2	Surface condenser . . . . .	30
8.3.3	Mixers . . . . .	31
8.4	Complete system . . . . .	31
<b>ENERGY MANAGEMENT IN MED PROCESSES DRIVEN BY VARIABLE ENERGY SOURCES</b>		<b>33</b>
Derived scientific contributions . . . . .		35
<b>9 Thermal desalination</b>		<b>37</b>
<b>10 SolarMED pilot plant</b>		<b>39</b>
10.1	Heat generation and storage subsystem . . . . .	39
10.1.1	Solar field . . . . .	39
10.1.2	Thermal storage . . . . .	40
10.2	Separation subsystem . . . . .	40
<b>11 Performance evaluation in Multi-Effect Distillation (MED) processes: standard methodology proposal</b>		<b>43</b>
11.1	Process analysis . . . . .	45
11.2	Performance metrics . . . . .	46
11.2.1	Separation metrics . . . . .	46
11.2.2	Energetic metrics . . . . .	47
11.2.3	Exergetic metrics . . . . .	48
11.3	Instrumentation . . . . .	50
11.3.1	Key Process Variable (KPV) . . . . .	50
11.3.2	Instrumentation requirements . . . . .	51
11.3.3	Uncertainty determination . . . . .	52
11.4	Monitoring and process control . . . . .	53
11.4.1	Monitoring: steady-state identification . . . . .	53
11.4.2	Control system . . . . .	53
11.5	Methodology application in an experimental campaign . . . . .	55
11.5.1	Implementation results . . . . .	56
11.5.2	Results analysis . . . . .	60
<b>12 Hybrid modelling of a solar driven MED system</b>		<b>63</b>
12.1	Introduction . . . . .	63
12.2	Dynamic modelling. Process variables . . . . .	63
12.2.1	Solar Field ( <i>sf</i> ) . . . . .	63
12.2.2	Thermal storage . . . . .	66
12.2.3	Heat exchanger . . . . .	66
12.2.4	MED . . . . .	67
12.2.5	Other components . . . . .	68
12.3	Discrete modelling. Operation state . . . . .	68
12.3.1	Heat generation and storage subsystem ( <i>sfts</i> ) . . . . .	68
12.3.2	Separation subsystem ( <i>med</i> ) . . . . .	68
12.4	Complete system model . . . . .	68
12.4.1	Validation . . . . .	69
<b>13 Towards the optimal coupling and operation of a solar driven MED system</b>		<b>71</b>
13.1	Introduction . . . . .	71
13.2	Problem description . . . . .	71
13.2.1	Implementation discussion . . . . .	72
13.4	Operation Plan Layer Description . . . . .	75
13.4.1	Candidate problems generation . . . . .	75
13.4.2	Update times generation . . . . .	75
13.5	Operation optimization layer description . . . . .	77
13.6	Optimization results . . . . .	78
13.6.1	Choosing an algorithm . . . . .	78
13.6.2	Choosing a candidate problem . . . . .	78
13.6.3	Simulation results . . . . .	79
13.6.4	Performance comparison with alternative strategies . . . . .	81

<b>CONCLUSIONS AND OUTLOOK</b>	<b>83</b>
Conclusions . . . . .	85
Outlook and future work . . . . .	85
Derived scientific contributions . . . . .	86
<b>Bibliography</b>	<b>87</b>
<b>Alphabetical Index</b>	<b>91</b>



## List of Figures

1	A rotated figure . . . . .	2
2	Condenser outlet temperature controller implementation . . . . .	5
3	Example figure. Try clicking or scanning the QR code to access the interactive version. [1ex] . . . . .	1
1.1	<b>Aerial view of the pilot plants at the Plataforma Solar de Almería (PSA), Spain.</b> The developments presented in this thesis have been developed and validated around two test-rigs: a Combined Cooling System (CCS) and a Solar-driven Multi-Effect Distillation (SolarMED) pilot plants. In the picture, the CCS plant is located on the left side, and the... . . . . .	8
2.1	ANN model configurations . . . . .	10
2.2	Considered ANN architectures . . . . .	11
8.1	Control volume in the exchange area of a wet cooling tower arrangement . . . . .	27
8.2	Inputs-outputs block diagram of the main model components . . . . .	31
8.3	Complete model diagram of the combined cooling system . . . . .	32
10.1	SolarMED process diagram . . . . .	39
10.2	MED plant at PSA with open effects for maintenance . . . . .	41
10.3	. . . . .	42
11.1	Inputs and outputs variables in an MED process. The dash line delimits the control volume . . . . .	46
11.2	Piping and Instrumentation Diagram (P&ID) with the required instrumentation, KPVs, and basic control loops (ANSI/ISA 5.1-2022) required in an MED plant . . . . .	51
11.3	Sensitivity index results for different variables. Useful to assess the impact of the different measured variables uncertainty on the performance metrics. KPVs are shown in bold notation . . . . .	52
11.4	Diagram of the steady-state identification procedure . . . . .	54
11.5	. . . . .	55
11.6	Ryznar Stability Index (RSI) values as a function of temperature and concentration before (left) and after (right) pre-treatment using nanofiltration . . . . .	56
11.7	Flowchart of finite state machines for plant start-up (left) and shutdown (right) . . . . .	57
11.8	Condenser outlet temperature controller implementation . . . . .	58
11.9	. . . . .	59
11.10	Temperature and concentration evolution for operation points at each effect in the MED plant. Surface represents the RSI. . . . .	61
11.11	Per effect comparison between low and high Top Brine Temperature (TBT) operation points . . . . .	61
12.1	Solar field process diagram. . . . .	64
12.2	Solar field and thermal storage electrical characterization tests. . . . .	65
12.3	Solar field flow for different pump configurations and their associated power consumption. [1ex]	66
12.4	Heat exchanger process diagram. . . . .	67
12.5	Complete SolarMED model architecture. TODO: Needs to be updated . . . . .	69
13.1	Decision tree resulting from the combinatorial nature of the integer part of the optimization problem. Text in nodes represents system states. . . . .	74
13.2	Proposed optimization strategy architecture . . . . .	74
13.3	Operation plan layer computation and updates distribution . . . . .	76
13.4	Fitness evolution for a particular startup-problem . . . . .	78
13.5	A rotated figure . . . . .	80

## List of Tables

1	MED plant at PSA specifications and nominal operating conditions . . . . .	2
10.1	MED plant at PSA specifications and nominal operating conditions . . . . .	41

10.2	Characteristics of the instrumentation installed at MED-PSA unit ( <sup>a</sup> value of the measured temperature in °C, <sup>b</sup> of reading, <sup>c</sup> full scale) . . . . .	41
11.1	RSI values and their interpretation in terms of scaling and corrosion risk [59] . . . . .	55
11.2	Experimental campaign design specifications . . . . .	56
11.3	Measured variables and performance metrics for some operation points of the experimental campaign. The values are expressed as mean ± standard deviation with a coverage factor of 2 (95% confidence interval). D is the duration of the steady state period. . . . .	60
12.1	Solar Field and Thermal Storage subsystem ( <b>sfts</b> ) FSM states definitions. $\wedge$ represents the logical AND operator and $\forall$ represents that all meet the condition. . . . .	68
12.2	Separation subsystem ( <b>med</b> ) FSM states definitions. $\wedge$ represents the logical AND operator, $\exists$ represents that at least one meets the condition, and $\forall$ represents that all meet the condition. . . . .	68
13.1	Operation plan. Start-up (1) and shutdown (2) degrees of freedom for changes in the operation state. . . . .	75

## List of Listings

# How to read this thesis

## TL;DR

This preliminary chapter explains how to read this thesis, mainly the different environment boxes used throughout the manuscript, why the large margins, what is placed in them, and how to use the interactive features of the manuscript. This is an example of a Too Long; Didn't Read (TL;DR) box. It contains an Abstract/Summary of the main point of the chapter and are placed at the beginning of every chapter.

This  $\text{\LaTeX}$  template is designed with large margins, on the one hand this allows to have shorter lines, which makes for an easier reading experience but most interestingly, it also allows to place additional information in the margins, such as side notes, side citations, figures, tables... your imagination is the limit! Or rather  $\text{\LaTeX}$  compilation errors and your patience are. Throughout this manuscript I will add side notes<sup>1</sup> to provide additional information and comments that would otherwise be too distracting and verbose to include in the main text, constantly interrupting the flow of the reading. The side notes are not essential to understand the content of the document, but mostly complementary.

1: Like this one! They are like footnotes, but placed in the margin of the page

## Boxed environments

Both problem definition boxes (e.g. ref) and model definition boxes (e.g. Model 0.2) are countered environments and can (and will) be referenced in the text.

### Problem: Problem definition box example

This is an example of a problem definition box. It is used to formally and concisely define an optimization problem.

$$\min_{\mathbf{x}, \mathbf{e}; \theta} J = f(\mathbf{x}, \mathbf{e}; \theta) = \text{XXXX}$$

with:

$$\begin{aligned} \text{out}_1, \text{out}_2 &= f(\text{in}_1, \text{in}_2, \dots, \text{in}_N) \\ \text{out}_1, \text{out}_2 &= f(\text{in}_1, \text{in}_2, \dots, \text{in}_N) \end{aligned}$$

- ▶ Decision variables

$$\mathbf{x} = [x_1, x_2]$$

- ▶ Environment variables

$$\mathbf{e} = [e_1, e_2, \dots, e_3]$$

- ▶ Fixed parameters

$$\theta = [\theta_1 = X, \theta_2 = Y]$$

subject to:

- ▶ Box-bounds

$$\begin{aligned} \cdot x_1 &\in [x_1, \bar{x}_1] \\ \cdot x_2 &\in [x_2, \bar{x}_2] \end{aligned}$$

- ▶ Constraints



**Figure 3:** Example figure. Try clicking or scanning the QR code to access the interactive version.



**Table 1:** MED plant at PSA specifications and nominal operating conditions

Parameter	Value
Capacity	72 m <sup>3</sup> /day
Number of effects	14
Feed type	Forward feed
Physical arrangement	Vertically stacked
Heat exchanger configuration	90/10 Cu-Ni HTE
Heat source type	Hot water
Top Brine Temperature (TBT)	70 °C
Condenser temperature	35 °C

2: I believe that this is a good way to make the document more accessible and to encourage readers to explore the content in more depth. However, the interactive features are optional and not necessary to understand the content of the document.



3:

¶: Like hoarding toilet paper

- $|out_X - out_Y| \leq \epsilon_1$
- $out_X \leq out_Z - \Delta Z$

### Model 0.2: Model definition box example

$out_1, out_2 = \text{some cool model}(in_1, in_2, in_3)$

### Other boxes

Other boxes are used to highlight important points, or to provide additional information that is not essential to the main text.

In order to make the book more interactive and link-friendly, I have enabled hyperlinks in the PDF. This means that you can click on the references, citations, and links to external resources, and they will take you to the corresponding location. This is standard latex, however to maintain a consistent experience in the physical version, QR codes are inserted in the margin next to the links. The reader is invited to scan them with a QR code reader to access the corresponding online resource<sup>2</sup>. Some figures also include QR codes that link to an interactive (HTML) version of the figure, see Figure 3 as an example.

The additional material as well as the source code of this document are hosted in a [Zenodo repository](#)<sup>3</sup>. Alternatively, a mirror repository is also available at:

<https://github.com/juan11iguel/my-thesis>

It seems unlikely that both Zenodo and GitHub will go down at a time where this document is still relevant, and if they do, I think there will be more important things to worry about than losing access to the interactive content of this thesis. ¶

## About the author

Un payaso

– Lidia Roca, probablemente

I am currently completing my PhD thesis, with the defense planned for October. My research interests lie primarily in automatic control, optimization, and robotics, especially as applied to solar thermal processes.

I think I am mostly a creative person, but in order to implement those ideas, throughout my work, I've gained experience with a variety of tools and technologies, including Linux, Python, Docker, LaTeX, and the Robot Operating System (ROS). I'm particularly passionate about open science and open source software, and I strive to contribute to communities that value transparency and collaboration.

For my bachelor's thesis, I created a mobile robotics lab in the University of Almería by deploying the [Duckietown project](#). This gave me the opportunity to interact and work with ROS, and since the whole project was deployed using Docker, to learn about containerization technologies. For my master's thesis, work was also software-related, but this time it was about the implementation of a SCADA-like system using Python. During my PhD, I have had four years to really delve into these technologies, so today they are an integral part of my workflow and I am confident to say they've helped me become effective at implementing those (sometimes too) many ideas.



Lidia esto solo lo he copiado  
por tener algo, ya lo mejoraré



## **INTRODUCTION**



asdad



**Figure 1.1:** Aerial view of the pilot plants at the PSA, Spain.

The developments presented in this thesis have been developed and validated around two test-rigs: a CCS and a SolarMED pilot plants. In the picture, the CCS plant is located on the left side, and the...

## 2.1 Performance metrics

To evaluate the quality of the models fit to the experimental data, four performance metrics were evaluated: coefficient of determination ( $R^2$ ), Root Mean Squared Error (RMSE), Mean Absolute Error (MAE) and Mean Absolute Percentage Error (MAPE). These metrics are described below.

**Coefficient of determination.**  $R^2$  measures the proportion of the variance in the predicted variable that can be attributed to the independent variable(s), in this case the considered system inputs. Values close to one indicate a better prediction accuracy. It is calculated as follows:

$$R^2 = 1 - \frac{\sum_{i=1}^n (y_i - \hat{y}_i)^2}{\sum_{i=1}^n (y_i - \bar{y})^2},$$

where  $y_i$  is the measured or observed value for the output variable, in the  $i$ -th observation,  $\hat{y}_i$  is the estimated value of the same variable and  $n$  is the total number of observations. Finally,  $\bar{y}$  is the mean value of the experimental values.

**Root Mean Square Error.** RMSE is a statistical measure of the difference between the values predicted by a model and the observed values. It is calculated as the square root of the mean of the squared differences between the predicted and observed values and it has its units.

$$\text{RMSE} = \sqrt{\frac{1}{n} \sum_{i=1}^n (y_i - \hat{y}_i)^2}$$

**Mean Absolute Error.** It represents the average absolute difference between predicted and actual values.

$$\text{MAE} = \frac{1}{n} \sum_{i=1}^n |y_i - \hat{y}_i|$$

**Mean Absolute Percentage Error.** As the MAE, it calculates the difference between the predicted and the actual values, but in this case it does so in relative terms:

$$\text{MAPE} = \frac{1}{n} \sum_{i=1}^n \left| \frac{y_i - \hat{y}_i}{y_i} \right| \times 100\%$$

## 2.2 First principle modelling

## 2.3 Data-driven modelling

Machine learning algorithms are unique in their ability to obtain models and extract patterns from data, without being explicitly programmed to do so. They

2.1	Performance metrics . . . . .	9
2.2	First principle modelling . . . . .	9
2.3	Data-driven modelling . . . . .	9
2.3.1	Gaussian Process Regression . . . . .	10
2.3.2	Artificial Neural networks . . . . .	10
2.3.3	Random Forest . . . . .	12
2.3.4	Gradient Boosting . . . . .	12
2.4	Hybrid modelling . . . . .	12
2.5	DD from FP. Sample generation . . . . .	12
2.6	Hybrid modelling by means of FSMs . . . . .	12

are more effective with large volumes of data but can also be applied to build steady state regression models with less information of a process.

### 2.3.1 Gaussian Process Regression

### 2.3.2 Artificial Neural networks

Artificial Neural Networks (ANNs), as the name suggests, have a behavior similar to biological neurons. Their structure is formed by a succession of layers, each one composed by nodes (or neurons) and they receive as input the output of the previous layer. This process is subsequently repeated until the final layer which has a number of neurons equal to the number of outputs.

There are important aspects to be considered in the ANN model design, such as the model configuration, the network architecture and the network topology. They are discussed below.

**Model configuration.** If the model has more than one output, several configurations are available for the implementation of the model as shown in Figure 8.2. The first one is a Multiple Inputs Multiple Outputs (MIMO) configuration, where a single network receives all the inputs and directly produces all predicted outputs. The second one is a cascade structure. This cascading approach involves training a network (*network A* in Figure 8.2 (b)) to predict one output using the available inputs. Subsequently, these inputs, along with the output from the first-output-predicting network, are fed into a second network (*network B* in Figure 8.2 (b)) that is in charge of forecasting the second output. This procedure can be repeated as many times as desired. A potential advantage of this configuration is that it may reduce the experimental data requirements to obtain satisfactory results. A third option is the combination of both configurations, where some networks may predict several outputs, while others are fed some of these outputs as subsequently use them as inputs.

**Network architectures.** Three network architectures have been implemented and tested:

1. Feed Forward (FF) network - Figure 2.2 (a). This is the base network architecture, where different layers are added sequentially and the flow of information is unidirectional. The transfer function adopted in the hidden layers is the differentiable *Log-Sigmoid*<sup>1</sup>, whereas the one employed in the output layer is a linear one with no saturations.
2. Cascade-forward (CF) network - Figure 2.2 (b). It is a variation on the feedforward network since it adds direct connections from the input and hidden layers to the output layer.
3. Radial Basis Function (RBF) network - Figure 2.2 (c). The transfer functions used in the first layer of the RBF network are different, they are local Gaussian like functions. Also, instead of multiplying by the weights, the distance between inputs and weights is computed and the bias is multiplied instead of added [1].

**Network topology.** Two-layer networks (one hidden and one output layer) can learn almost any input-output relationship, including non-linear ones. Adding more layers can improve the learning for more complex problems. However, increasing the number of layers or neurons per layer increases the training computational requirements, requires more data for a satisfactory model and can lead to overfitting. Therefore, the process is usually started with two layers and then the number of layers is increased if they do not perform satisfactorily [1]. In this study, for the feedforward and cascade-forward architectures, one and two hidden layers have been tested with the following configurations: 5, 10, 20, 5-5, 5-10, 10-5, 10-10. For the case of the RBF, it only has one hidden layer and

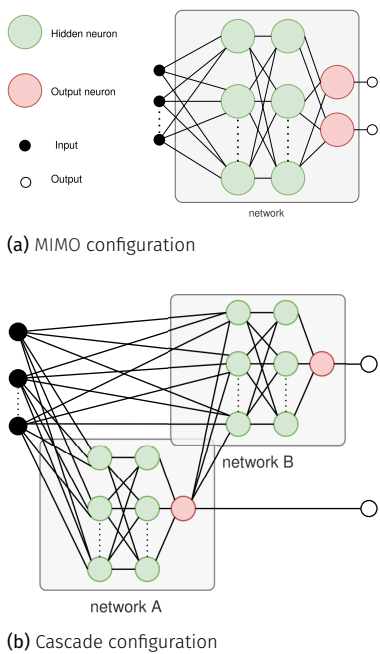


Figure 2.1: ANN model configurations

1: Defined as  $\text{logsig}(x) = 1/(1 + e^{-x})$ , mapping any real input to a value between 0 and 1.

[1]: Hagan et al. (2014), *Neural Network Design*

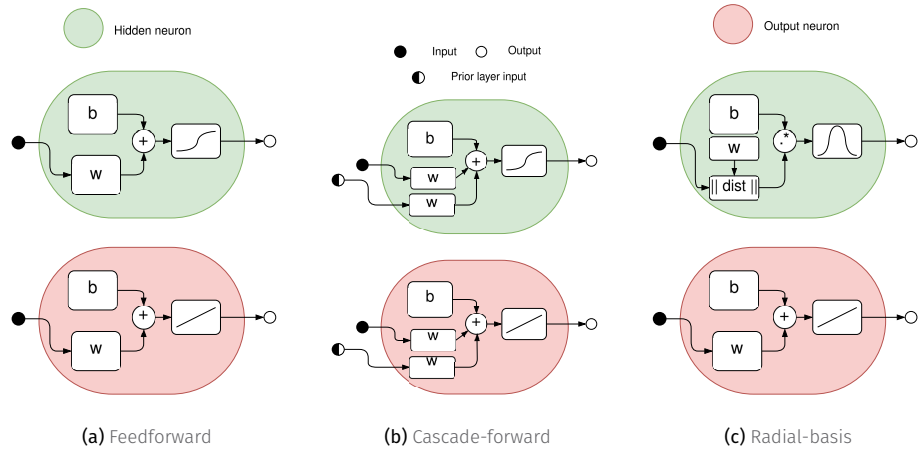


Figure 2.2: Considered ANN architectures

neurons are added sequentially during the training process up to a maximum which is set to 120 neurons.

**Training process.** The next important aspect to consider is the training process. For the FF and CF networks many Gradient- or Jacobian-based algorithms can be utilized. In this case, the Levenberg-Marquardt backpropagation algorithm [2] has been used. It is a fast algorithm, ideal for multilayer networks with up to a few hundred weights and biases enabling efficient training. The training in this case is done in batches since sequential training is slower and does not produce better results. All data have been normalized applying the z-score normalization method. The criteria established for deciding when to stop the training is the following one: when the performance on the validation set increases (worsens) or when the gradient is below a minimum ( $1 \times 10^{-7}$ ) for a number of iterations or epochs, or when a maximum number of 1000 epochs is reached. The number of iterations to wait, often referred as patience, is set to 6. Finally, the selected network parameters will be those of the best epoch.

[2]: Beale et al. (2010), "Neural Network Toolbox"

For each network architecture, the training process was repeated a total of ten times (this is the recommended practice if the computational requirements allow it, since it guarantees reaching a global optimum with a high degree of confidence [3]). The optimal architecture and training was selected according to a performance function, which in this case has been the Mean Squared Error (MSE) with the values normalized.

[3]: Hamm et al. (2007), "Comparison of Stochastic Global Optimization Methods to Estimate Neural Network Weights"

In the case of the RBF network, the chosen training method consists in two stages which treats the two layers of the RBF network separately. The first layer weights and biases are tuned based on the orthogonal least squares method [1], while for the second layer are computed in one step using a linear least-squares algorithm. During training, neurons are added to the first layer (in increments of 20) trying to minimize the MSE to some goal, which in this case is set depending on the case study: 10 for the MIMO configuration and 0 ( $^{\circ}\text{C}^2$ ) and 20 ( $\text{L}^2/\text{h}^2$ ) for temperature and water lost networks, respectively, for the cascade configuration. Finally, a parameter called spread is used to set the first layer biases. Larger values of this parameter promote a smoother approximation of the training data (more generalization), conversely, lower values provide a more exact fit to the training data. Values from 0.1 to 30 have been tested for this parameter.

[1]: Hagan et al. (2014), *Neural Network Design*

### 2.3.3 Random Forest

### 2.3.4 Gradient Boosting

## 2.4 Hybrid modelling

## 2.5 Data-driven from first-principles models. Sample generation

One important advantage that first-principles models have over data-driven is their scalability, that is, the ability to adapt a model developed and validated in a pilot-scale system, to a large scale one. This is true for many systems as long as the system configuration remains the same. This allows to study and analyze pilot scale plants and extrapolate the results to industrial sized plants. In addition, these type of model are also capable of predicting the behaviour of the modelled systems in conditions that have not been tested (e.g. different operating or environmental conditions), although the reliability of the model could be lower if these conditions move away from those experimentally used for some parameter calibration.

On the contrary, data-driven models are very specific to the system and operating ranges they are trained for. That is why training/calibrating a data-driven model with data from a first-principles model is a common practice to obtain a model that can be used in a larger range of operating conditions...

The process of generating samples from a first-principles model to train a data-driven model is called sample generation. It consists of running the first-principles model for a set of input parameters, which can be selected randomly or following a specific distribution, and then using the outputs of the first-principles model as the training data for the data-driven model.

The first step is to define the input parameters and their ranges. This can be done by selecting the most relevant parameters for the system and determining their ranges based on the system's operating conditions. The next step is to generate a set of input parameters, which can be done using different methods such as Latin Hypercube Sampling, Monte Carlo Sampling, Sobol Sampling, or simply grid sampling. These methods allow to generate a set of input parameters that cover the entire range of the input parameters and ensure that the generated samples are representative of the system's behaviour. Once the input parameters are defined, the first-principles model is run for each set of input parameters, and the outputs of the model are recorded. Finally, the recorded outputs are used to train the data-driven model.

## 2.6 Hybrid modelling by means of FSMs

A state machine is a model of behavior composed of a finite number of states and *transitions* between those states. Within each state and transition some *action* can be performed. A state machine needs to start at some *initial state*.

Core concepts description:

- ▶ **State.** A state represents a particular condition or stage in the state machine. It's a distinct mode of behavior or phase in a process.
- ▶ **Transition.** This is the process or event that causes the state machine to change from one state to another.
- ▶ **Action.** Specific operation or task that is performed when a certain event happens i.e. a state is entered, exited, or during a transition.

- ▶ **Model.** A stateful structure that holds information about the state of the machine. It gets updated during transitions and defines actions.
- ▶ **Machine.** This is the entity that manages and controls the model, states, transitions, and actions. It's the conductor that orchestrates the entire process of the state machine.



# 3

## Sensitivity analysis

It involves systematically assessing how variations in input parameters impact the model's outputs. In this case, the Sobol method [4], which is a variance-based approach, has been used. This method decomposes the total variance of the model output into contributions from individual input parameters and their interactions. By quantifying the relative importance of each parameter, Sobol analysis facilitates the identification of influential factors, enabling a more nuanced understanding of complex systems characterized by numerous interacting variables.

The analysis results are different sensitivities indices such as total sensitivity indices (total-order), first-order sensitivity indices (first-order), and interaction sensitivity indices (second-order). First-order measures the direct effect of an input variable on the output, excluding interaction effects with other variables, while the second-order measures specifically this interaction effects. Finally, total-order indices account for the total effect of an input variable, including both direct and interaction effects.

[4]: Nossent et al. (2011), "Sobol'sensitivity Analysis of a Complex Environmental Model"



The PID control algorithm continuously calculates and adjusts the control inputs based on the error between the desired setpoint and the actual system output, ensuring precise and stable control over various parameters.

4.1 PID controllers . . . . . 17

4.2 Hierarchical control . . . . . 17

#### 4.1 PID controllers

#### 4.2 Hierarchical control



# Optimization overview

A general expression to define an optimization problem is:

$$\min_{\mathbf{x}, \mathbf{e}; \theta} J = f(\mathbf{x}, \mathbf{e}; \theta) \quad \text{s.t.} \quad g_i(\mathbf{x}) \leq 0, \quad i = 1, \dots, m \quad (5.1)$$

where  $\mathbf{x}$  is the vector of decision variables,  $f(\mathbf{x})$  is the objective function to be minimized, and  $g_i(\mathbf{x})$  are the constraints of the problem. The objective function is a scalar function that maps the decision variables to a real number, representing the cost or performance of the system. The constraints are functions that restrict the feasible region of the problem, defining the set of values that the decision variables can take. The optimization problem is to find the values of the decision variables that minimize the objective function while satisfying the constraints.

Regarding the constraints, they can be categorized in two types depending whether they can be evaluated before evaluating the objective function or not:

- ▶ **Bounds.** These are constraints that limit the range of the decision variables, such as

$$x_i \in [l_i, u_i], \quad i = 1, \dots, n$$

where  $l_i$  and  $u_i$  are the lower and upper bounds of the decision variable  $x_i$ , respectively<sup>1</sup>.

- ▶ **Constraints.** These are constraints that restrict the feasible region of the problem, such as

$$g_i(\mathbf{x}) \leq 0, \quad i = 1, \dots, m$$

where  $g_i(\mathbf{x})$  are the constraint functions that depend on the decision variables  $\mathbf{x}$ , and  $m$  is the number of constraints. They can only be known after evaluating the objective function.

## 5.1 NLP problems

Non-Linear Programming (NLP)

## 5.2 MINLP problems

Mixed Integer Non-Linear Programming (MINLP)

## 5.3 A discussion on constraint handling

There are two main approaches to handle constraints in optimization problems:

- ▶ **Penalty methods.** These methods add a penalty term to the objective function to penalize the violation of the constraints. The penalty term is usually a function of the constraint violation, and it is added to the objective function to form a new objective function that is minimized. The penalty term can be linear or non-linear, and it can be adjusted during the optimization process to ensure that the constraints are satisfied. The main advantage of penalty methods is that they allow to handle constraints

5.1 NLP problems . . . . .	19
5.2 MINLP problems . . . . .	19
5.3 A discussion on constraint handling . . . . .	19
5.4 Multi-objective optimization . . . . .	20
5.5 Optimization algorithms . . . . .	20

<sup>1</sup>: Also known as box-bounds

in a flexible way, and they can be used with any optimization algorithm. However, they can also lead to suboptimal solutions if the penalty term is not properly tuned, and they can also lead to numerical instability if the penalty term is too large.

- ▶ **Constraint handling methods.** These methods handle the constraints directly, by either rejecting solutions that violate the constraints or by modifying the optimization algorithm to ensure that the constraints are satisfied. The main advantage of constraint handling methods is that they guarantee that the constraints are satisfied, and they can also lead to better solutions than penalty methods. However, they can also be more complex to implement, and they can also lead to numerical instability if the constraints are too restrictive. Specific constraint-handling capable algorithms are required to solve these type of problems.

By using inequality constraints, the optimization algorithm is forced to find the best solution that satisfies the constraints, however, in a problem with a horizon window, this would require returning a value of the constraint for each step in the horizon window. Thus, producing a large vector of inequality constraints and increasing the dimension of the problem (*i.e.* its complexity). On the other hand returning a single value for the whole episode gives little information to the algorithm on how to adapt its decision values to satisfy the constraint and thus might be unable<sup>2</sup> to converge to a solution.

Finally, non constraint-handling capable algorithms can be wrapped with constraint handling methods to solve problems with constraints [5], where they basically implement some type of penalty method.

2: By unable we are referring to requiring an unfeasible amount of objective function evaluations, too much time.

[5]: Farmani et al. (2003), "Self-Adaptive Fitness Formulation for Constrained Optimization"

[6]: Geem et al. (2001), "A New Heuristic Optimization Algorithm"

[7]: Biscani et al. (2020), "A Parallel Global Multi-objective Framework for Optimization: Pagmo"

3: While HS has shown competitive performance, it has also faced criticism—not for its results, but for its metaphor. The musical analogy adds little explanatory value and arguably obscures the algorithm's mechanics. At its core, HS operates similarly to Evolutionary Strategies or Genetic Algorithms, employing concepts like mutation and crossover.

## 5.4 Multi-objective optimization

## 5.5 Optimization algorithms

- ▶ **Improved Harmony Search algorithm (IHS)** [6, 7] is a metaheuristic optimization algorithm inspired by the improvisation process of musicians. In this analogy, each musician represents a decision variable, each note corresponds to a value, and the goal is to create the best possible harmony—analogous to finding the global optimum. In the algorithm, every member of the input population contributes to the search process. At each iteration, a new solution (individual) is generated. If this new solution outperforms the worst individual in the population, it replaces it. The total number of fitness function evaluations equals the number of iterations. An enhanced version of HS introduces dynamic parameters: the probability of selecting values from the decision vector is adjusted linearly, while the mutation rate changes exponentially over time. These improvements aim to balance exploration and exploitation more effectively.<sup>3</sup>
- ▶ Another

asdad

6.1 Hypothesis . . . . . 21

6.2 Objectives . . . . . 21

**6.1 Hypothesis****6.2 Objectives**



asdad



# Modelling of a combined cooling system

## TL;DR

This chapter describes the steady-state modelling of the different components of a combined cooling system, mainly a Wet Cooling Tower (WCT) and a Dry Cooler (DC). Different alternatives are presented: from physical models to data-driven approaches, including the generation of samples for data-driven models trained using data from a physical model. Models are also developed for the other components of the system and finally it is shown how they are integrated into a complete system model. The complete system model interface is defined at Model ?? and a block diagram is presented in Figure 8.3 including all relevant variables.

## Introduction

In order to study the potential advantages of making use of a combined cooling system, it is first necessary to develop the modelling of its components. Since the objective is performance prediction, this chapter focuses on the steady state modelling of the combined cooler main components, *i.e.* the WCT and the DC. More specifically, the aim is to compare two modelling strategies: that based on physical equations (Section 2.2) and that based on black box models (Section 2.3) such as ANNs, in order to see which one is more suitable for its integration in the optimization of the complete process.

This chapter presents a comparison between the two modelling approaches, at steady state and with a focus on optimization applications, in terms of predictive capabilities, experimental and instrumentation requirements, execution time, implementation and scalability. A sensitivity analysis is performed to further analyze and compare each case study. It also presents and evaluates all relevant aspects of interest in the development of such models, specifically for ANNs, model configuration, architecture and topology are discussed. Other system components are also described in Section 8.3 (Other components) and finally their integration is discussed in Section 8.4 (Complete system).

## 8.1 Wet cooler

In the case of the models based on physical equations, the analysis of wet cooling towers has its origin in [8], in which the theory for their performance evaluation was developed. Merkel proposed a model based on several assumptions to simplify the heat and mass transfer equations to a simple hand calculation. However, these assumptions mean that Merkel's method does not reliably represent the physics of the heat and mass transfer process in a cooling tower. This was already stated by Bourillot [9] who concluded that the Merkel method is simple to use and can correctly predict cold water temperature when an appropriate value of the coefficient of evaporation is used. However, it is insufficient for the estimation of the characteristics of the warm air leaving the fill and for the calculation of changes in the water flow rate due to evaporation. Jaber and Webb [10] developed the equations necessary to apply the effectiveness-NTU<sup>1</sup> method directly to counterflow or crossflow cooling towers. This approach is particularly useful in the latter case and simpler compared to a more conventional numerical procedure. Notice that the effectiveness-NTU

<b>8.1 Wet cooler . . . . .</b>	<b>25</b>
8.1.1 Poppe model . . . . .	26
8.1.2 Samples generation for first-principles to data-driven models . . . . .	28
8.1.3 Model interface . . . . .	28
<b>8.2 Dry cooler . . . . .</b>	<b>29</b>
8.2.1 Physical model . . . . .	29
8.2.2 Samples generation for first-principles to data-driven models . . . . .	29
8.2.3 Model interface . . . . .	29
<b>8.3 Other components . . . . .</b>	<b>30</b>
8.3.1 Electrical consumption . . . . .	30
8.3.2 Surface condenser . . . . .	30
8.3.3 Mixers . . . . .	31
<b>8.4 Complete system . . . . .</b>	<b>31</b>

Ahora mismo esta introducción es demasiado parecida al TL;DR, hay que distinguirla

[8]: Merkel (1925), "Verdunstungskühlung"

[9]: Bourillot (1983), "Hypotheses of Calculation of the Water Flow Rate Evaporated in a Wet Cooling Tower"

[10]: Jaber et al. (1989), "Design of Cooling Towers by the Effectiveness-NTU Method"

1: The effectiveness-NTU method estimates how well a heat exchanger transfers heat by comparing the actual heat transfer to the maximum possible, using a parameter, Number of Transfer Units (NTU), that reflects its size and flow characteristics.

[11]: Poppe et al. (1991), "Berechnung von Rückkühlwerken"

[12]: Kloppers et al. (2005), "A Critical Investigation into the Heat and Mass Transfer Analysis of Counterflow Wet-Cooling Towers"

[13]: Cutillas et al. (2021), "Energetic, Exergetic and Environmental (3E) Analyses of Different Cooling Technologies (Wet, Dry and Hybrid) in a CSP Thermal Power Plant"

[14]: Hosoz et al. (2007), "Performance Prediction of a Cooling Tower Using Artificial Neural Network"

2: The notation  $n_1 \dots n_l$  represents the architecture of the ANN model, where  $l$  is the number of layers and  $n_i$  are the nodes in each one of the layers.

[15]: Gao et al. (2013), "Artificial Neural Network Model Research on Effects of Cross-Wind to Performance Parameters of Wet Cooling Tower Based on Level Froude Number"

[16]: Song et al. (2021), "A Novel Approach for Energy Efficiency Prediction of Various Natural Draft Wet Cooling Towers Using ANN"

3: ANN uses as input  $f_{fan}$  whereas Poppe's model uses  $\dot{m}_a$ .

[17]: Navarro et al. (2022), "Critical Evaluation of the Thermal Performance Analysis of a New Cooling Tower Prototype"

method is based on the same simplifying assumptions as the Merkel method. On the other hand, Poppe and Rögner [11] developed the Poppe method. They derived the governing equations for heat and mass transfer in a wet cooling tower and did not make any simplifying assumptions as in the Merkel theory, which makes it a very precise model. As a matter of fact, predictions from the Poppe formulation have resulted in values of evaporated water flow rate that are in good agreement with full scale cooling tower test results [12]. This model has already been used for the evaluation of the thermal performance of solar power plants using different condensation systems (wet, dry and hybrid system), as can be found in Cutillas et al. [13].

In the case of black box models, numerous authors in the literature have designed ANN models for WCT with different objectives, such as performance prediction, simulation and optimization. One of the first works in this area is the one described in [14] where an ANN model was developed to predict the performance of a forced-counter flow cooling tower at lab scale. In this case, the input variables were the dry bulb temperature, the relative humidity of the air stream entering the tower, the temperature of the water entering the tower, the air volume flow rate and the cooling water mass flow rate. The outputs of this model were the heat rejection rate at the tower, the mass flow rate of water evaporated, the temperature of the cooling water at the tower outlet, the dry bulb temperature and the relative humidity of the air at the outlet of the tower. The results obtained with a 5-5-5<sup>2</sup> ANN demonstrated that wet cooling towers at lab-scale can be modelled using ANNs with a high degree of accuracy. There are also ANN models for Natural Draft Counter-flow Wet Cooling Towers (NDWCT) at lab-scale, such as the one proposed by [15]. In this case, the authors used a 4-8-6 ANN structure and considered some additional variables, such as air gravity, wind velocity, heat transfer coefficients and efficiency as outputs. All these works can be useful to validate the model development methodology but may fail predicting the performance of WCT at larger scale. In this sense, special attention deserves the study carried out by [16] where an 8-14-2 ANN model was proposed to predict the performance (the cooling number and the evaporative loss proportion) of NDWCTs at commercial scale. The model is based on 638 sets of field experimental data collected from 36 diverse NDWCTs used in power plants. It is a very challenging work since it covers samples from a wide range of tower sizes and capacities being the Mean Relative Error (MRE) below 5 %.

From the literature review, it can be stated that there are works based on Poppe and ANN models that evaluate the main output variables of WCTs. Nevertheless, to the author knowledge, there are no studies focused on the comparison between both modelling strategies. Also lacking is a comprehensive analysis of the different aspects that affect the models development and performance.

The static models presented in this section have been developed to predict two main outputs, the water temperature at the outlet of the WCT,  $T_{w,or}$  and the water consumed due to evaporation losses,  $\dot{m}_{w,lost}$ . The inputs variables required by both modelling approaches, Poppe model and ANN models, are: the cooling water flow rate ( $\dot{m}_w$ ), the water temperature at the inlet of the WCT ( $T_{w,i}$ ), the ambient temperature ( $T_\infty$ ), the ambient relative humidity ( $\phi_\infty$ ) and the frequency percentage of the fan ( $f_{fan}$ ) (or its equivalence in air mass flow rate<sup>3</sup>,  $\dot{m}_a$ ).

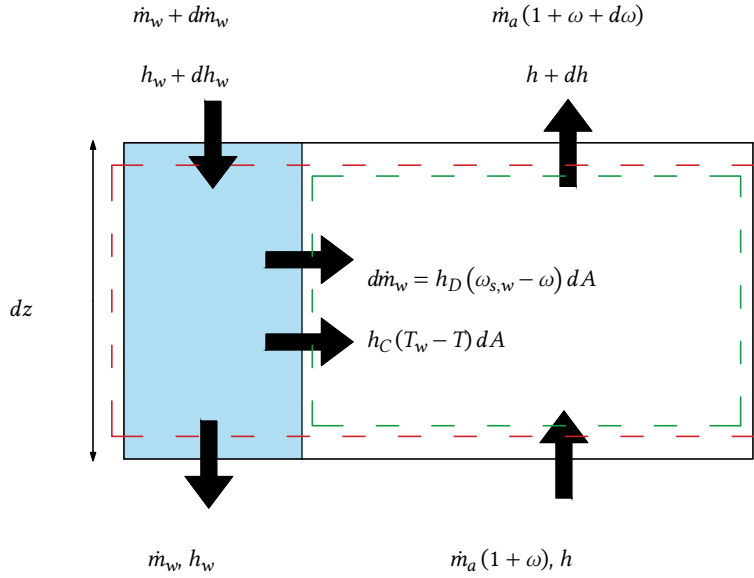
### 8.1.1 Poppe model

The well-known Merkel number is accepted as the performance coefficient of a wet cooling tower [17]. This dimensionless number is defined in Equation 8.1, and it measures the degree of difficulty of the mass transfer processes occurring in the exchange area of a wet cooling tower.

$$Me = \frac{h_D a_V V}{\dot{m}_w}, \quad (8.1)$$

where  $h_D$  is the mass transfer coefficient,  $a_V$  is the surface area of exchange per unit of volume and  $V$  is the volume of the transfer region.

The Merkel number can be calculated using the Merkel and Poppe theories for the performance evaluation of cooling towers. On the one hand, the Merkel theory [8] relies on several critical assumptions, such as the Lewis factor ( $Le$ ) being equal to 1, the air exiting the tower being saturated with water vapour and it neglects the reduction of water flow rate by evaporation in the energy balance. On the other hand, the Poppe theory [11], which is the one used in this work, do not consider simplifying assumptions, thus being the one most usually preferred. In this theory, the authors derived the governing equations for heat and mass transfer in the transfer region of the wet cooling tower (control volume shown in Figure 8.1) assuming a one dimensional problem. In this figure, the red and green dashed lines indicate the fill and air-side control volumes, respectively.



[8]: Merkel (1925), "Verdunstungskühlung"

[11]: Poppe et al. (1991), "Berechnung von Rückkühlwerken"

**Figure 8.1:** Control volume in the exchange area of a wet cooling tower arrangement.

Following the detailed derivation process and simplification of the previously-mentioned governing equations described in [17], the major following equations for the heat and mass transfer obtained, according to the Poppe theory, are:

$$\frac{d\omega}{dT_w} = \frac{c_{p_w} \frac{\dot{m}_w}{\dot{m}_a} (\omega_{s,w} - \omega)}{(h_{s,w} - h) + (Le - 1) [(h_{s,w} - h) - (\omega_{s,w} - \omega) h_v] - (\omega_{s,w} - \omega) h_w} \quad (8.2)$$

$$\frac{dh}{dT_w} = c_{p_w} \frac{\dot{m}_w}{\dot{m}_a} \left[ 1 + \frac{(\omega_{s,w} - \omega) c_{p_w} T_w}{(h_{s,w} - h) + (Le - 1) [(h_{s,w} - h) - (\omega_{s,w} - \omega) h_v] - (\omega_{s,w} - \omega) h_w} \right] \quad (8.3)$$

$$\frac{dMe}{dT_w} = \frac{c_{p_w}}{(h_{s,w} - h) + (Le - 1) [(h_{s,w} - h) - (\omega_{s,w} - \omega) h_v] - (\omega_{s,w} - \omega) h_w}, \quad (8.4)$$

where the quantity referred to as  $Me$  in Eq. 8.4, is the Merkel number calculated according to the Poppe theory. The above described governing equations can be solved by the fourth order Runge-Kutta method to provide the evolution of

[17]: Navarro et al. (2022), "Critical Evaluation of the Thermal Performance Analysis of a New Cooling Tower Prototype"

[18]: Ashrae (2004), "HVAC Systems and Equipment"

the air humidity ratio, air enthalpy and Merkel number inside the transfer area of the cooling tower (fill). Once these profiles are known, the amount of water lost due evaporation can be calculated as per Eq. Equation 8.6. Refer to [17] for additional information concerning the calculation procedure.

$$Me = \frac{h_D a_v V}{\dot{m}_w}, \quad (8.5)$$

$$\dot{m}_{w,lost} = \dot{m}_a (\omega_{a,o} - \omega_{a,i}) \quad (8.6)$$

It is important to mention that the Merkel number varies with the operation conditions and its value can be obtained using a correlation with the water-to-air mass flow ratio as an independent variable. One of the proposed correlations in ASHRAE [18] is:

$$Me = c (\dot{m}_w / \dot{m}_a)^{-n} \quad (8.7)$$

4: See Section ?? (??)

where the constants  $c$  and  $n$  can be obtained from the fitting of experimental data<sup>4</sup>.

### 8.1.2 Samples generation for first-principles to data-driven models

The first pair of input variables for the WCT sample generation are the wet bulb temperature ( $T_{wb}$ ) and the difference between this temperature and the system inlet temperature ( $\Delta T_{wb-in}$ ). The wet bulb temperature is used instead of the ambient temperature or the relative humidity, because as it can be derived from the physical model, it is the most relevant thermodynamic variable for the wet cooling tower performance. Using both the ambient temperature and the relative humidity would lead to a larger than necessary input space with many duplicate samples, as the wet bulb temperature is a function of both variables. The second pair of input variables are the cooling water flow rate ( $q_{wct}$ ) and, following the reasoning from the physical model, the air to water mass flow ratio ( $\dot{m}_a / \dot{m}_{wct}$ ), since it is a key parameter in defining the operating conditions of the tower. From the resulting 2D grid, valid combinations are obtained by calculating the air mass flow rate and finding if a valid fan speed can be obtained using an air mass flow rate to fan speed empirical correlation.

Finally, all valid thermodynamic and operational combinations are merged into a comprehensive sample set, enabling detailed system evaluations across a realistic and constrained input space.

### 8.1.3 Model interface

#### Model 8.1: Wet cooling tower

$$T_{wct,out}, C_{w,wct} = \text{wct model}(q_{wct}, \omega_{wct}, T_{amb}, HR, T_{wct,in})$$

### Model 8.2: Wet cooling system model

$T_{wct,out}, C_e, C_w, T_{c,in}, T_{c,out} = \text{wcs model}(q_{wct}, \omega_{wct}, T_{amb}, HR, T_{wct,in})$   
 $T_{c,in}, T_{c,out} = \text{condenser model}(q_c, \dot{m}_v, T_v)$   
 $T_{wct,out}, C_{w,wct} = \text{wct model}(q_{wct}, \omega_{wct}, T_{amb}, HR, T_{c,out})$   
 $C_{e,c} = \text{electrical consumption}(q_c)$   
 $C_{e,wct} = \text{electrical consumption}(\omega_{wct})$   
 $C_e = C_{e,wct} + C_{e,c}$   
 $C_w = C_{w,wct}$

## 8.2 Dry cooler

### 8.2.1 Physical model

a

Pendiente de basarse en el artículo del modelo físico del DC con Elxe

### 8.2.2 Samples generation for first-principles to data-driven models

Similar to the wet cooling tower case, setting absolute values for both the inlet temperature and the environment temperature will lead to many unfeasible combinations ( $T_{dc,in} \leq T_{db}$ ). So instead, values are generated for the temperature difference, therefore, a 2D grid is constructed using combinations of ambient/dry-bulb temperature ( $T_{amb}$ ) and the difference between inlet and ambient temperature ( $(\Delta T_{amb-in})$ ). For each valid temperature pair ( $T_{amb}, T_{dc,in}$ ), additional independent variables ( $q_{dc}, \omega_{dc}$ ) are combined via a Cartesian product, resulting in a full multidimensional grid of plausible operating points. This systematic procedure ensures a dense and uniform sampling across all relevant input dimensions. Finally, infeasible combinations are filtered based on physical constraints.

### 8.2.3 Model interface

#### Model 8.3: Dry cooler

$T_{dc,out} = \text{dc model}(q_{dc}, \omega_{dc}, T_{amb}, T_{dc,in})$

#### Model 8.4: Dry cooling system model

$$\begin{aligned}
 T_{dc,out}, C_e, T_{c,in}, T_{c,out} &= \text{dcs model}(q_{dc}, \omega_{dc}, T_{amb}, T_{dc,in}) \\
 T_{c,in}, T_{c,out} &= \text{condenser model}(q_c, \dot{m}_v, T_v) \\
 T_{dc,out} &= \text{dc model}(q_{dc}, \omega_{dc}, T_{amb}, T_{c,out}) \\
 C_{e,c} &= \text{electrical consumption}(q_c) \\
 C_{e,dc} &= \text{electrical consumption}(\omega_{dc}) \\
 C_e &= C_{e,dc} + C_{e,c}
 \end{aligned}$$

### 8.3 Other components

#### 8.3.1 Electrical consumption

Electrical consumption is modelled with polynomial regressions of order 3 from experimental data:

#### Model 8.5: Electrical consumption

$$\begin{aligned}
 C_e &= \text{electrical consumption model}(x) \\
 C_e &= p_1 \cdot x^3 + p_2 \cdot x^2 + p_3 \cdot x + p_4
 \end{aligned}$$

where  $C_e$  represents the electrical consumption, and  $x$  is the input variable (e.g., the recirculated cooling water flow rate, particular cooler fan speed, etc.). The coefficients  $p_i$  correspond to a polynomial regression and must be calibrated individually for each component.

#### 8.3.2 Surface condenser

The surface condenser is a heat exchanger that condenses steam into water, assuming that all the vapor that enters the condenser (at saturated conditions), leaves it as saturated liquid, it can be modelled by applying the first law of thermodynamics, which states that the heat lost by the steam (*released*) is equal to the heat gained by the cooling water (*absorbed*), and equal to the heat transferred by the condenser heat transfer surfaces (*transferred*).

**Model 8.6: Surface condenser**

$$T_{c,in}, T_{c,out} = \text{condenser model}(\dot{m}_c, T_v, \dot{m}_v)$$

$$LMTD = \frac{T_{c,out} - T_{c,in}}{\ln\left(\frac{T_v - T_{c,in}}{T_v - T_{c,out}}\right)}$$

$$\dot{Q}_{released} = \dot{m}_v \cdot (h_{sat,vap} - h_{sat,liq})$$

$$\dot{Q}_{absorbed} = \dot{m}_c \cdot c_p(T_{c,out} - T_{c,in})$$

$$\dot{Q}_{transferred} = U \cdot A \cdot LMTD$$

$$U = \dots$$

The condenser area ( $A$ ) is a constant parameter

where  $T_{c,in}$  and  $T_{c,out}$  are the cooling water inlet and outlet temperatures, respectively,  $\dot{m}_c$  the cooling water mass flow rate,  $T_v$  vapour temperature and  $\dot{m}_v$  its mass flow rate and  $h_{sat,vap}$  and  $h_{sat,liq}$  are the specific enthalpies of the steam at the inlet and outlet of the condenser, respectively.  $\dot{Q}$  represents the heat transfer rate i.e. the thermal power.

**8.3.3 Mixers**

The mixers outlet flow ( $q_{mix,out,i}$ ) and temperature ( $T_{mix,out,i}$ ) can be determined with a simple mass and energy balances from its inlets streams ( $q_{mix,in}$ ,  $T_{mix,in}$ ):

**Model 8.7: Mixer model**

$$q_{mix,out}, T_{mix,out} = \text{mixer model}(q_{mix,in,1}, T_{mix,in,1}, q_{mix,in,2}, T_{mix,in,2}) \quad (8.8)$$

$$q_{mix,out} = q_{mix,in,1} + q_{mix,in,2} \quad (8.9)$$

$$T_{mix,out} = T_{mix,in,1} \cdot \frac{c_p(T_{mix,in,1})}{c_p(T_{out,i})} \frac{q_{mix,in,1}}{q_{mix,out,i}} + \\ T_{mix,in,2} \cdot \frac{c_p(T_{mix,in,2})}{c_p(T_{out,i})} \frac{q_{mix,in,2}}{q_{mix,out,i}} \quad (8.10)$$

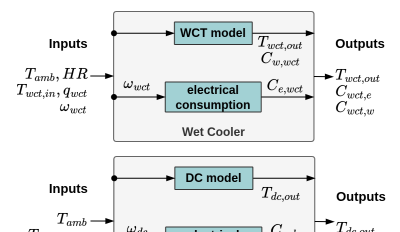
where  $c_p(\cdot)$  is the specific heat, which can be assumed to be the same for the mixing temperature differences of this type of system.

**8.4 Complete system**

The complete model of the combined cooling system integrates the models of the WCT and DC, along with the surface condenser and the mixers, as defined in Model 8.8 (Complete system)<sup>5</sup>. The full diagram, including all variables, is shown in Figure 8.3.

To solve the system, the condenser model is evaluated first, providing the inlet temperature for the dry cooler. Once the dry cooler is solved, the resulting temperatures allow for solving the wet cooling tower. Finally, the mixers are evaluated to determine the final outlet temperature of the combined cooler, which should match the condenser's inlet temperature.

5: Although the electrical consumption for cooling water recirculation is attributed to the condenser in this model, other components—particularly the hydraulic circuit and the dry cooler—also contribute significantly to circulation resistance



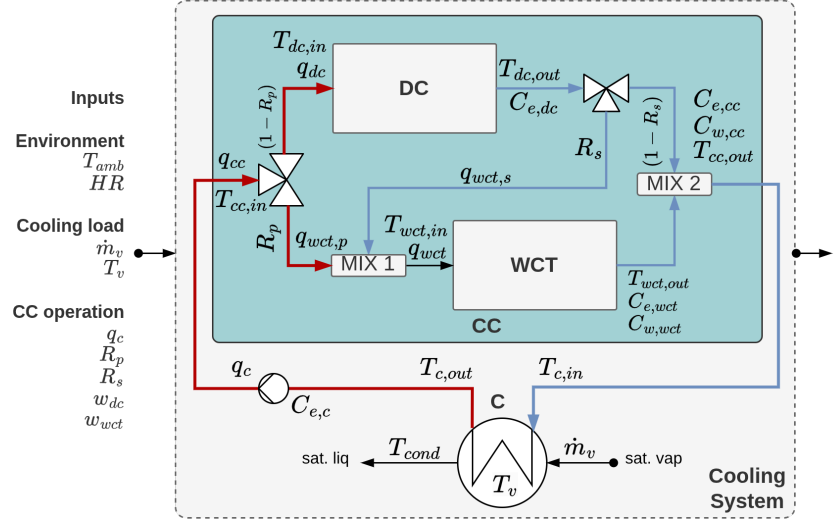


Figure 8.3: Complete model diagram of the combined cooling system

#### Model 8.8: Combined cooling system

$$\begin{aligned}
 & T_{cc,out}, C_e, C_w, T_{c,in}, T_{c,out} = ccs\_model(q_c, R_p, R_s, \omega_{dc}, \omega_{wct}, T_{amb}, HR_i, T_v, \dot{m}_v) \\
 & T_{cc,in} = T_{c,out} \\
 & T_{dc,in} = T_{cc,in} \\
 & q_{dc} = q_c \cdot (1 - R_p) \\
 & q_{wct,p} = q_c \cdot R_p \\
 & q_{wct,s} = q_{dc} \cdot R_s \\
 & T_{dc,out}, C_{e,dc} = dc\_model(q_{dc}, \omega_{dc}, T_{amb}, T_{dc,in}) \\
 & q_{wct}, T_{wct,in} = mixer\_model(q_{wct,p}, T_{cc,in}, q_{wct,s}, T_{dc,out}) \\
 & T_{wct,out}, C_{e,wct}, C_{w,wct} = wct\_model(q_{wct}, \omega_{wct}, T_{amb}, HR, T_{wct,in}) \\
 & T_{c,in}, T_{c,out} = condenser\_model(q_c, \dot{m}_v, T_v) \\
 & q_{cc}, T_{cc,out} = mixer\_model(q_{wct}, T_{wct,out}, q_{dc}, T_{dc,out}) \\
 & C_{e,c} = \text{electrical consumption}(q_c) \\
 & C_{e,dc} = \text{electrical consumption}(\omega_{dc}) \\
 & C_{e,wct} = \text{electrical consumption}(\omega_{wct}) \\
 & C_e = C_{e,dc} + C_{e,wct} + C_{e,c} \\
 & C_w = C_{w,wct}
 \end{aligned}$$

## **ENERGY MANAGEMENT IN MED PROCESSES DRIVEN BY VARIABLE ENERGY SOURCES**



 WORK IN PROGRESS

Esta sección no está terminada. Siquieres puedes echarle un ojo para ver la estructura y cómo encaja con el resto pero no merece la pena revisarla en detalle en el estado actual.

TL;DR

...

a

Add visual abstract

Derived scientific contributions

Structure



## Thermal desalination



Esta sección no está terminada. Siquieres puedes echarle un ojo para ver la estructura y cómo encaja con el resto pero no merece la pena revisarla en detalle en el estado actual.

Desalination is increasingly recognized as a key strategy to address global freshwater scarcity, driven by the combined pressures of climate change and population growth. Regions already facing drought and water stress, such as parts of Spain, are expected to see growing dependence on desalinated water to meet rising demand. While desalination technologies—particularly membrane-based systems like Reverse Osmosis (RO)—have seen rapid expansion, the energy intensity of the process remains a major challenge. To mitigate this, efforts have focused on improving energy efficiency and integrating renewable energy sources such as solar or geothermal heat. In particular, thermal desalination technologies like MED are gaining renewed interest due to their compatibility with low-exergy heat sources (e.g. waste heat) and the ability to treat high-salinity brines. These thermal processes also align better with circular economy approaches, allowing the concentration of brine and the recovery of valuable minerals such as lithium or magnesium, an emerging field known as brine mining.



**WORK IN PROGRESS**

Esta sección no está terminada. Si puedes echarle un ojo para ver la estructura y cómo encaja con el resto pero no merece la pena revisarla en detalle en el estado actual.

<b>10.1 Heat generation and storage subsystem</b>	39
10.1.1 Solar field	39
10.1.2 Thermal storage	40
<b>10.2 Separation subsystem</b>	40

The SolarMED system is an MED plant that receives its thermal energy from a solar field connected to a two-tank thermal storage system. It is one of the experimental facilities located in PSA as can be seen in Figure 1.1.

The different components are interconnected as depicted in Figure 10.1: a flat plate collector solar field which is the heat source, a pressurized hot water two-tank thermal storage system, and an MED plant which uses this heat to separate seawater into fresh water and brine. The solar field and thermal storage circuits are separated by a heat exchanger. Two subsystems are differentiated: the **sfts** subsystem and the thermal load that makes use of this heat for some useful application, in this case, to produce separation by means of the MED: the separation subsystem.

A esta figura quitar colores de decision variable and environment

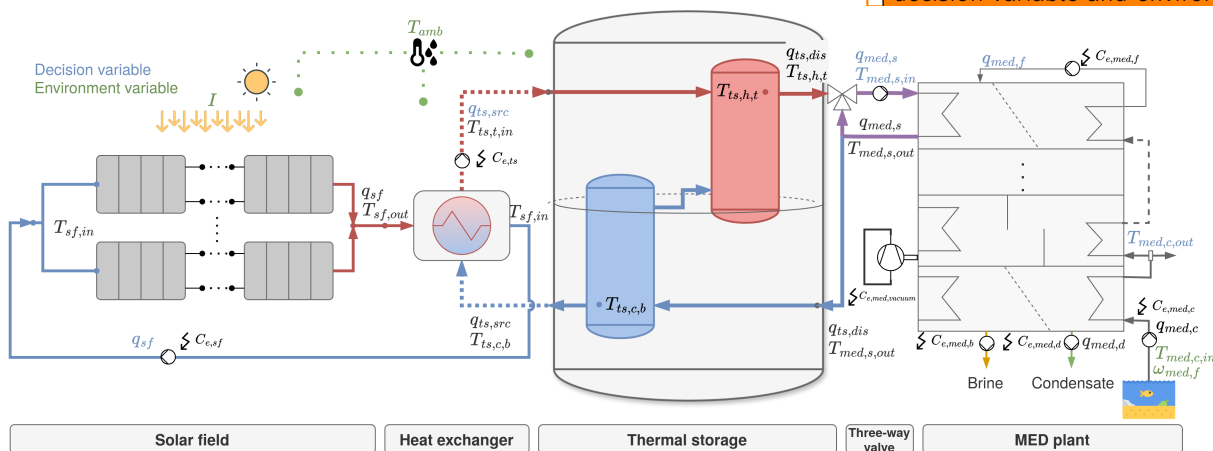


Figure 10.1: SolarMED process diagram

## 10.1 Heat generation and storage subsystem

Two pressurized water tanks coupled to a solar field composed of static flat plate collectors.

### 10.1.1 Solar field

The solar field is basically a converter of electrical to thermal energy conditioned to the availability of solar irradiance. It has a total aperture area of  $606 \text{ m}^2$  and can generate a maximum thermal power of  $323 \text{ kW}_{th}$  with a  $1000 \text{ W/m}^2$  solar irradiance. It is composed of 4 loops each with 2 rows of collectors...

The parameters are the collector aperture ( $A_c$  ( $m^2$ )), number of parallel collectors in each loop ,number of serial connections of collectors rows ( $n_s$ ), number of parallel tubes in each collector ( $n_t$ ) and the length of the collector inner tube ( $L_t$ ). Their values are shown in Table ??.

### 10.1.2 Thermal storage

1: See Figure 10.1 - *Thermal storage*

The thermal storage system<sup>1</sup> consists on a two-tank system designed to ensure thermal stratification. It has a total capacity of 40 m<sup>3</sup>. One of the tanks (the red tank in the diagram) operates at a higher temperature, receiving heat from the energy source and delivering it to the load. The return flow from the load enters the bottom of the cold tank (blue tank in the diagram) before circulating back to the hot tank, where it absorbs heat from the source.

## 10.2 Separation subsystem

patricia

The MED pilot plant was built in 1988 within the Solar Thermal Desalination project [REF]. It is a 14 effect, vertically stacked, forward-feed plant initially built to use low-pressure saturated steam as heat source for the first effect and later replaced to use hot water within the XXX project in 2005. An image of the facility in its current state can be seen in Figure 10.2It has been operated in different experimental campaigns and configurations robustly for more than two decades, as can be seen in Figure 10.3, which shows the operation history of the plant (starting from 2009). The campaign from 2009 to 2012 focused on ... [patricia] while the campaign from 2015 to 2016.... Finally, within the research work presented in this thesis, a new campaign was performed to validate a standardization methodology proposal and experimentally characterize the behaviour of the system at higher temperatures. This is explained in detail in the following chapter (Chapter 11 (Performance evaluation in MED processes: standard methodology proposal)).

Some particularities of this system are explained hereinafter:

- ▶ VFDs are used to control all flow rates in the system: heat source, cooling, feed, brine and distillate.
- ▶ As mentioned, the external heat source driving the process, is hot water from a thermal storage system. Water is drawn from one of the tanks and mixed with the water at the outlet of the first effect through a three-way valve, allowing independent regulation of flow and temperature.
- ▶ The inland location of this experimental plant is another particularity of the system. A fixed amount of seawater (30 m<sup>3</sup>), stored in a reservoir, is available to be used in the process and replenished as needed. The effluents from the plant are mixed in a different reservoir (5 m<sup>3</sup>), and returned to the feed in a close loop operation. Because water exits the process at a higher temperature than when it enters, this type of operation implies an ever-increasing heat sink temperature. A wet cooling tower, installed between the two reservoirs, is used to mitigate this effect.
- ▶ The previous particularity leads to a significant variation in the inlet water temperature from day to day and also within the same day depending on the operation conditions. To ensure the stability of the condenser (i.e. a constant vapor pressure and outlet cooling water temperature), the cooling flow rate is regulated. This allows to have a stable system representative of a real plant operating under normal conditions. However, this can lead to variable electrical consumption of the cooling pump.

- The vacuum system of the plant is based on two hydro-ejectors and a pump. The pump is operated always at fixed speed and its electrical consumption has been characterized with measurements under various conditions as being near-constant and independent of the operation conditions. Its associated nominal power is 5 kW<sub>e</sub>.
- The salinity of the feedwater is checked before every test measuring its conductivity with a conductivity meter (see Table ??).

A summary of its main specifications is shown at Table Table 11.1.

The facility's instrumentation is shown in Table 10.2. As can be seen, Platinum temperature transducer, 100 ohms at 0 °C (PT100) sensors are used to measure all liquid temperatures (TT01..TT05), while a PT1000 sensor is used to measure the ambient temperature (TT06). The pressure inside the first effect and condenser (PT01 and PT02, respectively) is measured by two different pressure transducers which fundamentally differ in their measurement range. To monitor the power consumption of the system, various subsystems have been individually instrumented using a power meter (JT01..JT04). Conductivity is measured using a portable conductivity meter (CT01, CT02), to which a calibration is periodically performed to convert conductivity to salinity. Flow rates (FT01..FT04) are measured using different types of flowmeters depending on the characteristics of the fluid being evaluated. Electromagnetic flowmeters are used for conductive fluids, while vortex flowmeters are used for non-conductive fluids. All sensors transmit a 4–20 mA analog signal that is converted to digital by Analog-to-Digital Converter (ADC) converters.

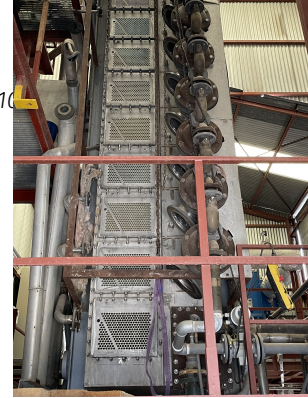


**Figure 10.2:** MED plant at PSA with open effects for maintenance

**Table 10.1:** MED plant at PSA specifications and nominal operating conditions

Parameter	Value
Capacity	72 m <sup>3</sup> /day
Number of effects	14
Feed type	Forward feed
Physical arrangement	Vertically stacked
Heat exchanger configuration	90/10 Cu-Ni HTE
Heat source type	Hot water
Vacuum system	Hydro-ejectors
Heat source flow rate	12 L/s
Feed water flow rate	8 m <sup>3</sup> /h
Brine rejection	5 m <sup>3</sup> /h
Distillate production	3 m <sup>3</sup> /h
Cooling flow rate at condenser	8-20 m <sup>3</sup> /h (10-25 °C)
Thermal power consumption	190 kW
Top Brine Temperature (TBT)	70 °C
Condenser temperature	35 °C

Measured variable	Instrument	Model	Range	Measurement uncertainty
Water temperature, TT01..TT05	PT100 Class A	SEDEM OF12871	0 - 100°C	± 0.15 + 0.002·T <sup>a</sup>
Distillate flow rate, FT03	Vortex flow meter	ABB TRIO-WIRL VT4	1.6 - 18 m <sup>3</sup> /h	± 0.75% o.r. <sup>b</sup>
Hot water flow rate, FT01	Electromagnetic	Endress+Hauser Proline Promag 50P	2.42 - 78.33 L/s	± 0.5% o.r.
Feedwater flow rate, FT02	Electromagnetic	Proline Promag P 300	2.1 - 66 m <sup>3</sup> /h	± 0.5% o.r.
Ambient temperature, TT05	PT1000	-	-40 - 60 °C	± 0.15 + 0.002·T
Pressure, PT01	Pressure capacitive	Endress+Hauser Cerabar T-PMC131	0 - 1 bar	± 0.5% FS <sup>c</sup>
Pressure, PT02	Piezoresistive sensor	WIKA S-10	0 - 0.6 bar	± 0.5% FS
Level, LT01, LT02	Magnetic level gauge	IGEMA NAV-50	0-750 mm	± 5 mm
Power, JT01..JT04	Power meter Class 1	Circutor CM31	0-7 kW	±1% o.r.
Conductivity, CT01..CT02	Conductivity meter	Prominent Portamess 911	0.1µS/cm - 1000 mS/cm	± 0.5% o.r. < 500 mS/cm ± 1% o.r. ≥ 500 mS/cm

**Table 10.2:** Characteristics of the instrumentation installed at MED-PSA unit (<sup>a</sup> value of the measured temperature in °C, <sup>b</sup> of reading, <sup>c</sup> full scale).

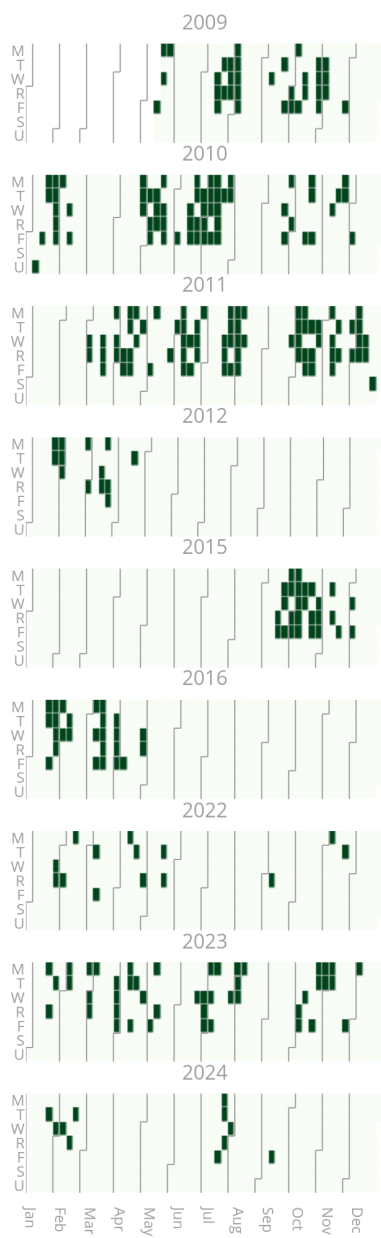


Figure 10.3: Operation history of the pilot plant.



## TL;DR

This chapter presents a standardized method for evaluating the performance of MED processes, which can also be extended to other thermal separation technologies. The method addresses key aspects such as instrumentation requirements, process control, and the suitability of performance metrics, including the uncertainties associated with their determination. Additionally, an algorithm has been developed for the automatic detection of steady-state operation, enhancing the reliability and robustness of evaluations under variable conditions. Experimental results confirm that the proposed method is both robust and reliable, enabling fair comparisons of MED processes across different operating scenarios.

The experimentation includes the evaluation of the process at high TBTs. The results are analyzed using different performance metrics and the scale formation risk is estimated by the RSI. The results show that the MED process can be operated at high TBTs without significant scale formation and achieve higher concentrations, but without significant improvements in thermal performance and limited reconcentration capacity if no changes to its design are made.

## Introduction

The future of MED in desalination and brine concentration applications depends on the technical development of the process and its integration with other technologies [19, 20]. The performance of this technology and how it is evaluated plays an important role in this development.

Although efforts have been made to propose performance metrics to evaluate the multi-effect evaporation process, there is neither consensus in which metrics are the most suitable [21] nor standards on how to evaluate the experimental process. The only standard existing in MED is not related to performance evaluation, but to cost structures and determinants [22].

For the performance evaluation of MED processes, originally, the index Gain Output Ratio (GOR) was used for plants operating with steam as external energy source. In order not to be limited to steam-driven systems and to take into account sensible heat sources, a new performance index was defined: the Performance Ratio (PR) [23, 24], which is currently the most widely adopted for MED performance evaluation although it is constrained by using a reference enthalpy of 2326 kJ equivalent to 1000 BTU. In [25], a variation of this metric called the Waste Heat Performance Ratio ( $PR_{WH}$ ) was suggested to account for the potential of low-grade waste heat sources. Another widespread thermal performance metric that has been used in MED is the Specific Thermal Energy Consumption (STEC) and its electrical equivalent, the Specific Electrical Energy Consumption (SEEC). However, there are certain limitations in the aforementioned metrics that challenge making a fair comparison between desalination systems that use different energy sources *i.e.* electrical and thermal<sup>1</sup>. Furthermore, the ability of thermal energy to perform work changes with its temperature, so it is essential to consider the quality of the thermal energy used in desalination processes. This limitation of traditional energetic metrics was showcased in Bouma et al. [27] where they compared four different configurations of MED plants: a low temperature MED configuration (LT-MED), a MED unit incorporating Thermal

11.1	Process analysis . . . . .	45
11.2	Performance metrics . . . . .	46
11.2.1	Separation metrics . . . . .	46
11.2.2	Energetic metrics . . . . .	47
11.2.3	Exergetic metrics . . . . .	48
11.3	Instrumentation . . . . .	50
11.3.1	KPV . . . . .	50
11.3.2	Instrumentation requirements	51
11.3.3	Uncertainty determination .	52
11.4	Monitoring and process control	53
11.4.1	Monitoring: steady-state identification . . . . .	53
11.4.2	Control system . . . . .	53
11.5	Methodology application and results . . . . .	55
11.5.1	Implementation results . . .	56
11.5.2	Results analysis . . . . .	60

[19]: Ghenai et al. (2021), "Performance Analysis and Optimization of Hybrid Multi-Effect Distillation Adsorption Desalination System Powered with Solar Thermal Energy for High Salinity Sea Water"

[20]: Son et al. (2020), "Pilot Studies on Synergistic Impacts of Energy Utilization in Hybrid Desalination System"

[21]: Burgess et al. (2000), "Solar Thermal Powered Desalination: Membrane versus Distillation Technologies"

[22]: Pinto et al. (2017), "Desalination Projects Economic Feasibility"

[23]: Mistry et al. (2011), "Entropy Generation Analysis of Desalination Technologies"

[24]: El-Dessouky et al. (2002), *Fundamentals of Salt Water Desalination*

[25]: Christ et al. (2014), "Thermodynamic Optimisation of Multi Effect Distillation Driven by Sensible Heat Sources"

1: the value of 1 kWh electric differs from that of 1 kWh thermal in terms of their ability to produce work, as the latter is constrained by the Carnot efficiency [26]

[27]: Bouma et al. (2020), "Metrics Matter"

[28]: Darwish et al. (2006), "Multi-Effect Boiling Systems from an Energy Viewpoint"

[29]: Shahzad et al. (2019), "A Standard Primary Energy Approach for Comparing Desalination Processes"

[26]: Lienhard et al. (2017), "Thermodynamics, Exergy, and Energy Efficiency in Desalination Systems"

[30]: Brogioli et al. (2018), "Thermodynamic Analysis and Energy Efficiency of Thermal Desalination Processes"

[31]: Spiegler et al. (2001), "El-Sayed, Y.M."

[32]: Sharqawy et al. (2011), "On Exergy Calculations of Seawater with Applications in Desalination Systems"

[33]: Sharqawy et al. (2010), "Formulation of Seawater Flow Exergy Using Accurate Thermo-dynamic Data"

[34]: Mistry et al. (2012), "Effect of Nonideal Solution Behavior on Desalination of a Sodium Chloride (NaCl) Solution and Comparison to Seawater"

[35]: Mistry et al. (2013), "Generalized Least Energy of Separation for Desalination and Other Chemical Separation Processes"

[36]: Thiel et al. (2015), "Energy Consumption in Desalinating Produced Water from Shale Oil and Gas Extraction"

[37]: Valenzuela et al. (2014), "Optical and Thermal Performance of Large-Size Parabolic-Trough Solar Collectors from Outdoor Experiments"

[38]: Prahl et al. (2018), "Protocol for Characterization of Complete Solar Concentrators Using Photogrammetry or Deflectometry"

[39]: Bayón et al. (2019), "Development of a New Methodology for Validating Thermal Storage Media"

Vapor Compression (MED-TVC), a MED unit using nanofiltration (NF-LT-MED) for feedwater pretreatment, and a combination of TVC and nanofiltration. Although the STEC values favored the use of TVC, a more rigorous analysis revealed that the most efficient systems were those that used lower temperature heat sources (LT-MED and NF-LT-MED).

Some authors have carried out exergy analyzes to overcome the limitations aforementioned of energy performance metrics. Darwish et al. [28] proposed two new metrics: Specific Fuel Energy and Equivalent Specific Work. The first compares the energy used for the desalination process that could otherwise be used for energy generation in a turbine for which it was assumed a value for the efficiency of the power plant. The second sets the work potential of the extracted steam as a baseline, considering the desalination plant separation efficiency and adding the energy consumption for pumping. The problem of this study is that it is limited to cogeneration schemes (joint electricity and water production) and would not be useful in the case of desalination with low-temperature sources. Shahzad et al. [29] developed an approach based on the second law of thermodynamics, which is also useful only for cogeneration schemes. They proposed a common metric called the Standard Universal Performance Ratio to compare desalination processes using different kinds of energy, which is based on conversion of different types and grades of energies to standard primary energy. In this case, conversion factors were proposed to convert the derived energy input to the standard primary energy. Other authors have performed exergy analyses for stand-alone desalination processes, as is the case of Lienhard et al. [26] and Brogioli et al. [30], who considered desalination processes as a black box and the ideal work or the thermodynamic limit for the separation of dissolved salts in seawater as the Carnot work.

The problem with the exergy analyses is that they are more complex [31] due to the need to consider several aspects not present in simple energetic metrics: definition of dead state and control volume [32], chemical exergy modeling of seawater [33, 34] and minimum energy reference (least and minimum work of separation) [35, 36]. Probably because of their complexity, they have not been widespread in the performance evaluation of practical setups. Also, none of the works published so far in the scientific literature addresses specifically the exergetic evaluation when using non-conventional energy sources such as waste heat.

Two important requirements for an accurate and reliable performance assessment, yet to be dealt with in thermal desalination, are the steady state identification and the uncertainty of both the direct measurement and that associated with the performance metric determination. With respect to the former, it is highly recommended to use automatic procedures that increase the reliability of the measurements. The steady state evaluation carried out manually so far by qualified operators [37–39], leads to high time consumption and full dependence on the operators' attention, leading to potential unreliable identifications. With respect to the latter, it allows for a more comprehensive and nuanced approach to performance evaluation, since it increases the robustness of the evaluation while providing information on the reliability of the results. Therefore, there is a gap in the establishment of standard methodologies that include all the necessary requirements for the reliable assessment of the performance of thermal desalination processes. This chapter aims to address this gap by proposing a method with potential for a broader application in other thermal desalination processes. The method is applied and validated in an experimental MED plant as part of a high TBT experimental campaign.

This chapter is structured as follows: first in the Section 11.1 (Process analysis) a process analysis focused on performance evaluation is done to clearly define the scope of the evaluation and the inputs and outputs of the process. Then in Section 11.2 (Performance metrics), the performance metrics are defined, including separation, energetic, and exergetic. Section 11.3 (Instrumentation)

is related to the instrumentation of the system: KPVs, instrumentation requirements and uncertainty determination for both direct measurement and derived metrics. Section 11.4 (Monitoring and process control) presents the proposed steady state identification algorithm for stable operation monitoring and the controllers to be implemented. Finally, in Section 11.5 (Methodology application in an experimental campaign) the proposed methodology is applied to a case study: a pilot MED plant evaluated in a TBT experimental campaign. The results from the campaign are also analyzed in this section.

## 11.1 Process analysis

Metrics are defined based on some criteria, and this criteria is of paramount importance because resources and efforts are invested in optimizing the process in its direction. In order to adequately define these criteria, it is important to have an overall perspective of the process: defining its inputs and useful outputs, from a qualitative point of view, as well as a clear delineation of the scope of the evaluation.

Metrics can be related either to the operation – isolated MED operation or considering primary energy [27] – or to the design of the system<sup>2</sup>. This chapter focuses on the operation of an isolated MED system.<sup>3</sup>

**Application.** Two applications are distinguished:

- ▶ **Seawater desalination.** The objective is to obtain fresh water. The level of separation achieved is a secondary (not useful) output.
- ▶ **Brine concentration.** The objective is to extract resources from the brine in order to valorize it. Here, the level of separation is a crucial factor to consider.

**External heat source type.** Two types of external heat sources are distinguished:<sup>4</sup>

- ▶ **Process heat.** Process heat is the heat utilized by a system and its associated costs are related to the amount of energy consumed.
- ▶ **Waste heat.** Waste heat is the heat utilized by a system that would otherwise be lost to the environment. It has no associated costs to the amount of heat used, though there are other costs associated with its use [40, 41]<sup>5</sup>. Here the paradigm is different as described by Christ et al [25, 42, 43], the goal is to maximize the amount of product by maximizing the utilization of the waste source.

### Process vs waste heat take on efficiency

In a process heat driven system, between two plants that produce the same amount of useful product, the most efficient one is the one that uses the least external heat to do so, whereas in a waste heat driven system, the two plants would be considered as efficient since the unused heat would be wasted to the environment. A more intuitive definition would be:

Given two plants that consume the same waste heat, the most efficient one is the one that produces more product with the available heat.

Based on the above considerations, Figure 11.1 shows the control volume of the MED process with the inputs and outputs used for the definition of the performance metrics. From left to right, seawater (including cooling water,  $c$ , and feed,  $f$ ) enters the control volume at the seawater intake conditions ( $T_{c,in}$ ). The cooling water is rejected at  $T_{c,out}$ . On the right side, the distillate and the brine are discharged from the MED system at temperatures  $T_{d,out}$  and  $T_{b,out}$  and mass fractions  $w_d$  and  $w_b$ , respectively. The temperatures of all these outlet streams,

2: e.g. specific area [24]

[27]: Bouma et al. (2020), "Metrics Matter"

3: It is as if an already built system is provided, so decision over its design parameters and energy source conditions is not an available degree of freedom, only optimization in its operational variables.

4: The use of electrical work will always be desired to be minimized, so the distinction is not needed.

[40]: Mistry et al. (2013), "An Economics-Based Second Law Efficiency"

[41]: Christ et al. (2017), "Techno-Economic Analysis of Geothermal Desalination Using Hot Sedimentary Aquifers"

5: e.g. a less efficient system will require a larger heat exchanger area to extract more energy from the waste source, directly increasing the cost of the system

[25]: Christ et al. (2014), "Thermodynamic Optimisation of Multi Effect Distillation Driven by Sensible Heat Sources"

[42]: Christ et al. (2015), "Application of the Boosted MED Process for Low-Grade Heat Sources — A Pilot Plant"

[43]: Christ et al. (2015), "Boosted Multi-Effect Distillation for Sensible Low-Grade Heat Sources"

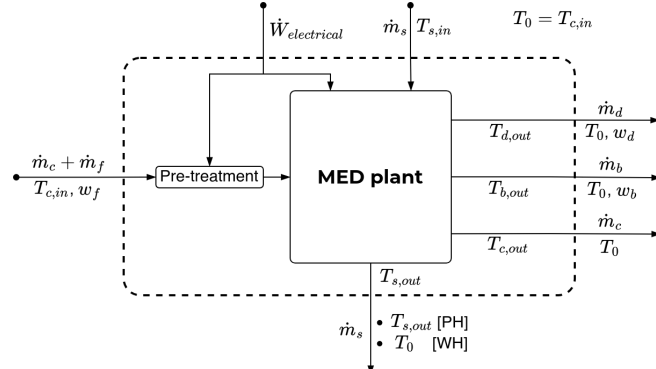


**Figure 11.1:** Inputs and outputs variables in an MED process. The dash line delimits the control volume

6: It is heat that is lost to the environment, no additional work can be feasibly extracted from these streams

from a qualitative (*i.e.* exergetic) point of view, are useless and thus considered to be at  $T_0$  when leaving the control volume<sup>6</sup>.

From top to bottom, the energy sources for the system are depicted. Electrical work is depicted as  $\dot{W}_{electrical}$  and it may include pumping, vacuum system, and feed water pretreatment, among others. The heat source is represented by the subscript ( $s$ ) and as shown in the figure, it enters the MED plant at  $T_{s,in}$  and leaves it at  $T_{s,out}$  after releasing part of its energy. When leaving the control volume,  $T_{s,out}$  value depends on the type of heat source:

- ▶ Process heat (PH). The value of  $T_{s,out}$  does not change. In case steam is used, the primary energy driver is the latent heat of phase change and  $T_{s,out}$  is usually similar to or equal to  $T_{s,in}$ . In case a sensible heat source is used, the driving force is the temperature difference and  $T_{s,out}$  is between  $T_{s,in}$  and  $T_0$ .
- ▶ Waste heat source (WH). In this case,  $T_{s,out}$  is considered to be at the sink conditions,  $T_0$ , since this heat is not reused but lost to the environment.

## 11.2 Performance metrics

A performance metric is a quantitative measure used to evaluate the effectiveness or efficiency of a system. It provides objective information that can be used to monitor progress, identify areas for improvement, and inform decision making. A metrics division in three categories is proposed: separation, energetic, and exergetic metrics. A detailed description of each of them within each category is presented below.

### 11.2.1 Separation metrics

[44]: Jones et al. (2019), "The State of Desalination and Brine Production"

[45]: Palenzuela et al. (2015), *Concentrating Solar Power and Desalination Plants*

The Recovery Ratio (RR) represents the flow ratio of unit of distillate produced per unit of feed and is very useful in seawater brine concentration applications [44]. It is related to electricity consumption, since the lower the RR the higher the feed pumping needs are for the same distillate production [45]. It is determined as follows:

$$RR = \frac{\dot{m}_d}{\dot{m}_f} \times 100 [\%], \quad (11.1)$$

where  $\dot{m}_d$  is the mass flow rate of distillate and  $\dot{m}_f$  is the feedwater mass flow rate, both in kg/s.

An equivalent metric is the concentration factor, which accounts for how many times the brine is concentrated with respect to the feed concentration:

$$CF = \frac{w_b}{w_f} = \frac{\dot{m}_f}{\dot{m}_f - \dot{m}_d} [-], \quad (11.2)$$

where  $w_b$  is the brine concentration and  $w_f$  is the feedwater concentration, both in g/kg.

Apart from the already known previous metrics, a new one is proposed in this work that can be useful for seawater brine concentration applications. This metric is called Reconcentration Index (RI), and it allows to determine how close the separation achieved (RR) is to the theoretical maximum recovery ratio ( $RR_{max}$ ). It is defined as:

$$RI = RR/RR_{max} [-], \quad (11.3)$$

where  $RR_{max}$  is calculated as follows [36]:

$$RR_{max} = w_{w,f} \left( 1 - \frac{b_{NaCl,f}}{b_{NaCl,sat}} \right) \times 100 [\%], \quad (11.4)$$

[36]: Thiel et al. (2015), "Energy Consumption in Desalinating Produced Water from Shale Oil and Gas Extraction"

where  $w_{w,f}$  is the water mass fraction in the feed (which is  $1 - w_{sol,f}$ , where  $w_{sol,f}$  is the mass fraction of the solutes in the feed) and  $b_{NaCl,f}$  is the molality of sodium chloride in the feed, in mol<sub>NaCl</sub>/kg<sub>w</sub> (both can be obtained from a feedwater chemical analysis). On the other hand,  $b_{NaCl,sat}$  is the molality of sodium chloride at saturation conditions (see Section ?? for more details of its estimation)<sup>7</sup>.

<sup>7</sup>: sodium chloride is the only solute considered, as it sets the concentration limit being the solute in seawater with the highest concentration and the greatest solubility [36]

## 11.2.2 Energetic metrics

The energetic metrics are metrics that consider only the first law of thermodynamics (*i.e.* quantity). They are: GOR, STEC, and SEEC and are described in the following.

Regarding the GOR, a universal definition of this metric that avoids the limitations of some of the commonly used definitions mentioned<sup>8</sup> is the ratio between the energy in the form of latent heat required to vaporize all the distillate produced and the external thermal energy contributed to the system (Eq. 11.5) [46].

$$GOR = \frac{\dot{m}_d \cdot \Delta h_{avg}}{\dot{Q}_{in}} \quad (11.5)$$

<sup>8</sup>: Limited to steam or 1000 BTU as arbitrary conversion factor

[46]: Lienhard V et al. (2012), "SOLAR DESALINATION"

where  $\Delta h_{avg}$  is the latent heat of vaporization at the average vapor temperature between the first effect and the last effect, in kJ/kg, and  $\dot{Q}_{in}$  is the external thermal energy consumption required to drive the process, in kW. It is determined by  $\dot{m}_s$  (mass flow rate of the external energy source supplied in the first effect, in kg/s) and  $\Delta h_s$ , which can be calculated as  $h_{s,in} - h_{s,out}$  (in case of sensible heat) or as  $h_{s,sat,vap} - h_{s,sat,liq}$  (in case of latent heat of phase change at saturation conditions from vapor to liquid at temperature  $T_{s,in}$ ).

In case waste heat is used as external thermal energy source for the MED system,  $\dot{Q}_{in}$  is determined with  $\dot{m}_s$  and  $\Delta h$  but referred to the lowest temperature of the system ( $T_{c,in}$ ).

Another performance index widely used in thermal desalination is the STEC. For desalination applications, it is defined as the input heat to the system per unit

of product (distillate). This index has units of energy per fraction of volume and its expression is shown in Eq. 11.6.

$$STEC = \frac{\dot{m}_s \cdot (h_{s,in} - h_{s,out})}{\dot{m}_d} \cdot \rho_d \cdot \frac{1 \text{ kWh}}{3600 \text{ kJ}} \left[ \frac{\text{kWh}_{\text{th}}}{\text{m}^3} \right]. \quad (11.6)$$

For brine concentration applications, it is named as  $STEC_{bc}$  and it is determined as the energy required (in kJ) per unit of feed (in kg) (i.e.  $\dot{m}_f$  in the denominator) [47].

Both STEC and GOR are equivalent and are related via Eq. 11.7.

$$STEC = \frac{2326 \text{ kJ/kg}}{GOR} \cdot \rho_d \cdot \frac{1 \text{ kWh}}{3600 \text{ kJ}}, \quad (11.7)$$

where  $\rho_d$  is the density of the distillate in  $\text{kg/m}^3$ .

For the cases in which waste heat source is used as energy source, a variation of the STEC is proposed: the waste heat STEC. For desalination applications, it is determined as follows:

$$STEC_{wh} = \frac{\dot{m}_s \cdot (h_{s,in} - h_{c,in})}{\dot{m}_d} \cdot \rho_d \cdot \frac{1 \text{ kWh}}{3600 \text{ kJ}} \left[ \frac{\text{kWh}_{\text{th}}}{\text{m}^3} \right]. \quad (11.8)$$

As before, for brine concentration applications,  $\dot{m}_d$  would be replaced by  $\dot{m}_f$  in the denominator.

Another important index in desalination is the SEEC, which represents the total electrical consumption of the plant and its auxiliary systems per unit of distillate water produced. These are the subsystems that should be considered:

- ▶  $J_s$ . External energy source
- ▶  $J_f$ . Feed pumping
- ▶  $J_c$ . Cooling
- ▶  $J_d, J_b$ . Discharge extractions
- ▶  $J_{vacuum}$ . Vacuum system
- ▶  $J_{aux}$ . Auxiliary consumptions. Represents any additional power that the system may require to function (e.g., electrical consumption for the feedwater pretreatment such as nanofiltration)

For desalination applications, the following equation is used for the calculation of this metric:

$$SEEC = \frac{\sum_{i=1}^N (J_i)}{\dot{m}_d} \left[ \frac{\text{kWh}_e}{\text{m}^3} \right], \quad (11.9)$$

where  $J_i$  is the electrical consumption of the  $i_{th}$  subsystem. In the case of brine concentration applications, the index is called  $SEEC_{bc}$  and the denominator would be replaced by  $\dot{m}_f$ .

### 11.2.3 Exergetic metrics

Exergy is the maximum amount of work achievable when a system is brought into equilibrium from its initial state to a reference state (known as the dead state and represented by the subscript “0”) [32, 48]. This reference state is usually established for desalination applications as the seawater intake temperature

$(T_{c,in})$ . In contrast to the energetic metrics, it considers not only the first law of thermodynamics (quantity), but also the second law (quality).

The most widespread exergetic metric is the second law efficiency ( $\eta_{II}$ ) [26], which accounts for irreversible losses within a system. It is calculated as the ratio of the useful exergy output of a system ( $\dot{E}x_{out,useful}$ ) to the exergy input given to the system ( $\dot{E}x_{in}$ ) (a further explanation of how to determine the different exergy flows can be found in Section ?? (??)):

$$\eta_{II} = \frac{\dot{E}x_{out,useful}}{\dot{E}x_{in}} \times 100 [\%]. \quad (11.10)$$

Considering exergy losses, which are the sum of exergy destroyed in each individual component ( $\dot{E}x_{destroyed}$ ) and exergy losses due to discharge streams in disequilibrium to the environment ( $\dot{E}x_{streams}$ ), the previous equation can be written as follows:

$$\eta_{II} = 1 - \frac{\dot{E}x_{destroyed} + \dot{E}x_{streams}}{\dot{E}x_{in}} \times 100 [\%]. \quad (11.11)$$

For brine concentration applications and in case waste heat is used, the metric is called  $\eta_{II,wh}$  and  $\eta_{II,bc}$ , respectively, to distinguish between the type of application and external energy source.

Another useful metric is the Specific Exergy Consumption (SEXC), which was firstly referenced as specific consumed available energy in [28]. Similarly to SEEC and STEC, it accounts for the exergy input to the system per unit of distillate produced (Eq. 11.12) and it is determined as follows [27]:

$$SEXC = \frac{\dot{E}x_{in}}{\dot{m}_d} \left[ \frac{\text{kWh}_{\text{ex}}}{\text{m}^3} \right]. \quad (11.12)$$

It is important to note that the terms  $\dot{E}x_{out,useful}$  and  $\dot{E}x_{in}$  from the previous exergetic metrics are determined depending on what is considered as useful exergy leaving the process and what is deemed as exergy input to the system.<sup>9</sup>

**Useful exergy output** . The useful exergy output of the system ( $\dot{E}x_{out,useful}$ ) depends on what is considered the valuable product generated by the process. In a separator in which the objective is to separate water and brine, the useful exergy is the chemical exergy of separation. As discussed in [26], for seawater desalination applications, where the valuable product is fresh / pure water, the chemical exergy of separation corresponds to that of a reference ideal separator that achieves the *minimum separation work* ( $\dot{W}_{least}^{min} = \dot{W}_{least}|_{RR \rightarrow 0}$ ). The objective is to minimize the required energy consumption to produce fresh / pure water, regardless of how much separation takes place ( $RR \rightarrow 0$ ), so  $\dot{E}x_{out,useful} = \dot{W}_{least}^{min}$ .

On the other hand, in brine concentration applications, since the objective is to maximize the separation achieved, the separator takes into account the amount of separation achieved ( $\dot{W}_{least}|_{RR}$ ), and  $\dot{E}x_{out,useful} = \dot{W}_{least}$  [36]. The definition and determination of the least and minimum least work of separation can be found in Section ??.

**Exergy input** . The exergy input ( $\dot{E}x_{in}$ ) is determined according to the type of external heat source. In case process heat is used, the exergy input is determined as:

$$\dot{E}x_{in} = \dot{E}x_{s,in} - \dot{E}x_{s,out} + \sum_i \dot{E}_i, \quad (11.13)$$

[26]: Lienhard et al. (2017), "Thermodynamics, Exergy, and Energy Efficiency in Desalination Systems"

[28]: Darwish et al. (2006), "Multi-Effect Boiling Systems from an Energy Viewpoint"

[27]: Bouma et al. (2020), "Metrics Matter"

9: It mirrors the qualitative analysis presented in Section 11.1

[26]: Lienhard et al. (2017), "Thermodynamics, Exergy, and Energy Efficiency in Desalination Systems"

[36]: Thiel et al. (2015), "Energy Consumption in Desalinating Produced Water from Shale Oil and Gas Extraction"

where  $\dot{E}x_{s,in}$  and  $\dot{E}x_{s,out}$  are the exergy flows associated with the thermal energy source at the inlet and outlet, respectively.

When using waste heat sources, the exergy input is determined as:

$$\dot{E}x_{in} = \dot{E}x_{s,in} - \dot{E}x_{s,out}^{wh} + \sum_i \dot{E}_i, \quad (11.14)$$

where  $\dot{E}x_{s,out}^{wh}$  is the outlet heat source exergy flow, which is evaluated at temperature  $T_0$  (dead state).

## 11.3 Instrumentation

### 11.3.1 KPV

The KPVs are those variables that uniquely define an operating point, which is obtained by averaging all monitored variables when stable operation is achieved. In other words, any change in the key variables is associated with a different operating point, since the plant outputs are affected accordingly. The following selected variables apply to any MED plant with any configuration in terms of seawater flow direction, tube arrangement in tube bundles, or effect layout [45]. They are represented in Figure 11.2 and described hereinafter:

- ▶ Heat source flow rate ( $\dot{m}_s$  - FT01), inlet temperature and pressure ( $T_{s,in}$  and  $P_{s,in}$  - TT01 and PT03) for sensible heat sources, and just FT01 and TT01 if saturated steam is used (otherwise steam quality needs to be estimated). They determine the hot side conditions, which usually take place in the first effect that is at the highest temperature and pressure. If multiple effects receive external heat sources, each one has to be monitored.
- ▶ Feed water flow rate ( $\dot{m}_f$  - FT02), which affect the overall plant operation conditions. A precise and stable input feed flow rate ensures consistent heat transfer rates, residence times, and separation efficiencies.
- ▶ Distillate flow rate ( $\dot{m}_d$  - FT03). It is a basic variable that gives information about the production of the system. As long as this output variable is stable, it can be assumed that the sum of it plus the brine flow rate is equal to the feed flow rate.
- ▶ Condenser pressure / temperature ( $P_{v,c}$  - PT02 /  $T_{v,c}$ ) or condenser outlet temperature ( $T_{c,out}$  - TT02). The stability of any of these variables, together with that of the distillate production, establish a stable heat sink.
- ▶ Effect pressure / temperature ( $P_{v,1}$  - PT01 /  $T_{v,1}$ ) or heat source outlet temperature ( $T_{s,out}$  - TT05), which is always required in case that sensible heat source is considered as the external energy source. The stability of this output variable determines a stable hot side. In case other effects, apart from the first one, receive external heat sources, each one has to be monitored.
- ▶ Feed water salinity ( $w_f$  - CT01). It affects the overall plant operation conditions since any stream with different salinity would have different thermodynamic properties (i.e. boiling point elevation) and therefore, different energy requirements to perform the separation.
- ▶ Condensate salinity ( $w_d$  - CT02). This variable together with the distillate flow rate gives information on the levels of salt separation from water achieved.
- ▶ Ambient temperature ( $T_{amb}$  - TT06). The ambient conditions determine the losses to the environment which can change the results for the, otherwise, same operating conditions.
- ▶ Seawater temperature or condenser inlet temperature ( $T_{c,in}$  - TT04). It is another environment variable that sets the minimum achievable temperature in the system.

[45]: Palenzuela et al. (2015), *Concentrating Solar Power and Desalination Plants*

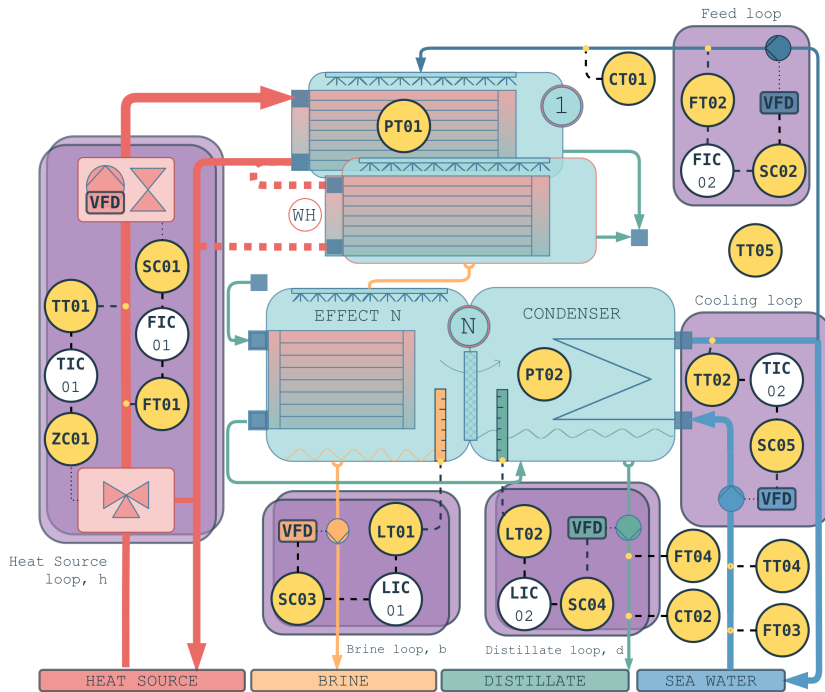


**Figure 11.2:** P&ID with the required instrumentation, KPVs, and basic control loops (ANSI/ISA 5.1-2022) required in an MED plant

- Last effect ( $L_b$  - LT01) and condenser ( $L_d$  - LT02) levels. In the case of the final condenser, it is a vessel in which the vapor coming from the final effect condenses, producing distillate that is continuously extracted from the system. The stability in this vessel is achieved when the extraction rate is equal to the condensate production rate. A higher extraction rate would eventually lead to unstable production, while a lower extraction rate would cause an increase in the vapor pressure, which would lead to induced lower production caused by misoperation. A stable level throughout the operation can ensure that the extraction and production rates ( $\dot{m}_d$ ) are in balance. In the case of the last effect, it is important to keep the level as low as possible in order to avoid brine contamination in the final condenser.

### 11.3.2 Instrumentation requirements

The installed instrumentation must measure magnitudes such as flow rate (mass or volumetric), temperature, pressure, water conductivity, level, and power. First, it is important to account for the influence of the quality of each measured variable on the reliability of the performance metrics, which is determined by a sensitivity analysis.

#### Reminder: How to interpret Sensitivity Analysis (SA) results

The results are different sensitivity indices such as total sensitivity indices (total-order), first-order sensitivity indices (first-order), and interaction sensitivity indices (second-order). First-order measures the direct effect of an input variable on the output, excluding interaction effects with other variables, while the second-order measures specifically these interaction effects. Finally, total-order indices account for the total effect of an input variable, including both direct and interaction effects.<sup>a</sup>

<sup>a</sup> More in Chapter 3 (Sensitivity analysis)

All KPVs must be monitored regardless of their influence on the performance metric being evaluated because, as mentioned above, the average values of these variables at steady state conditions define an operating point.

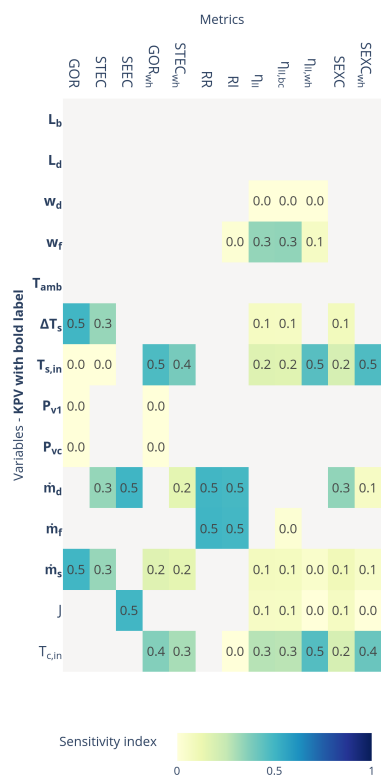


**Figure 11.3:** Sensitivity index results for different variables. Useful to assess the impact of the different measured variables uncertainty on the performance metric. KPVs are shown in bold notation

[50]: Smith (2013), *Uncertainty Quantification*

Figure 11.3 shows the results obtained from the sensitivity analysis in terms of total-order Sensitivity Index (SI). The closer the SI is to 1, the greater the influence of the variable (shown on the left axis) on the reliability of the performance metric (shown on the top). In other words, the quality of the variable measurement should be higher for variables with a higher SI. The cases where no sensitivity index is obtained indicate that the variable has no effect on the metric.

In general, monitoring of these variables must be performed online for each operating point evaluated. However, some of the variables rarely change and can be measured periodically or offline. This is the case of environment variables such as  $w_f$ ,  $w_d$ ,  $T_{amb}$ .

Another aspect that deserves careful consideration is the measurement of the temperature of the heat source. To determine the thermal efficiency of the system when a sensible heat source is utilized, it is crucial to accurately measure the temperature difference between the inlet and outlet of this energy source ( $\Delta T_s$ ). Using temperature transmitters with high accuracy rates (i.e. PT100), uncertainties of about 0.5 °C or below 1 % for the absolute temperature can be expected at temperatures exceeding 60 °C. However, when considering the small temperature differences between the inlet and outlet, which can be as low as 2 °C, the resulting relative uncertainty could be up to 25 %. To address this problem, it is recommended that both temperature transmitters are identical and calibrated simultaneously, using the same calibration pattern, which translates into observed values for the uncertainty of the temperature difference in the range of 0.1 °C or 5 %.

On the other hand, the total electrical energy consumption (represented as JT01 in Figure 11.2 can be monitored as global system consumption, or independently per subsystem ( $J_s$ ,  $J_c$ ,  $J_f$ ,  $J_d$ ,  $J_b$ ,  $J_{vacuum}$ ,  $J_{aux}$ ).

### 11.3.3 Uncertainty determination

Uncertainty determination is particularly valuable in assessing the reliability and validity of predictions, forecasts, or results evaluation. The framework on which the uncertainty assessment of this paper is based is JCGM 100:2008 [49].

In an uncertainty analysis, the uncertainties of direct measurements must first be determined. The uncertainty of each direct measure ( $\Delta X_i$ ) consists of the sum of two components, as indicated below:

$$\Delta X_i = \Delta X_{sensor} + \Delta X_{control}$$

where:

- ▶  $\Delta X_{sensor}$  is the contribution of the sensor, which depends on its accuracy, calibration and conversion errors, and should be available from the instrument datasheet.
- ▶  $\Delta X_{control}$  is the uncertainty attributed to the quality of the control and is estimated using the standard deviation of the measurement throughout the period considered as stable.

On the other hand, when working with derived variables, i.e. quantities that are calculated based on other measured or known quantities, the uncertainty is determined through uncertainty propagation. There are several analytical and numerical methods to propagate uncertainty [50]. One simple approach is the use of first-order Taylor series approximation, obtained calculating the partial derivative of the different direct measurements ( $X_i = 1..N$ ) that take part in the calculation of an output ( $y$ ):

$$Y = f(X_1, \dots, X_N),$$

$$\Delta Y = \left( \sum_{i=1}^N \left( \left| \frac{\delta Y}{\delta X_i} \right| \Delta X_i \right) \right)^{1/2},$$

where  $\Delta Y_i$  can be expressed in terms of absolute uncertainty, relative, or standard uncertainty [51]. This alternative provides a simple mathematical expression to directly estimate uncertainty. Expressions for the uncertainty estimation of energetic and separation metrics of MED processes with this approach are available in Section ???. However, first-order Taylor series approximation has certain limitations, being the main one that it is not adequate for highly non-linear models, where a higher order Taylor expansion is required, or when uncertainties are far from the mean. Also, when working with complex models, as in the case of exergetic metrics, its expression can not be practically obtainable. For these cases, the recommended approach are numerical methods, specifically the Monte Carlo method [52], which despite its higher computational requirements does not have the aforementioned limitations [53].

[51]: nist (), "NIST Guidelines for Evaluating and Expressing the Uncertainty of NIST Measurement Results Cover"

[52]: (2008), JCGM101:2008. *Evaluation of Measurement Data — Supplement 1 to the "Guide to the Expression of Uncertainty in Measurement" — Propagation of Distributions Using a Monte Carlo Method*

[53]: Wolff (2007), "Monte Carlo Errors with Less Errors"

## 11.4 Monitoring and process control

### 11.4.1 Monitoring: steady-state identification

The evaluation of the system performance must be carried out when the plant is at steady state conditions, that is, when the mass and energy balances are in equilibrium and thus do not change with time; otherwise, erroneous results can be obtained. Steady-state conditions can be identified by observation by qualified and experienced plant operators. However, the use of automatic detection algorithms is recommended for experimental facilities where a wide range of operating conditions are involved. In this work, an automatic detection algorithm has been purposely developed and implemented to identify the steady state of the process. The methodology is based on the idea presented by M. Korbel [54] et al. and consists of combining an algorithm to detect anomalies, such as the wavelet transform [55, 56] (which allows detecting abrupt signal changes and distinguishing between high-frequency noise, transient states and steady states), with a trend detection method to identify smooth ramps as non-steady states. Whereas M. Korbel [54] et al propose a statistical trend detection approach, in this paper the derivative of the signal is used due to its simplicity (only one parameter, the threshold, must be established). A diagram of the steady-state detection procedure is shown in Figure 11.4, where three parameters are mainly required: wavelet transform threshold ( $y_a$ ), derivative threshold ( $y_d$ ) and time window duration ( $T_{ss}$ ). At each  $k$ -sample time, a new value is read, and the *Anomaly detection* algorithm is applied (in this case the wavelet transform). If the output is positive (true, no anomaly), the second step is to analyse the *Trend detection*. Only if all elements in the result vector are positive along  $T_{ss}$ , is the value considered to be at steady state (ss) conditions. As a final step, the *Global steady state evaluation* identifies a steady-state period if all the values of the  $N$  variables involved have been previously classified as ss.

[54]: Korbel et al. (2014), "Steady State Identification for On-Line Data Reconciliation Based on Wavelet Transform and Filtering"

[55]: Jiang et al. (2003), "Application of Steady-State Detection Method Based on Wavelet Transform"

[56]: Jiang et al. (2000), "Industrial Application of Wavelet Transform to the On-Line Prediction of Side Draw Qualities of Crude Unit"

[54]: Korbel et al. (2014), "Steady State Identification for On-Line Data Reconciliation Based on Wavelet Transform and Filtering"

### 11.4.2 Control system

Figure 11.2 shows the control loops to be implemented in an MED unit, whose subsystems and their control are described below:

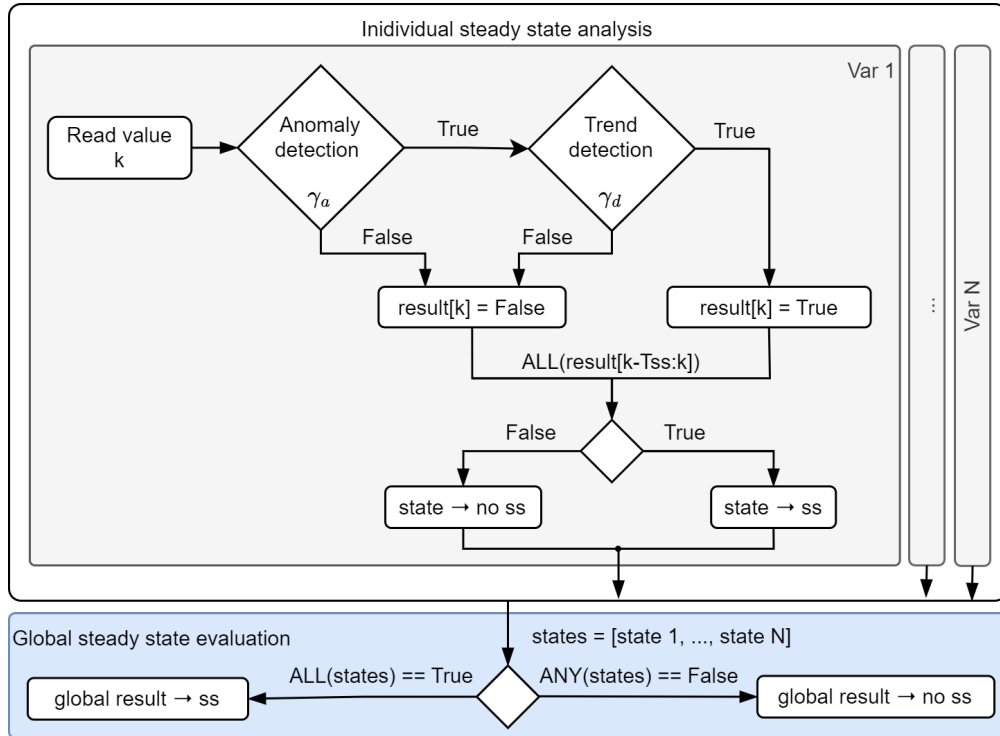


Figure 11.4: Diagram of the steady-state identification procedure

► **Heat source** (*Heat Source loop* in Figure 11.2). Both the inlet temperature (TT01) / pressure (PT03) and the flow rate of the heat source (FT01) must be controlled. It can be done either by direct control over the heat source obtaining heat under the required operating conditions or by performing a transformation. Depending on the heat source characteristics, this transformation involves:

For sensible heat sources, independent variation of temperature and flow rate can be achieved by means of: 1) a mixing three-way valve that mixes part of the return fluid, at temperature TT05, with the inlet fluid, at TT01 by acting over ZC01, the control signal for temperature regulation and; 2) flow (FT01) regulation by acting over the control signal SC01, which can be a Variable Frequency Drive (VFD) or valve. This decoupled regulation is shown in Figure 11.2, where ZC01 represents the control signal for temperature regulation. The flow rate regulation (FT01) is achieved by acting on the selected actuator (SC01), which can be a VFD or a valve<sup>10</sup>. For latent heat sources (steam), the pressure-flow-independent regulation is not possible since they are intrinsically coupled variables. In this case, a pressure regulator valve (ZC01) can be used to control either the flow rate (FT01) or the pressure (PT03).

► **Cooling** (*Cooling Loop* in Figure 11.2). The pressure inside the condenser (PT02) or the condenser outlet temperature (TT02) can be controlled by regulating the cooling flow rate (FT03), being the cooling water inlet temperature (TT04) a disturbance. This control loop (TIC02) consists in turn in two control loops (cascade control [57]), where an outer loop sets a reference flow rate value to achieve the desired condenser outlet temperature (or pressure), and an inner loop (not shown in Figure 11.2) acts on SC05 (VFD's frequency) to achieve the desired flow rate. Direct regulation of condenser outlet temperature using the VFD is also valid in case the measurement of the cooling flow rate is not available.

► **Brine extraction** (*Brine loop* in Figure 11.2). The brine level in the last effect

10: It should be noted that this decoupling is at the expense of energy losses in the mixing process

[57]: Åström et al. (1995), *PID Controllers: Theory, Design, and Tuning*

## 11.5 Methodology application in a high TBT experimental campaign at the pilot plant

(LT01), or in all effects if a parallel feed configuration is used, is controlled by the brine flow rate (see control loop LIC01 in Figure 11.2). In this case, the controller can act directly on the VFD frequency (SC03) to avoid the need for an additional flow meter.

- ▶ **Distillate extraction** (*Distillate loop* in Figure 11.2). As in the previous case, the distillate level (LT02) is controlled by acting on the control variable (SC04).
- ▶ **Feedwater** (*Feed loop* in Figure 11.2). The feed water flow rate is regulated by the FIC02 control loop, using a VFD (SC02) and a flow meter (FT02).

### A standard method for performance evaluation of thermal separation processes

1. Define the KPVs (Section 11.3.1)
2. Select the required performance metrics to be evaluated according to the application and type of energy source(s) (Section 11.1).
3. Define the required instrumentation of the KPVs and of any additional variables needed for the target performance metrics (Section 11.3.2).
4. Define the uncertainty associated with the measurement and that associated with the performance metric determination (Section 11.3.3).
5. Implement the required actuators and integrate them into a control system to ensure the stability of the plant operation (Section 11.4.2).
6. Identify a time window where stable operation is achieved (Section 11.4.1).

## 11.5 Case study: methodology application in a high TBT experimental campaign at the pilot plant

### Reminder: Performance of a thermal separator

The performance of a thermal process, such as MED, is dictated by the Carnot cycle [30], which sets the theoretical maximum efficiency for any heat engine. The efficiency of the Carnot cycle is limited by the temperature difference between the hot and cold sinks, which determine the amount of thermal energy that can be converted into useful (separation) work.

An approach to bring the MED closer to its thermodynamic limit can be achieved by raising the TBT, which allows to increase the number of effects [58] while maintaining an optimal temperature drop across them<sup>11</sup>. This leads to an improvement in the thermal performance of traditional desalination or an increase of the concentration factors that can be achieved, potentially enabling applications such as brine mining, introduced in Chapter 9 (Thermal desalination).

In practice, the TBT in the MED system is limited to 70°C. As shown in Figure 11.6, higher TBTs increase the risk of precipitation of divalent ions, which tend to form incrustations on the heat exchange surfaces. These deposits reduce heat transfer efficiency, as noted in [24]. For un-treated feedwater (Figure 11.6 - left) this risk of precipitation is present at almost any temperature due to its composition<sup>12</sup>. A nanofiltration pre-treatment<sup>13</sup> is used to selectively remove the divalent ions while leaving relatively unaffected the components to be separated in the MED process, *i.e.* NaCl. This allows the operation of MED processes at higher TBTs or higher feed concentration, with only severe scaling above 80°C and  $\approx 100$  g/kg as shown in Figure 11.6 - right.

To showcase the application and usefulness of the proposed methodology, a case study consisting on the application of the methodology to an experimental campaign at the SolarMED pilot plant is presented. The campaign was designed

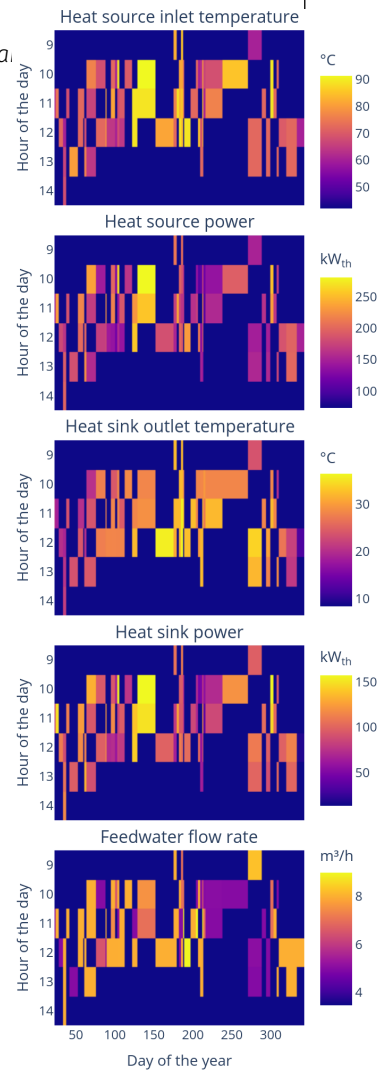


**Figure 11.5:** Visualization of the different process inputs values during the experimental campaign.



11: With limitations, on each effect a considerable exergy is destroyed. It has been shown that around XX effects is the limit ...

**Table 11.1:** RSI values and their interpretation in terms of scaling and corrosion risk [59].

RSI > 9	Severe corrosion
7.5 < RSI < 9	Heavy corrosion
7 < RSI < 7.5	Significant corrosion
6 < RSI < 7	Stable water
5 < RSI < 6	Moderate to light scaling
4 < RSI < 5	Severe scaling

12: Figure 11.6 - seawater in center bar plot

13: Figure 11.6 - pretreated water in center bar plot

to evaluate the performance of the MED process under different operating conditions (see Table 11.2 and Figure 11.5), with the aim of improving its thermal performance and assessing the feasibility of using higher TBTs.

### 11.5.1 Implementation results

**Table 11.2:** Experimental campaign design specifications

Variable	Unit	Range
$T_{s,in}$	°C	60-89
$q_s$	l/s	7-14
$T_{c,out}$	°C	20-40
$q_f$	m <sup>3</sup> /h	5-9
$w_f$	g/kg	40

The experimental facility at PSA is a complex system of considerable size for a pilot plant. It includes over 100 variables, between inputs and monitored outputs. Additionally, due to the large number of target operating points, each experimental campaign requires a significant number of test days. Achieving a valid steady state takes approximately 20–30 minutes, not including the transition time between operating points. On a good day, 3–4 stable operating points can be reached; on a bad day, due to for example unfavorable environmental conditions, none may be achieved. This makes the duration of experimental campaigns complex and extensive as illustrated in Figure 10.3, making it highly suitable for extensive subsystem automation. The following sections describe the implementation of the methodology, which is showcased in Figure 11.9 for one particular test and further discussed in the following.

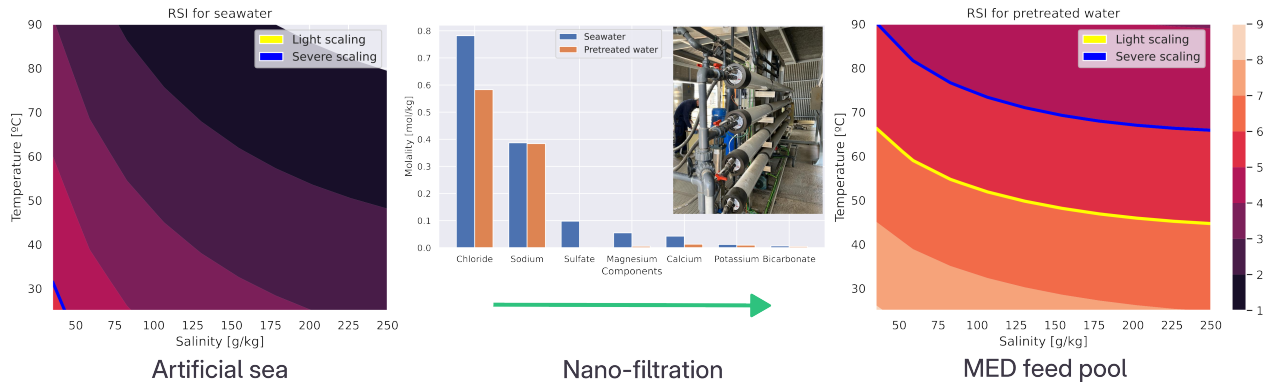


**Figure 11.6:** RSI values as a function of temperature and concentration before (left) and after (right) pre-treatment using nanofiltration.

### Monitoring and control system

**Finite state machines.** Each day of operation requires starting up and shutting down the system, making it a repetitive and sufficiently complex process that requires an experienced operator. Manual management of the process leads to errors that cause setbacks or, in the worst cases, premature failures in the facility: contamination of the condenser with brine due to erratic draining of the last effect, accumulation of scale on the surfaces of heat exchangers due to rapid cooling after shutdown, pumps cavitating because they are not stopped when the water flow at the intake ceases, etc. For this reason, two finite state machines have been implemented to manage the startup and shutdown of the facility. These have been designed to perform a sequence of operations that take the plant from an initial state to a final state following proper operating practices. A diagram of the process is shown in Figure 11.7.

The machines are responsible for managing the activation and deactivation of devices as well as controllers. Additionally, they set reference values for these based on a previously established configuration and evaluate whether the reference has been reached before proceeding to the next step. They also adjust certain parameters of the control system (level control) and restore the initial values once the task is completed.

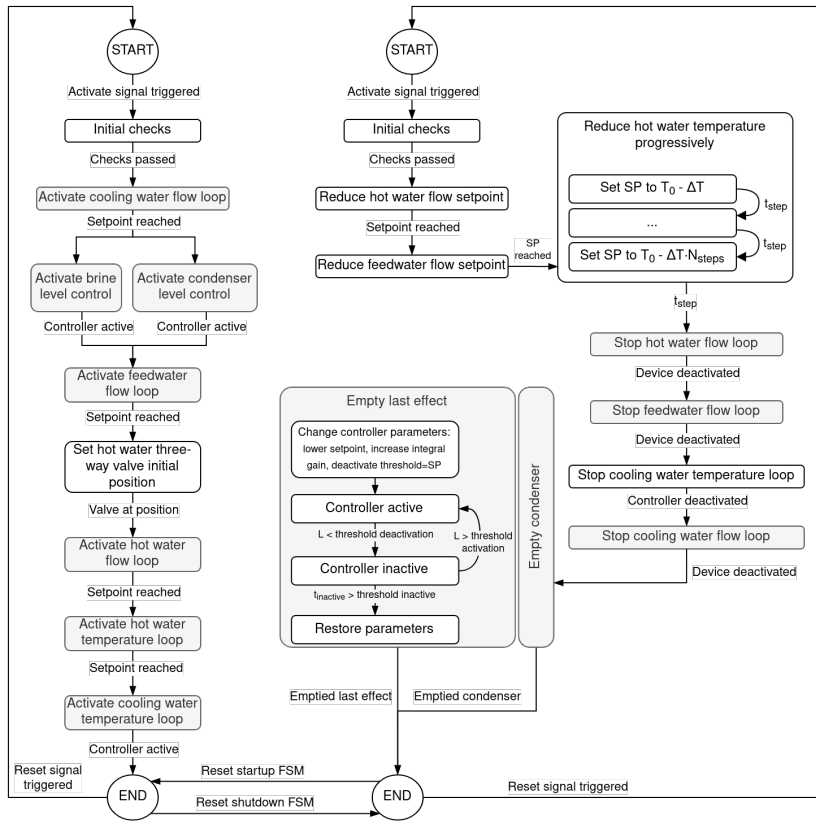
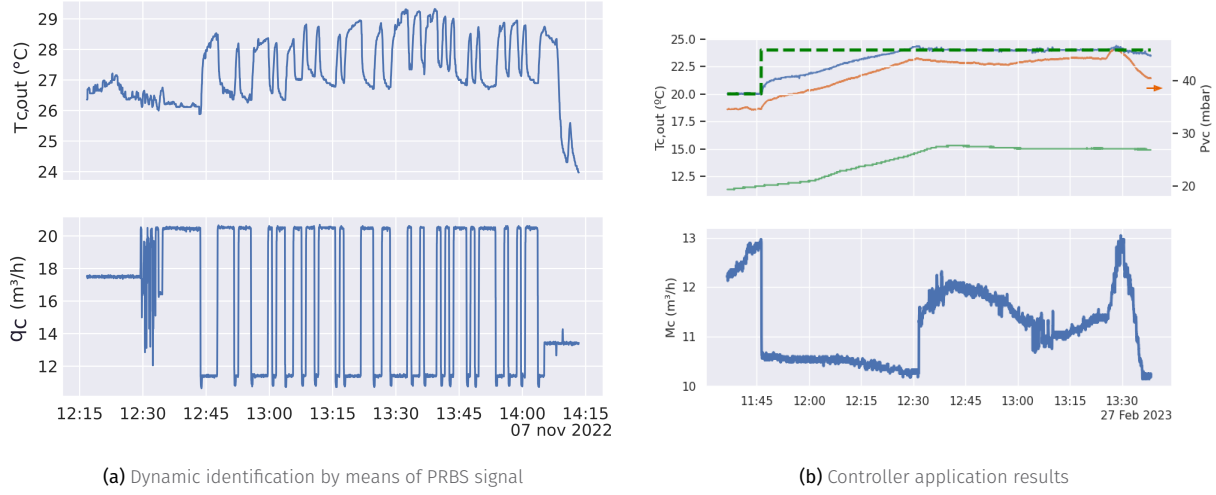


Figure 11.7: Flowchart of finite state machines for plant start-up (left) and shutdown (right)

In Figure 11.9 the activation sequence can be visualized at the beginning of the test (09:49–10:00): extractions → cooling → feedwater and heat source. The Flows are activated in about two minutes followed by another minute for the inlet temperature. Then the system is left to stabilize. At 09:52 the delay between activating the feedwater and it reaching the last effect is completed and the brine extraction pump starts operating. Pressures, temperatures and the distillate level in the system progressively evolve up to 10:00 when the conditions are changed for the first operation point for the day. The distillate level control action is delayed further until 10:04 when the first distillate is produced.

Regarding the shutdown procedure, the two most delicate processes are the cooling of the first effect (which has the highest scaling potential if not done properly) and the complete draining of the last effect and condenser. For the gradual cooling of the first effect, after the plant shutdown signal, the hot water temperature is reduced in 5-minute steps starting from the last recorded value until a final temperature of 50°C is reached. To drain the levels, a reference value well below the normal operating level is set, and the controller parameters are changed to more aggressive ones. Additionally, the device is deactivated each time the reference is reached and is not reactivated until the level reaches a specified value. This activation and deactivation process continues while the feedwater finishes draining from the upper effects of the plant. Once the control system has been deactivated for longer than a preset time, the plant shutdown procedure is considered complete, and the level controller parameters are restored.

This procedure can be observed in Figure 11.9 starting from 13:07. After a decrease in flow rates, the first effect heat load is progressively decreased until 13:34. From this time, pumps are stopped and the extraction cycles begin as can be noted by the high oscillations in the *Electrical consumption –  $J_b$*  and  *$J_d$*  and *Levels*.



**Figure 11.8:** Condenser outlet temperature controller implementation. On (b) the perturbation (inlet temperature) is shown with a solid-green line, while the output (condenser outlet temperature) is shown with a solid-blue line. The reference is a thick dashed-green line.

**Steady state identification.** The steady state identification algorithm has been implemented in the control system. It allows the automatic detection of stable operation points. This is done by monitoring the KPVs and applying the algorithm described in Section 11.4.1. In Figure 11.9, steady state periods are highlighted with a yellow background, which indicates that the algorithm has detected a stable operation point. Two are detected, the first one from 11:00 to 11:55 and the second one from 12:16 to 12:59.

**Control.** In terms of control, a Proportional-Integral-Derivative controller (PID) control has been implemented to effectively regulate and maintain the desired setpoints of the subsystems mentioned in Section 11.4.2. This approach enables the system to respond quickly to changes, minimize steady state errors, reject disturbances, and enhance overall performance and reliability. Figure 11.8 shows the development procedure for one of the main loops, the condenser outlet temperature control. To tune the controller, the system was excited with a Pseudo-Random Binary Sequence (PRBS) signal (a), obtaining an ARX model ( $n_a = 20$ ,  $n_b = 49$ ,  $n_k = 5$ , 96.38% fit) using the *System Identification Toolbox* from MATLAB, this allowed to extract an approximate first-order dynamic with which to tune the controller. Figure 11.8 (b) shows the controller performance for a particular test. Initially, the control signal ( $q_c$ ) increases to compensate for the trend observed in the condenser inlet temperature. At 11:45 the setpoint<sup>14</sup> is changed to 24 °C, to which the controller immediately adapts by decreasing its input and allowing the temperature to increase. The system progressively evolves towards the new setpoint, reached at 12:30 the controller then maintains the desired temperature compensating for other - not shown in the figure - disturbances. A similar situation can be observed in the showcased test of Figure 11.9 – Temperatures and Flows. For the first operation point (11:00 onwards), the continuously increasing inlet temperature ( $T_{c,in}$ ) is compensated by the controller, which increases the cooling flow rate to maintain the condenser outlet temperature at the setpoint. For the second operation point (12:16) the higher outlet temperature setpoint and turning on of the cooling tower allowing the inlet temperature to stabilize permits the controller to reduce the cooling flow rate and remain relatively unchanged.

14: i.e. reference

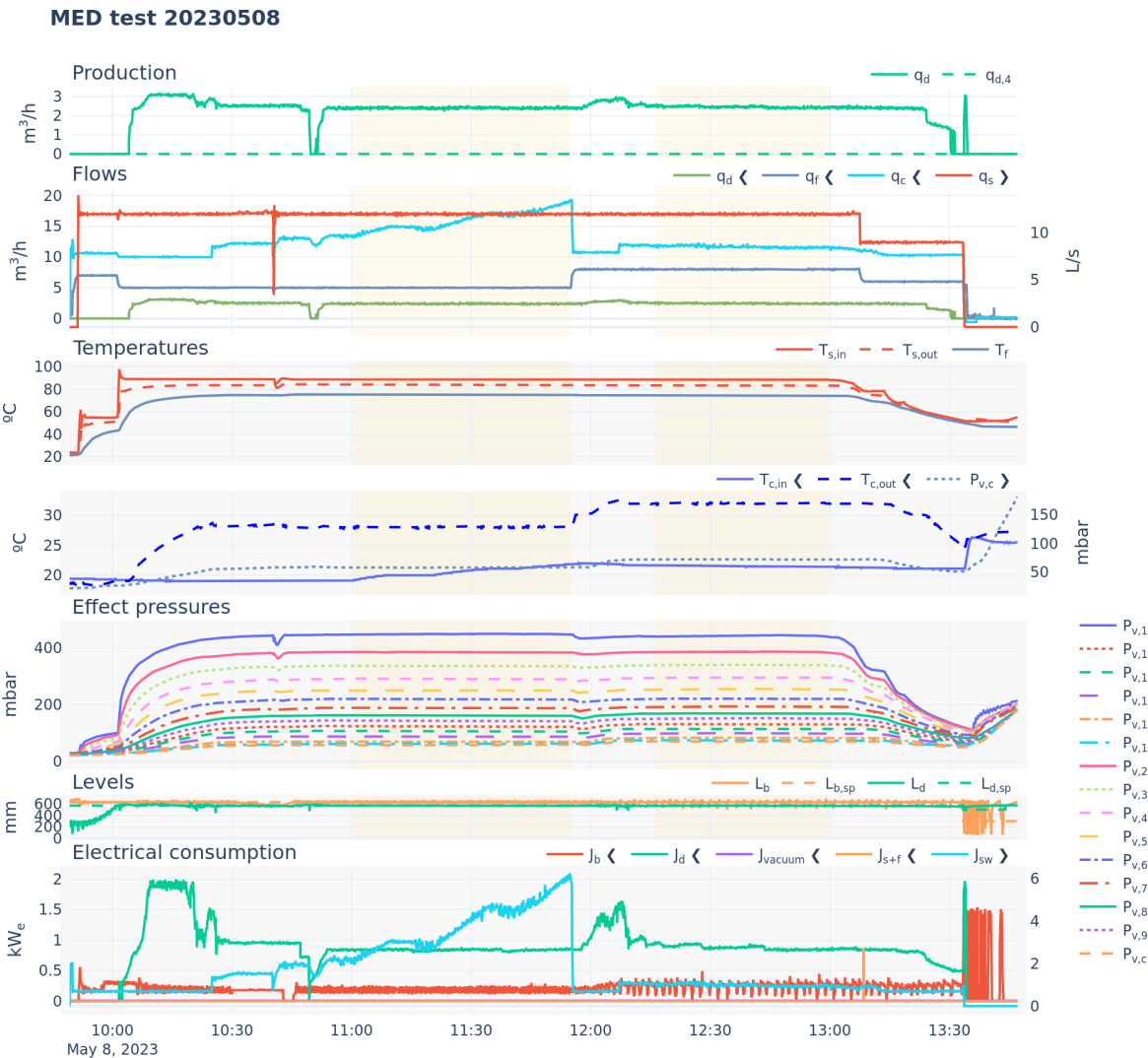


Figure 11.9: Test results. Several days available in interactive version



### Reproducibility and the effect of the steady state duration

The operation points pairs 1–2 and 3–4 in Table 11.3 are the same test, *i.e.* the same operating conditions, but performed on different days. Particularly for 1–2, the duration of the steady state is significantly different (16 and 76 minutes, respectively). The obtained performance metrics are similar, with almost identical values for the energetic and separation metrics. Slight differences, but still within the uncertainty margin are observed in metrics influenced by electrical consumption—which vary between tests due to differences in the cooling water inlet temperature: 17 (1) vs 13 (2)  $\text{m}^3/\text{h}$  for the cooling water flow rate, translates into a 0.3% difference in second law efficiency and 0.1  $\text{KWh}_e$  for SEEC. Inlet condenser temperature conditions are more similar in 3–4 (22.6 vs

**Table 11.3:** Measured variables and performance metrics for some operation points of the experimental campaign. The values are expressed as mean  $\pm$  standard deviation with a coverage factor of 2 (95% confidence interval).  $D$  is the duration of the steady state period.

	Test date (UTC)	D (min)	Performance metrics						
			GOR (-)	STEC (kW <sub>th</sub> )	SEEC (kW <sub>e</sub> )	RR (-)	RI (-)	$\eta_{II}$ (%)	SEXC (kWh <sub>ex</sub> /m <sup>3</sup> )
1	20230331 12:15	16	11 $\pm$ 1	60 $\pm$ 6	3.9 $\pm$ 0.2	29 $\pm$ 1	0.35 $\pm$ 0.02	8.0 $\pm$ 0.6	10.9 $\pm$ 0.8
2	20230418 12:22	76	11 $\pm$ 1	59 $\pm$ 6	4.0 $\pm$ 0.2	29 $\pm$ 2	0.35 $\pm$ 0.02	7.7 $\pm$ 0.6	11.3 $\pm$ 0.9
3	20230329 13:10	24	10.1 $\pm$ 0.7	66 $\pm$ 5	3.9 $\pm$ 0.2	30 $\pm$ 2	0.35 $\pm$ 0.02	6.9 $\pm$ 0.4	12.7 $\pm$ 0.8
4	20230414 12:51	27	10.2 $\pm$ 0.7	65 $\pm$ 5	3.9 $\pm$ 0.2	30 $\pm$ 2	0.36 $\pm$ 0.02	6.8 $\pm$ 0.4	12.8 $\pm$ 0.8
5	20230511 11:23	32	8.1 $\pm$ 0.4	81 $\pm$ 4	3.2 $\pm$ 0.2	44 $\pm$ 2	0.52 $\pm$ 0.02	4.6 $\pm$ 0.3	17.8 $\pm$ 0.9
6	20230414 11:49	18	11 $\pm$ 1	59 $\pm$ 5	3.8 $\pm$ 0.2	47 $\pm$ 3	0.56 $\pm$ 0.03	7.2 $\pm$ 0.5	11.9 $\pm$ 0.9
7	20230508 11:00	54	7.0 $\pm$ 0.4	93 $\pm$ 6	3.7 $\pm$ 0.2	48 $\pm$ 3	0.57 $\pm$ 0.03	3.9 $\pm$ 0.3	21 $\pm$ 1

	Measured variables										
	$T_{c,in}$ (°C)	$T_{c,out}$ (°C)	$q_s$ (L s <sup>-1</sup> )	$q_f$ (m <sup>3</sup> h <sup>-1</sup> )	$q_d$ (m <sup>3</sup> h <sup>-1</sup> )	$T_{s,out}$ (°C)	$T_{c,in}$ (°C)	$w_f$ (mS cm <sup>-1</sup> )	$w_d$ (μS cm <sup>-1</sup> )	$q_c$ (m <sup>3</sup> h <sup>-1</sup> )	J (kW)
1	64.0 $\pm$ 0.8	28.1 $\pm$ 0.6	12.0 $\pm$ 0.2	8.0 $\pm$ 0.1	2.4 $\pm$ 0.1	61.1 $\pm$ 0.7	24.5 $\pm$ 0.7	67.4 $\pm$ 0.7	8.00 $\pm$ 0.08	17 $\pm$ 1	(8.0 $\pm$ 0.2) $\times$ 10 <sup>3</sup>
2	64.0 $\pm$ 0.7	28.0 $\pm$ 0.6	12.0 $\pm$ 0.3	8.0 $\pm$ 0.1	2.3 $\pm$ 0.1	61.2 $\pm$ 0.7	23 $\pm$ 1	67.4 $\pm$ 0.7	8.00 $\pm$ 0.08	13 $\pm$ 2	(8.1 $\pm$ 0.2) $\times$ 10 <sup>3</sup>
3	68.0 $\pm$ 0.7	28.0 $\pm$ 0.6	12.0 $\pm$ 0.2	8.0 $\pm$ 0.1	2.4 $\pm$ 0.1	64.8 $\pm$ 0.7	22.6 $\pm$ 0.6	67.4 $\pm$ 0.7	8.00 $\pm$ 0.08	13.8 $\pm$ 0.8	(8.1 $\pm$ 0.2) $\times$ 10 <sup>3</sup>
4	68.0 $\pm$ 0.7	27.9 $\pm$ 0.8	12.0 $\pm$ 0.3	8.0 $\pm$ 0.1	2.4 $\pm$ 0.1	64.8 $\pm$ 0.6	21.4 $\pm$ 0.8	67.4 $\pm$ 0.7	8.00 $\pm$ 0.08	10.9 $\pm$ 0.9	(8.1 $\pm$ 0.2) $\times$ 10 <sup>3</sup>
5	88.9 $\pm$ 0.9	29 $\pm$ 1	12.0 $\pm$ 0.3	7.0 $\pm$ 0.1	3.1 $\pm$ 0.1	83.8 $\pm$ 0.9	22 $\pm$ 1	64.7 $\pm$ 0.6	8.00 $\pm$ 0.08	20.1 $\pm$ 0.3	(7.9 $\pm$ 0.3) $\times$ 10 <sup>3</sup>
6	68.0 $\pm$ 0.7	28.0 $\pm$ 0.5	12.0 $\pm$ 0.3	5.0 $\pm$ 0.1	2.4 $\pm$ 0.1	65.2 $\pm$ 0.7	20.8 $\pm$ 0.6	67.4 $\pm$ 0.7	8.00 $\pm$ 0.08	10.1 $\pm$ 0.4	(7.9 $\pm$ 0.3) $\times$ 10 <sup>3</sup>
7	89.0 $\pm$ 0.7	28.1 $\pm$ 0.6	12.0 $\pm$ 0.3	5.0 $\pm$ 0.1	2.4 $\pm$ 0.1	84.4 $\pm$ 0.8	21 $\pm$ 2	64.5 $\pm$ 0.7	8.00 $\pm$ 0.08	16 $\pm$ 3	(7.8 $\pm$ 0.3) $\times$ 10 <sup>3</sup>

21.4 °C), making differences for all metrics negligible.

Thus, it can be stated that the proposed methodology provides reproducible results and that the quality of stable operation and the ability to correctly identify it are of greater importance than the specific duration of the steady state.

## 11.5.2 Results analysis

In Table 11.3 operation points 4-5 and 6-7 compare low and high TBT operation. Two of them (4 and 6) receive heat at 68°C, while they differ in the feedwater flow rate ( $q_f$ ), one (4) with a higher value (8 m<sup>3</sup>/h) and the other (6) at a lower one (5 m<sup>3</sup>/h). The other two operation points receive heat at 89°C and similar feedwater flow rate<sup>15</sup>. The first two operation points result in an approximate TBT of 61.5°C while the last two operation points have an approximate TBT of 79.2°C. This operation points selection is made to compare the performance of the plant at low and high TBT operation with otherwise equivalent conditions.

**Performance analysis.** The first immediate observation is that contrary to what stated in the introduction, the performance of the plant does not improve with higher heat source temperatures, on the contrary it decreases: GOR -20% and -36% for the low (4-5) and high (6-7)  $q_f$  scenario, respectively. Results are even worse in terms of second law efficiency: -32% and -46%, respectively, since higher quality heat is being destroyed. In summary, more energy, of better quality is being consumed to produce distillate less efficiently

This can be explained by the fact that the increase in the heat source temperature is not taken advantage of by introducing more effects, which would provide the increase in efficiency.

On the other hand, the concentration achieved does increase significantly for the high  $q_f$  scenario, with a 47% increase in the recovery ratio. This is not the case for the low  $q_f$  scenario, where the recovery ratio is similar to the low temperature operation point. A possible explanation is presented hereinafter.

Using a physical model of the plant<sup>16</sup>, a better insight into the inner working of the plant can be obtained. The model is based on the energy and mass balances of the system, and it is used to estimate different outputs at the effect level, such as the temperature and pressure of the vapor, the distillate production, and the brine concentration. This allows to analyze the temperature and concentration

15: Equal between 4 and 5, slightly different but comparable between 6 and 7

comprobar números

16: See Section ??

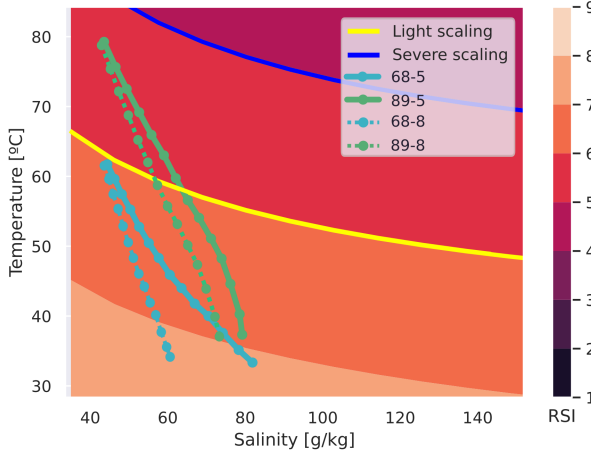


**Figure 11.10:** Temperature and concentration evolution for operation points at each effect in the MED plant. Surface represents the RSI.

evolution and visualize it as shown in Figure 11.10. According to the RSI, the high temperature operation points (5, 7) do get into the light scaling zone for the first 7 effects, while the low temperature operation points (4, 6) remain in the stable water zone for all effects.

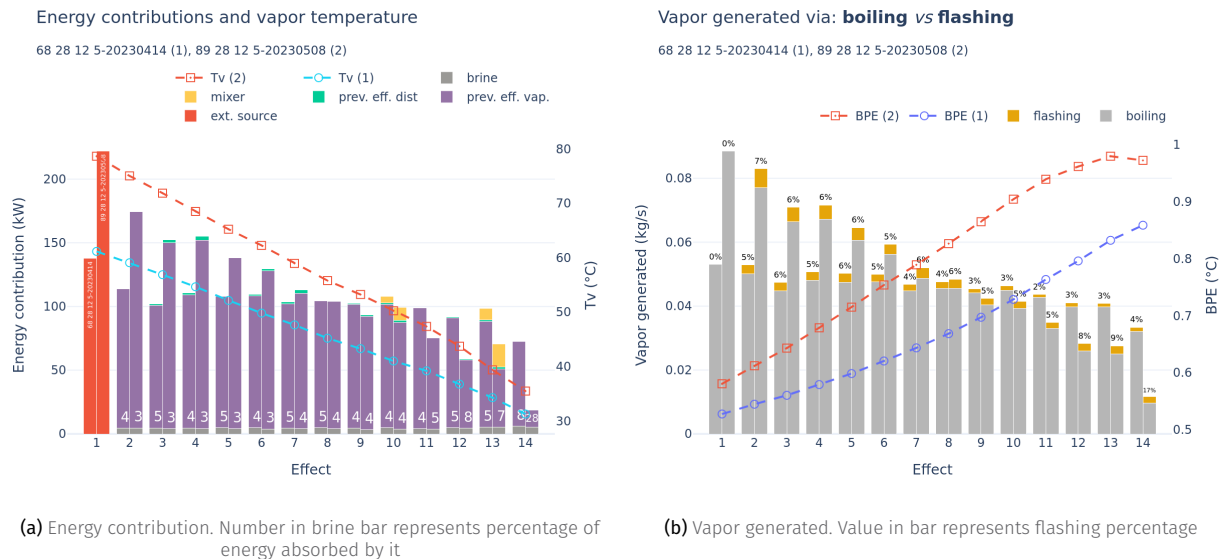


**Figure 11.11:** Per effect comparison between low and high TBT operation points

A per effect comparison can also be made in terms of energy contribution for vapor generation. This is shown in Figure 11.11 (a) for the low  $q_f$  scenario. In the first effect a stark difference between low and high operation can be seen, with almost double the power released, producing almost double the vapor (Figure 11.11 – (b)). However this difference is not maintained in the following effects, but an opposite trend is observed. Effect 8 is the crossing point and from there on the low temperature operation point produces more vapor. Another interesting comparison is the mixer energy contribution, the higher temperature of the distillate produced in the first effects becomes a significant contributor in the later effects, with a greater impact compared to the low temperature operation. Thus, distillate distribution is more effective when total plant temperature

differences are higher.

An explanation as to why vapor generation seems limited and thus the achieved concentration, can be the Boiling Point Elevation (BPE) of the brine (see Figure 11.11 (b)), which is a function of temperature and concentration, increasing with the latter. This means that the temperature difference between the brine and the vapor is reduced, and, which in turn reduces the boiling driving force. In the visualized case, the final BPE value for the low-temperature operation is reached by effect 9 of the high temperature one. In an MED plant, the vapor generated in the previous effect is the driving force for the next effect (Figure 11.11 – (a)), low vapor production on one effect means a diminished force for heat transfer in the next one, which in turn reduces the vapor production on that effect. It is an exponential decay process. That is why despite the larger energy availability in the first effects, the better balanced effects of the low temperature operation turns out to ultimately produce similar levels of separation [60].

[60]: Lienhard V (2019), "Energy Savings in Desalination Technologies"

In this figure, it can be seen than flashing takes a more relevant role in vapor generation in the latter effects of the high temperature alternative, since it is not affected by BPE (8,9 and 17% of the total vapor generated in effects 12, 13 and 14, respectively). This indicates that maybe flashing is a good alternative to increase the vapor production in the latter stages of a thermal brine concentrator plant.

**Remark 11.5.1** A MED-MSF hybrid could be a good alternative to increase the brine concentration in the last effects, where the vapor production is limited by the BPE. Another option worth exploring is variable geometry effects, in order to increase temperature differences and maintain vapor production at higher concentrations.

17: Section 14 (Reproducibility and the effect of the steady state duration)

**Scaling assessment.** To assess whether scaling occurred during high-temperature operation, control tests were conducted both before the high-temperature tests and repeated after about 30 hours of operation. In Table 11.3 the same operation points used to validate the reproducibility<sup>17</sup>, i.e.: 1-2 and 3-4 can be used to draw conclusions. Aside from the mentioned differences in metrics influenced by electrical consumption, the performance metrics values are consistent across tests, suggesting that the system is operating efficiently without significant fouling or scaling.

Incluir una gráfica de los coeficientes de transferencia para ambos tests?

## 12.1 Introduction

The behavior of the SolarMED process is controlled by acting on two components, a continuous and a discrete one, described Section 12.2 (Dynamic modelling. Process variables) and Section 12.3 (Discrete modelling. Operation state), respectively. Then, they are combined to create a complete model of the SolarMED process.

- ▶ Operation state.
- ▶ Process variables. Regulates the continuous-dynamic behavior of the process. Specifically, two recirculation flow rates for the sfts subsystem, five flow and temperature variables for the MED.

## 12.2 Dynamic modelling. Process variables

The dynamic behavior of the SolarMED regulates the values of the different process variables. This behaviour is modelled by integrating a set of models for each component of the SolarMED system.

Even though this modelling component models the dynamic behavior of the system, many of the models described in the following sections are steady-state models. This can lead to discrepancies between the model predictions and the actual system behavior, particularly during transient events. However, this is not deemed a significant limitation since the model is intended to be used for an optimization approach where the model sample rate is in the order of minutes, and inputs for slower component dynamics are changed sparingly, typically starting from 30 minutes and above, more than enough time for the system to reach steady state.

### 12.2.1 sf

The solar field is basically a converter of electrical to thermal energy dependent on the irradiance availability. The two main outputs, in terms of operation of the solar field, are the conversion factor ( $kW_e/kW_{th}$ ) and the temperature the heat is obtained.

The diagram illustrates the individual loops that make up the field. In the model, it is assumed that all loops have equal flow rates and temperatures (*i.e.*, a balanced flow distribution). As a result, the system can be simplified to a single loop with a collector area equal to the sum of the areas of the individual loops.

A first-principles based on the one presented in Ampuño et al. [61] is used to model the solar field. The model has two types of parameters: dynamic and constant. The dynamic parameters are the thermal loss coefficient ( $H \left( \frac{J}{s \cdot C} \right)$ ) and the collector efficiency factor ( $\beta(m)$ ), which are calibrated based on experimental data. The constant parameters are the ones defined in

12.1	Introduction	63
12.2	Dynamic modelling	63
12.2.1	sf	63
12.2.2	Thermal storage	66
12.2.3	Heat exchanger	66
12.2.4	MED	67
12.2.5	Other components	68
12.3	Discrete modelling	68
12.3.1	Heat generation and storage subsystem (sfts)	68
12.3.2	Separation subsystem (med)	68
12.4	Complete system model	68
12.4.1	Validation	69

[61]: Ampuño et al. (2018), “Modeling and Simulation of a Solar Field Based on Flat-Plate Collectors”

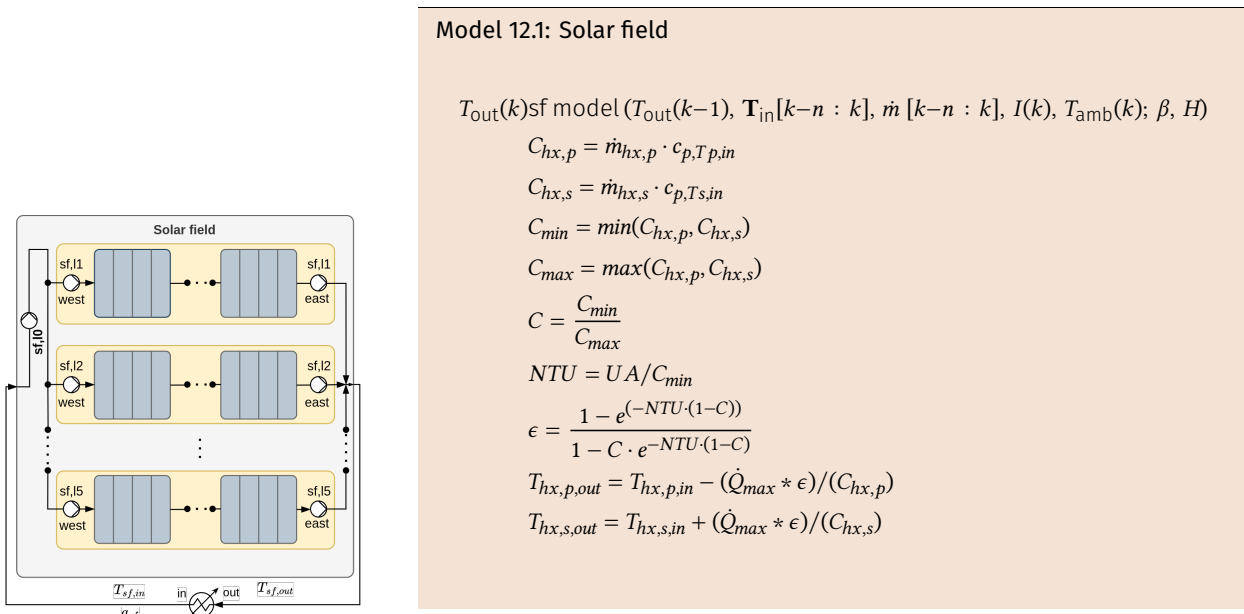


Figure 12.1: Solar field process diagram.

[62]: Ampuño et al. (2019), "Apparent Delay Analysis for a Flat-Plate Solar Field Model Designed for Control Purposes"

1: Transport delays are a common feature in dynamic systems, where the response of the system to an input is not instantaneous, but rather delayed by a certain amount of time. This delay can be caused by various factors, in this particular system, is due to the time it takes for the water to flow through the solar field and reach the temperature sensors.

[63]: Normey-Rico et al. (1998), "A Robust Adaptive Dead-Time Compensator with Application to A Solar Collector Field"

2: observe the trend in Figure 12.2 - Temperatures

3: In Figure 12.2, from 20240927 07:35 to 08:20

The main difference with respect to the model presented in is how the apparent transport delay is handled [62]<sup>1</sup>. In this implementation, the transport delay is simplified to a single parameter based on the work presented in Normey-Rico et.al [63].

### Electrical consumption

**Definition 12.2.1 Step train test.** Variations in the VFD pump speed from a minimum to a maximum value, with fixed increments.

The AQUASOL solar field is composed by a set of pumps that recirculate the water through the solar field. The pumps are controlled by VFDs that allow to vary the flow rate through the solar field. A main recirculation pump ( $P_{l0}$ ) is responsible for the primary flow, while additional pumps ( $P_{l1}, P_{l2}$ , etc.) are used in the individual loops to either increase the total flow rate or to operate with the isolated loop. This redundancy means that the same flow rate can be achieved with different pump configurations.

Then, prior to modelling the electrical consumption of the solar field, a prior step is to characterize the electrical consumption of the system. This is done by determining the relationship between flow rate and power consumption for every configuration and to find the best configuration, that is, the one that minimizes the electrical consumption across the range of flow rates that the solar field operates at.

In order to characterize the electrical consumption of the solar field, a series of tests were performed as can be seen in Figure 12.2. The tests were carried out in two different dates since they have to be performed early, before the solar field is irradiated by the sun and the field heats up<sup>2</sup>. In the first day, step trains are applied to the main loop and individual isolated loops (20240925 07:15 - 08:30). On the second day, different speeds levels were set for the main recirculation pump (10% - 100%, 10% increments) while step trains were applied to the individual loops (40% - 100%, 20% increments)<sup>3</sup>.

Figure 12.3 shows the relationship between flow rate and power consumptions for different configuration and pump speeds. Up to 90 l/min the best configuration

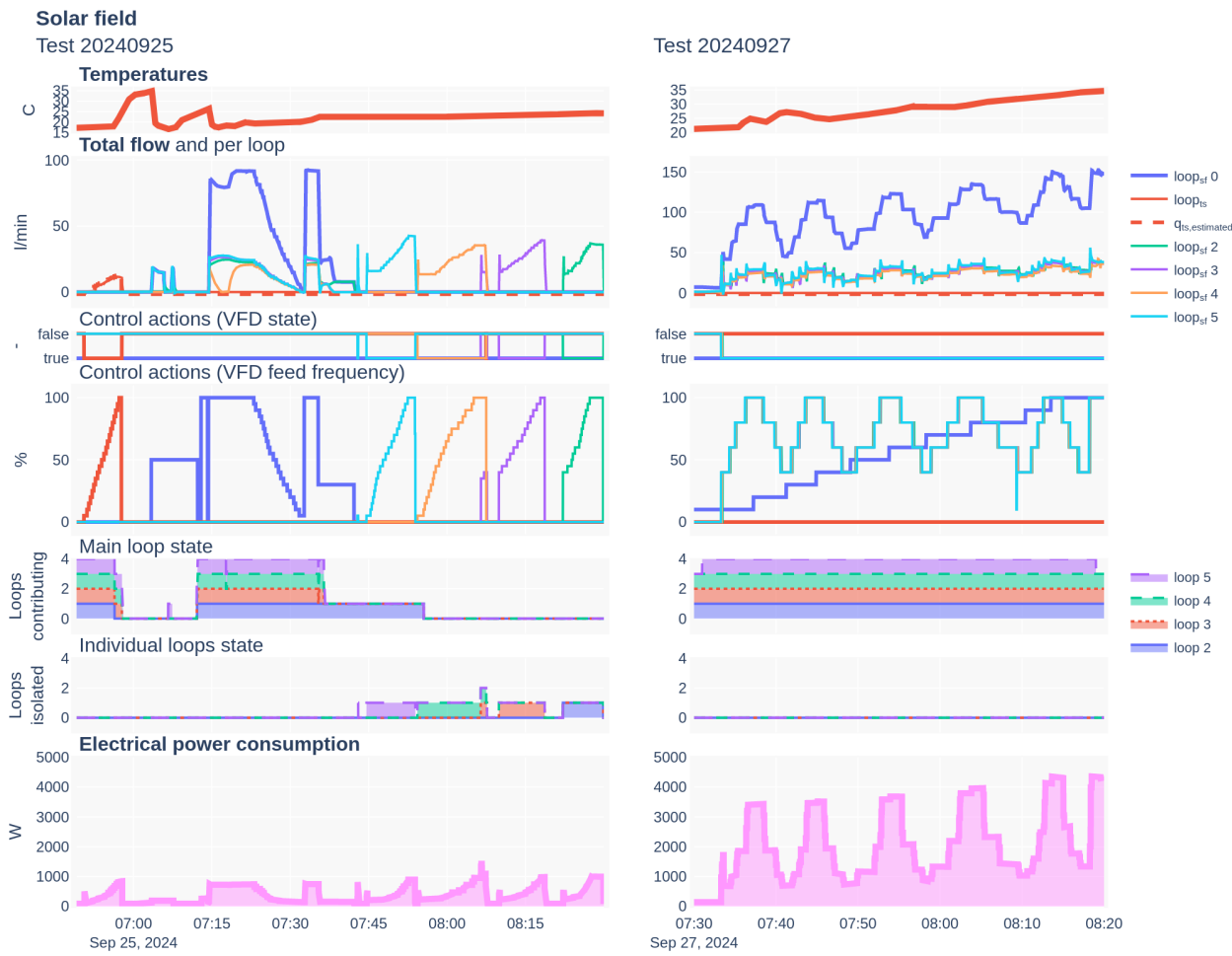


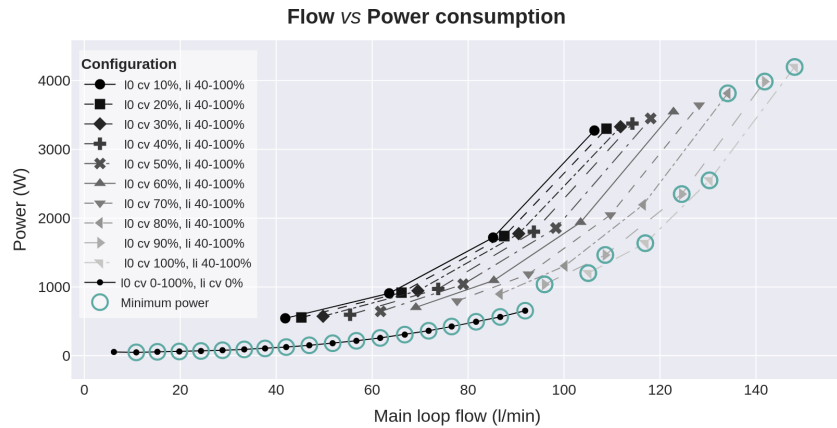
Figure 12.2: Solar field and thermal storage electrical characterization tests.



is to just use the main recirculation pump. Above this flow rate, the main pump is used in combination with the individual loops. First a combination of main pump from 85 to 100% and individual loops at their 40% minimum speed, then the main pump at 100% and individual loops at increasing values up to 100%. With this selection, a two degree order polynomial regression is fitted to the data, as shown in Figure ??.

Summarizing, the electrical consumption of the solar field is modelled as a function of the flow rate through the solar field from a minimum value of XX m<sup>3</sup>/h to a maximum value of YY m<sup>3</sup>/h. This is achieved as a result of the combination of the main recirculation pump and the individual loops.

**Figure 12.3:** Solar field flow for different pump configurations and their associated power consumption.



### Validation

#### 12.2.2 Thermal storage

### Electrical consumption

### Validation

#### 12.2.3 Heat exchanger

The solar field and thermal storage are interfaced by a Heat Exchanger (hex), particularly a counter-flow heat exchanger. The component is modelled using a first-principles steady state model based on the effectiveness-NTU method[64, 65].

[64]: Çengel et al. (2015), *Heat and Mass Transfer*

[65]: Kays et al. (1958), *Compact Heat Exchangers*

Modelling considerations [64]:

- ▶ It has been assumed that the rate of change for the temperature of both fluids is proportional to the temperature difference; this assumption is valid for fluids with a constant specific heat, which is a good description of fluids changing temperature over a relatively small range. However, if the specific heat changes, the Logarithmic Mean Temperature Difference (LMTD) approach will no longer be accurate.
- ▶ It has also been assumed that the heat transfer coefficient ( $U$ ) is constant, and not a function of temperature.
- ▶ No phase change during heat transfer.
- ▶ Changes in kinetic energy and potential energy are neglected.

### Model 12.2: Heat exchanger

$$T_{hx,p,out}, T_{hx,s,out} = \text{hx model}(T_{hx,p,in}, T_{hx,s,in}, \dot{m}_p, \dot{m}_s, T_{amb}, (UA)_{hx}, H)$$

$$C_{hx,p} = \dot{m}_{hx,p} \cdot c_{p,Tp,in}$$

$$C_{hx,s} = \dot{m}_{hx,s} \cdot c_{p,Ts,in}$$

$$C_{min} = \min(C_{hx,p}, C_{hx,s})$$

$$C_{max} = \max(C_{hx,p}, C_{hx,s})$$

$$C = \frac{C_{min}}{C_{max}}$$

$$NTU = UA/C_{min}$$

$$\epsilon = \frac{1 - e^{(-NTU \cdot (1-C))}}{1 - C \cdot e^{-NTU \cdot (1-C)}}$$

$$T_{hx,p,out} = T_{hx,p,in} - (\dot{Q}_{max} * \epsilon) / (C_{hx,p})$$

$$T_{hx,s,out} = T_{hx,s,in} + (\dot{Q}_{max} * \epsilon) / (C_{hx,s})$$

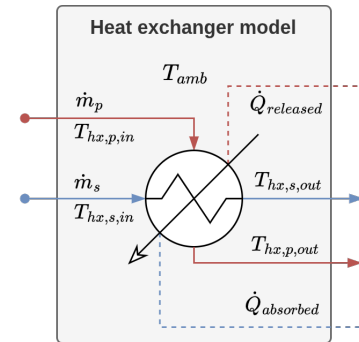


Figure 12.4: Heat exchanger process diagram.

Where  $p$  references the primary circuit (solar field side) and  $s$  the secondary circuit (thermal storage side). As shown in the Model 12.2, first the heat capacity  $C$  is determined in order to calculate the effectiveness ( $\epsilon$ ) of the heat exchanger. Finally, after determining the maximum heat transfer rate ( $\dot{Q}_{max}$ ), the outlet temperatures can be obtained.

### Validation

In order to calibrate the two parameters of this model ( $UA$  and  $H$ ), one experimental test used where the parameters are varied in order to minimize the error between the model and the experimental data. The obtained values are shown in Table ?? and the dynamic behavior of the model is shown in Figure ???. It can be seen than the model performs fairly well even in transient conditions, with a mean absolute error of XX% and a coefficient of determination  $R^2$  of YY%.

Several more tests are evaluated and the performance obtained is shown in Table ???. On average, the model has a mean absolute error of XX% and a coefficient of determination  $R^2$  of YY%. The model is able to predict the outlet temperatures of the heat exchanger with a good accuracy, even in transient conditions, which is a good indication of the model's reliability.

### 12.2.4 MED

The MED is modelled statically, that is, considering that changes in the system operating conditions happen at a slow enough rate that the dynamic behavior between stable states can be neglected, and thus, only those stable states are considered. The model is a data driven one, specifically an ANN that has been trained with data from an experimental campaign in the pilot plant<sup>4</sup>.

4: Referencia a donde se mencione o algún artículo de Patricia

## Electrical consumption

### Validation

#### 12.2.5 Other components

##### Three-way valve

## 12.3 Discrete modelling. Operation state

The second modelling component defines the discrete state of the system, that is, its *operation state*. This component is modelled by means of FSMs.

### Reminder: FSMs

A finite state machine is a model of behavior composed of a finite number of states and transitions between those states. Within each state and transition some action can be performed<sup>a</sup>.

<sup>a</sup> See Section 2.6 (Hybrid modelling by means of FSMs) for a more detailed description.

The complete system is divided into two subsystems: the heat generation and storage subsystem and the separation subsystem.

### 12.3.1 Heat generation and storage subsystem (**sfts**)

This subsystem encompasses the **sf** and the Thermal Storage (**ts**). The subsystem can be modelled with a simple FSM as shown in Figure ??, where the states are defined based on whether water is being recirculated in each circuit. Four states are defined as shown in Table 12.1.

### 12.3.2 Separation subsystem (**med**)

## 12.4 Complete system model

Aquí describir cómo se combinan los componentes en función del estado del sistema y cómo ello depende de las máquinas de estado finito.

To refer to the operational state of the system, a three digit number is used, where the first two digits represent the **sfts** state and the last one the **med** state. For example, the state **005** represents an inactive **sfts** subsystem with an active **med**. **101** represents a warming-up solar field while vacuum is being generated in the MED system.

Hello, here is some text without a meaning. This text should show what a printed text will look like at this place. If you read this text, you will get no information. Really? Is there no information? Is there a difference between this text and some nonsense like “Huardest gefburn”? Kjift – not at all! A blind text like this gives you information about the selected font, how the letters are written and an impression of the look. This text should contain all letters of the alphabet and it should be written in of the original language. There is no need for special content, but the length of words should match the language. Hello, here is some text without a meaning. This text should show what a printed text will look like at this place. If you read this text, you will get no information. Really? Is there no information? Is there a difference between this text and some nonsense like

**Table 12.1:** **sfts** FSM states definitions.  $\wedge$  represents the logical AND operator and  $\forall$  represents that all meet the condition.

State	Name	Condition
0	Off	$\forall q == 0$
1	Generating vacuum	$med_{vac} == 2$
2	Idle	$\forall q == 0 \wedge med_{vac} == 1$
3	Starting-up	$\forall q > q \wedge med_{vac} \geq 1 \wedge \forall T > T$
4	Shutting down	$\exists q < q$
5	Active	$\forall q > q \wedge med_{vac} \geq 1 \wedge \forall T > T$

"Huardest gefburn"? Kjift – not at all! A blind text like this gives you information about the selected font, how the letters are written and an impression of the look. This text should contain all letters of the alphabet and it should be written in of the original language. There is no need for special content, but the length of words should match the language.

### 12.4.1 Validation

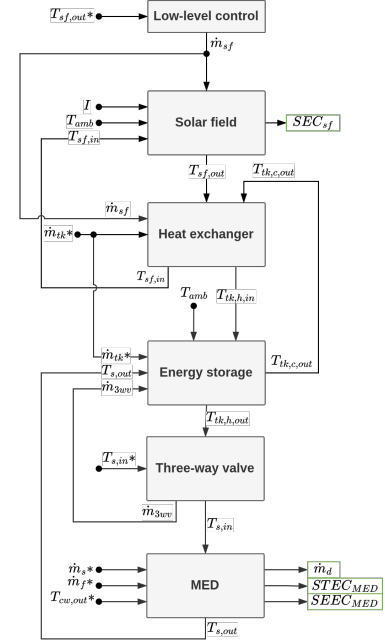


**Figure 12.5:** Complete SolarMED model architecture. TODO: Needs to be updated



## TL;DR

This chapter describes a method to develop an operational strategy enabling the seamless integration of a solar driven MED system in an autonomous and optimal manner, including decisions on when to start or stop each subsystem and how to regulate them during operation.

The method is based on a hierarchical control approach consisting of three layers, where the upper operation plan solves a MINLP problem. Results for a week long simulation of the system are compared against two alternative strategies: a baseline operation and only operation optimization strategies show that the proposed method is able to significantly increase the water production by XX % by taking full advantage of the solar resource and flexibility of the thermal storage.

13.1	Introduction . . . . .	71
13.2	Problem description . . . . .	71
13.2.1	Implementation discussion .	72
13.3	Proposed strategy . . . . .	74
13.4	Operation Plan Layer Description . . . . .	75
13.4.1	Candidate problems generation	75
13.4.2	Update times generation . .	75
13.5	Operation optimization layer description . . . . .	77
13.6	Optimization results . . . . .	78
13.6.1	Choosing an algorithm . . . .	78
13.6.2	Choosing a candidate problem	78
13.6.3	Simulation results . . . . .	79
13.6.4	Performance comparison with alternative strategies . . . . .	81

## 13.1 Introduction

LRoca, Carballo, Juan Diego

## 13.2 Problem description

The behavior of the SolarMED process is controlled by acting on two components, a discrete (operation state) and a continuous one (process variables).

The goal is to design an operational strategy that enables the seamless integration of both subsystems in an autonomous and optimal manner, including decisions on when to start or stop each subsystem and how to regulate them during operation. Therefore, considering the whole system as a MINLP optimization problem<sup>1</sup> that aims to maximize the water production while minimizing the (electrical) consumption of the system. Decisions on when to operate the system are weighted considering an optimization horizon, approximating the operation strategy of the system to the optimum:<sup>2</sup>

### Problem: SolarMED

$$\min_{\mathbf{x}, \mathbf{e}; \theta} J = f(\mathbf{x}, \mathbf{e}; \theta) = \sum_{i=1}^{n_{steps}} (J_{e,i} - J_{w,i})$$

with:

for  $i = 1 \dots n_{steps}$  :

- $J_{w,i} = q_{d,i} \cdot P_{w,i}$  if valid operation else 0
- $J_{e,i} = C_{e,i} \cdot P_{e,i}$
- $q_{d,i}, C_{e,i}$ , valid operation = solarmed model( $x_{c,i}, x_{p,i}, \dots$ )

- Decision variables

$$\mathbf{x} = [\mathbf{med}_{mode}, \mathbf{sfts}_{mode}, \mathbf{qsf}, \mathbf{qts,src}, \mathbf{qmed,s}, \mathbf{qmed,f}, \mathbf{T}_{med,s,in}, \mathbf{T}_{med,c,out}]$$

1: See Section 5.2 (MINLP problems)

2: In general  $q$  represents flow rates while  $T$  are temperatures. Figure 10.1 can be consulted for subscript reference.

$\forall i = 1 \dots n_{steps}$  is a notation to indicate that a condition must be held at every step  $i$  in the optimization horizon ( $n_{steps}$ ).  
Bold variables represent vectors.

where  $\mathbf{x}_{nx \times \sum n_{updates,xi}} = [x_{1,i}, \dots, x_{1,n_{updates,x_1}}, \dots, x_{n_x,n_{updates,x_{n_x}}}]$

- ▶ Environment variables

$$\mathbf{e} = [\mathbf{I}, \mathbf{T}_{\text{amb}}, \mathbf{P}_e, \mathbf{P}_w]$$

where  $\mathbf{e} = [e_{1,1}, \dots, e_{1,n_{steps}}, \dots, e_{n_e,n_{steps}}]$

- ▶ Fixed parameters ??

$$\theta = [R_p = 1, R_s = 0, \omega_{dc} = 0]$$

subject to:

- ▶ Box-bounds

- $\text{med}_{\text{mode}} \in [0, 1] \subset \mathbb{Z}$
- $\text{sfts}_{\text{mode}} \in [0, 1] \subset \mathbb{Z}$
- $q_{sf} \in [q_{sf}, \bar{q}_{sf}] \subset \mathbb{R}$
- $q_{ts,src} \in [q_{ts,src}, \bar{q}_{ts,src}] \subset \mathbb{R}$
- $q_{med,s} \in [q_{med,s}, \bar{q}_{med,s}] \subset \mathbb{R}$
- $q_{med,f} \in [q_{med,f}, \bar{q}_{med,f}] \subset \mathbb{R}$
- $T_{\text{med,s,in}} \in [T_{\text{med,s,in}}, \bar{T}_{\text{med,s,in}}] \subset \mathbb{R}$
- $T_{\text{med,c,out}} \in [T_{\text{med,c,out}}, \bar{T}_{\text{med,c,out}}] \subset \mathbb{R}$

valid operation conditions,  $\forall i = 1 \dots n_{steps}$ :

- ▶  $T_{sf,out} \leq \bar{T}_{sf,out}$

Where the objective is to minimize the cumulative cost of operation ( $J$ ). Fresh water ( $q_{med,d}$ ) sold ( $J_w$ ) at price  $P_w$  is the negative term while electrical consumptions ( $C_e$ ) at price  $P_e$  make up the positive cost term ( $J_e$ ). The benefit ( $B$ ) of operation is simply the inverse of the cost of operation.

The environment is represented by the vector  $\mathbf{e}$ , which includes the global solar irradiance ( $\mathbf{I}$ ), ambient temperature ( $\mathbf{T}_{\text{amb}}$ ), and the prices of water ( $\mathbf{P}_w$ ) and electricity ( $\mathbf{P}_e$ ).

The decision vector  $\mathbf{x}$  is composed of the decision variables for both the discrete and the continuous space. Two decision variables are defined to manipulate the discrete state of each subsystem defined in Section 12.3:  $\text{med}_{\text{mode}}$  and  $\text{sfts}_{\text{mode}}$ . These binary ( $\subset \mathbb{Z}$ ) variables establish whether the particular subsystem is active ( $x_i = 1$ ) or inactive ( $x_i = 0$ ). This is directly related to the operation state of the particular subsystem<sup>34</sup> and accounted for in the models by the integrated finite-state machines as explained in Section 12.3. For the continuous space, the decision variables include the ones that define the operating conditions (i.e. operation point) of the MED system, and the two recirculation flow rates that determine the conditions of the heat source ( $q_{sf}, q_{ts,src}$ ).

3: As defined in Tables 12.1 and 12.2

4: Once the values for these decision variables are provided, the low-level control layer is in charge of safely transitioning between operation states e.g.  $\text{med}_{\text{mode}} : 0 \rightarrow 1$ , med state: off → generating vacuum → starting-up → active

### 13.2.1 Implementation discussion

#### On the constraint handling

The reader might notice that no constraints are explicitly defined in the problem definition. This is because the constraints are implicitly defined in the model equations, which are used to evaluate the objective function. This design decision is motivated to avoid the need for a constraint-handling capable optimization algorithm, limiting the choice for an already complex MINLP problem<sup>5</sup>. Specifically, two aspects demand further consideration:

5: See Section 5.3 (A discussion on constraint handling) for a more detailed discussion on the topic

1. The decision value for the MED outlet condenser temperature ( $T_{med,c,out}$ ) is not a direct input to the system, but rather a setpoint to be followed by a low-level control loop by manipulating the cooling water flow rate ( $q_{med,c}$ ). This input might saturate and thus not be able to achieve the desired setpoint. In this case, a new value for the decision variable is computed, which is the minimum value that can be achieved (with  $\overline{q_{med,c}}$ ).

In this case, the value used in the SolarMED and the output from the optimization to the low-level control layer would be the validated value for  $T_{med,c,out}$ . No additional actions are needed.

2. In the solar field, in order to not constantly interrupt the evaluation due to the solar field temperature going above  $\overline{T}_{sf,out}$  (120 °C), the model saturates this temperature when going above and sets a flag. The limitation of this approach is that when there is low energy demand from the load, and likely because it favors energy transfer in the heat exchanger<sup>6</sup>, the optimizer tends to minimize the solar field flow, and systematically lets the solar field outlet temperature reach the limit. To avoid this situation, the positive term of the objective function is nullified in iterations where the constraint is not met.

Here, in order to ensure *valid operation* the fitness function is manipulated to de-incentivize decision variable values that lead to unfeasible operation.

<sup>6</sup>: greater temperature difference in primary side instead of greater mass flow rate with its associated increase in pumping power

### On the prediction horizon

The problem is designed as an optimization problem with a shrinking horizon. The horizon size should be large enough so that decisions on how to operate the system are made with perspective, taking into account how they will affect the system in the future, but not so large that current decisions have no impact on the far future, and making the problem dimensionality become unmanageable.

For this case study, this parameter should be chosen based on the hours of capacity of the thermal storage to operate the MED system.

The thermal storage capacity is XXX which allows the system to operate with no supply from the solar field for up to XX hours. This means that depending on the charge state of the thermal storage, the system could start operation independently of the irradiance conditions, or operate at different levels of temperature. Considering this the optimization horizon, in time units, chosen was 36 hours. This means that if the optimization is evaluated at 5:00 on day 1, the fitness function is evaluated until 19:00 of day 2 *i.e.* including the end of operation for day 2.

#### Reminder: Shrinking horizon optimization

An optimization where the horizon end is fixed, and as time progresses, the start of the horizon moves forward.<sup>9</sup>

<sup>9</sup> See Chapter 5 (Optimization overview)

### On solving the optimization problem

Solving the optimization problem for this MINLP formulation presents significant challenges due to the combinatorial nature of the integer decision variables [66]. As shown in Figure 13.1, each combination of integer decisions, such as the operational modes of the separation subsystem ( $med_{mode}$ ) and the solar field thermal storage subsystem ( $sfts_{mode}$ ), leads to a different system trajectory along the prediction horizon<sup>7</sup>.

[66]: Grossmann (2021), Advanced Optimization for Process Systems Engineering

The number of possible operation trajectories increases exponentially with both the number of integer variables ( $n_{xi}$ ) and the number of decision updates ( $n_{updates,xi}$ ), following the expression<sup>8</sup>:

$$n_{problems} = n_{xi}^{n_{updates,xi}}. \quad (13.1)$$

<sup>7</sup>: This will be referred to as: **operation plan**

<sup>8</sup>: For example:  $n_{updates,xi} = 6 \rightarrow n_{problems} = 64$ ,  $n_{updates,xi} = 24 \rightarrow n_{problems} = 16\,777\,216$

This exponential growth makes the search space extremely large and complex.

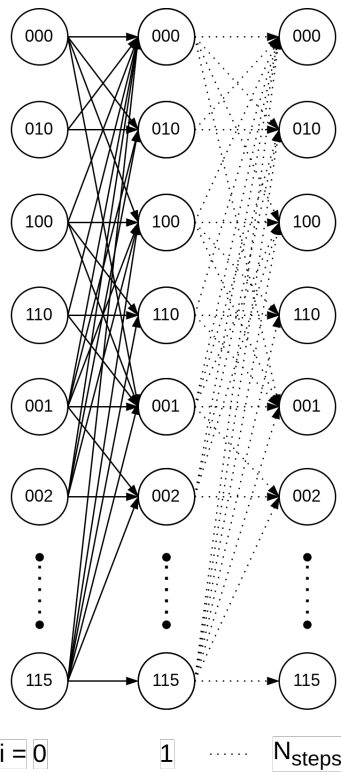


**Figure 13.1:** Decision tree resulting from the combinatorial nature of the integer part of the optimization problem. Text in nodes represents system states.

An important design consideration when solving the optimization problem is whether the sequence of integer decisions (*i.e.*, operational mode transitions over time) is predefined or whether the optimization algorithm is allowed to explore the decision tree freely and determine the optimal sequence. The latter case requires more computational effort but allows for potentially better-performing solutions by dynamically adjusting to system conditions.

#### On the decision variables update frequency

Apart from the integer decision variables, if a fixed decision variable update frequency is chosen for all continuous decision variables, the size of the decision vector for a large horizon like the one chosen can become large with diminishing returns. Instead, a new design parameter is introduced: the number of decision variable updates ( $n_{\text{updates},x_i}$ ) for each decision variable in the optimization problem.

Thus, the decision vector is formed by each individual decision variable repeated as many times as updates for it:

$$X_{nx \times \sum n_{\text{updates},xi}} = [x_{1,k}, \dots, x_{1,n_{\text{updates},x_1}}, \dots, x_{n_x,n_{\text{updates},x_n}}]$$

The number of updates of the decision variable ( $n_{\text{updates},x_i} \in [1, n_{\text{steps}}]$ ) can be chosen individually. More updates are assigned to variables regulating faster dynamics ( $q_{sf}, q_{ts,src}$ ), and these updates of the decision variables are evenly distributed throughout the *active* period of the subsystem within the horizon. This is a crucial design consideration since otherwise the limited number of updates would be assigned to long inactive periods (between end of operation in day 1 and start on day 2).

It also means that the continuous component of the decision vector can only be assigned timestamps after the integer part is defined. Once timestamps are associated with each decision variable, the decision vector values can be resampled to match the desired sampling time of the optimization problem. This is done by forward filling [67] the values of the decision vector until the next update time.

### 13.3 Proposed optimization strategy

A hierarchical control approach (see Figure 13.2) was chosen consisting of three layers: operation plan, operation optimization, and control. This scheme was chosen for two main reasons. On the one hand, the time scales of the different aspects of the operation of the system (operation mode changes, process variables setpoint changes, regulatory control, respectively) can differ substantially. Secondly, it allows to abstract process complexity from the more computationally demanding upper layers by allocating it into the downstream layers. The operation plan layer makes decisions for the *operation modes*, the operation optimization layer sets the setpoints given to the continuous *process variables* that are to be followed by the low-level regulatory control layer.

Both operation plan and operation optimization layers share the same underlying problem structure, the difference being that the operation plan layer evaluates a predefined library of  $n_{\text{problems}}$  combinations of the binary decision variables  $\text{med}_{\text{mode}}$  and  $\text{sfts}_{\text{mode}}$  twice; once to decide the operation start, and another to end operation. The operation optimization layer periodically solves a single NLP problem with the selected values for these two variables fixed. They are further described in the following sections.

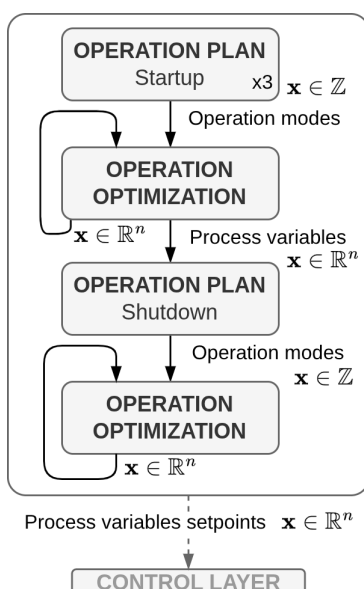


**Figure 13.2:** Proposed optimization strategy architecture

## 13.4 Operation Plan Layer Description

This layer determines the integer decision variables of the MINLP problem, namely, the sequence of operation modes producing an operation plan. To make the problem computationally tractable, only a limited number of combinations,  $n_{problems}$ , are evaluated. This transforms the mixed-integer problem into a simpler form by moving the integer variables from the decision to the environment space. In effect, the original MINLP is decomposed into a library of nNLP problems that are individually evaluated<sup>9</sup>.

To improve robustness, the layer can be evaluated multiple times ( $n_{evals}$ ) under different scenarios—typically reflecting variations in forecasted environmental conditions. The final operation plan is selected as the best compromise across these scenarios.

The time required to perform this layer's computation is denoted  $\Delta t_{eval,plan}$ .

The number of updates available for each integer variable  $n_{updates,xi}$  will be interchangeably referred to as Degrees of Freedom (DoF).

9: MINLP → nNLP

### 13.4.1 Candidate problems generation

Given the available computational resources and the complexity of the objective function, it has been found feasible to evaluate in the order of  $n_{problems} \sim 100$  candidate combinations. This constraint informs how many DoF (*i.e.* number of updates available for the operation modes) can be defined by using Equation 13.1. The particular design choice for the number of updates per subsystem is shown in Table 13.1. In total, 101 distinct operation plans are generated for the start-up evaluation and 144 for the shutdown<sup>10</sup>.

Subsystem	Degrees of freedom				$n_{problems}$	
	Day 1		Day 2			
	Start	Stop	Start	Stop		
Evaluation: Start-up (1)	sfts	3	3	1	1	
	med	3	3	1	1	
Evaluation: Shutdown (2)	sfts	-	3	2	144	
	med	-	3	2	144	

10: Notice the total number does not match exactly Equation 13.1 since special cases are added (subsystem inactive)

**Table 13.1:** Operation plan. Start-up (1) and shutdown (2) degrees of freedom for changes in the operation state.

### 13.4.2 Update times generation

Up to this stage the operation plans generated just consist of a list of ones and zeros for each subsystem, indicating whether the subsystem is active or inactive in the particular update. The next step is to assign the operation mode updates to specific time instants, which then can be resampled to match the desired sampling time of the optimization problem<sup>11</sup>.

In order to maintain the solution close to the optimal one, while keeping the number of problems reasonable, decision updates are distributed throughout the prediction horizon at strategic time instants. Since the case study system is fundamentally a solar process, the operation is strongly dependent on the irradiance availability, and thus operation changes are likely to take place at the start and end of the solar day.

The operation mode updates are distributed temporally as shown in Figure 13.3 (b) depending on the number of updates available (DoF). These update times are dependent on the solar irradiance profile and are bounded by lower- and upper-level thresholds. Depending on the plan action (start-up or shutdown), they are named early-late start or early-late stop thresholds, respectively.

In Figure 13.3 (b) up to three DoF are visualized. If only one update is available, the update time is set at the mean of the early and late thresholds. If two DoF are available, for the sfts subsystem, they are placed halfway between the

11: As with the continuous component of the decision vector, this is done by forward filling [67] the values of the decision vector until the next update time. This is also known as *Last Observation Carried Forward*

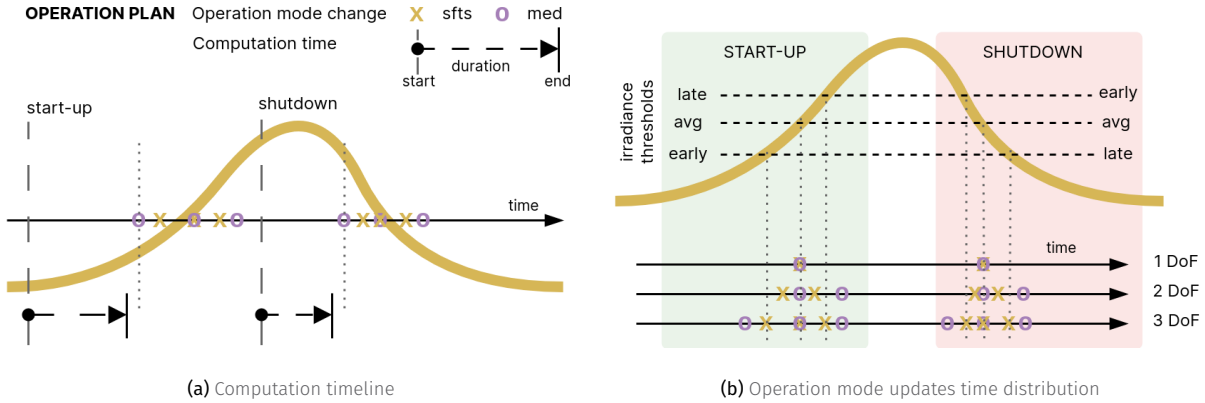


**Figure 13.3:** Operation plan layer computation and updates distribution. The yellow line represents the irradiance illustrating the solar day.

early threshold and the mean, and the late threshold and the mean, respectively. For the MED subsystem, updates are delayed. Finally, with three DoF, updates for the sfts subsystem are placed at the early, mean and late thresholds, while for the MED subsystem, the leftmost and rightmost updates are shifted to the left and right, respectively. If more updates for the particular action are available *i.e.* DoF, additional thresholds can be added.

Given a number of updates per subsystem and the update times assigned. The potential operation time change candidates are defined as:

$$t_{mode-change,candidates} = [t_0, t_1, \dots, t_{max(n_{updates}, \forall x_i)}]$$

Ordered in ascending order, where  $t_0$  is the earliest potential operation change time and  $t_{max(n_{updates}, \forall x_i)}$  is the latest potential operation change time. Based on this definition, the earliest potential subsystem start-up would be at  $t_{\uparrow,candidates}(0)$ . Similarly, the earliest potential shutdown would be at  $t_{\downarrow,candidates}(0)$ .

### Start-up

The most important aspect of this evaluation is to find the right time to bring the subsystems online, and secondary is to provide a preliminary estimate for their shutdown timing.

This is the first evaluation of the proposed methodology (see Figure 13.2) and is computed ahead of the first potential operation mode change (Figure 13.3 (a) - *start-up*), with enough lead time to complete the analysis before any potential change in operation mode ( $t_{\uparrow,candidates}(0)$ ):

$$t = t_{\uparrow,candidates}(0) - (\Delta t_{eval,plan} \times n_{evals})$$

Being the earliest evaluation, it has the longest prediction horizon and thus the highest predicted variables uncertainty. As a counterpart, as shown in Figure 13.3 (a), this early evaluation start allows sufficient computation time, even several hours in advance, to perform several evaluations. Specifically three evaluations ( $n_{evals}$ ) are performed: a nominal scenario with the forecasted environmental conditions, a pessimist one with a 20% decrease in the expected solar irradiance and finally an optimist one with a 20% increase in the expected solar irradiance.

## Shutdown

A second evaluation is performed later in the day (see Figure 13.2), before system shutdown. This aims to determine the most suitable time to stop operations using the most recent system state information. It includes DoF regarding the operation schedule for the following day, allowing the shutdown decision for day 1 to account for its impact on the start and end times of day 2<sup>12</sup>.

12: See Table 13.1

Only one evaluation is performed, as the uncertainty in the prediction horizon is significantly lower than in the start-up evaluation. It is evaluated in parallel to the operation optimization layer and just before the earliest expected shutdown time of the subsystems from Section 11 (Start-up),  $t_{\downarrow, \text{candidates}}(0)$ , considering subsystem shutdown.

$$t = t_{\downarrow, \text{candidates}}(0) - (\Delta t_{\text{eval, plan}} \times \text{somenumber})$$

Once computed the integer decision are updated in this layer. The faster the computation the better, since it will allow the operation optimization layer to optimize operation for the actual shutdown time and adapt accordingly.

## 13.5 Operation optimization layer description

As mentioned, this middle layer establishes the setpoints for the continuous process variables, *i.e.* the continuous part of the MINLP problem. The operation optimization layer evaluates periodically, with a sample time  $T_{\text{eval, optim}}$ , a NLP problem where the integer decision variables are fixed to the values provided by the operation plan layer<sup>13</sup>. It uses the latest available state of the system and environment predictions to evaluate the objective function.

13: It is exactly equivalent to the operation plan layer problem, just making  $n_{\text{problems}} = 1$

The layer computation time is named  $\Delta t_{\text{eval, optim}}$ .

### SolarMED optimization methodology

1. Generate operation mode change candidates based on the available updates per subsystem and irradiance thresholds.
2. Before the first potential operation change and considering the evaluation time,  $t = t_{\uparrow, \text{candidates}}(0) - (\Delta t_{\text{eval, plan}} \times n_{\text{evals}})$ , evaluate the operation plan layer to establish the operation start of the subsystems and an estimation of when to stop.
3. Before the established startup and considering the layer evaluation time,  $t = t_{\uparrow} - \Delta t_{\text{eval, optim}}$ , start evaluating the operation optimization layer periodically ( $T_{\text{eval, optim}}$ ) to establish the setpoints for the continuous process variables.
4. Before the earliest subsystem projected shutdown and considering the operation optimization layer evaluation time,  $t = t_{\downarrow, \text{candidates}}(0) - \Delta t_{\text{eval, plan}}$ , evaluate the operation plan layer, in parallel to the operation optimization layer, to establish the shutdown time of the subsystems.
5. Continue evaluating the operation optimization layer periodically ( $T_{\text{eval, optim}}$ ) until the last subsystem is shutdown.

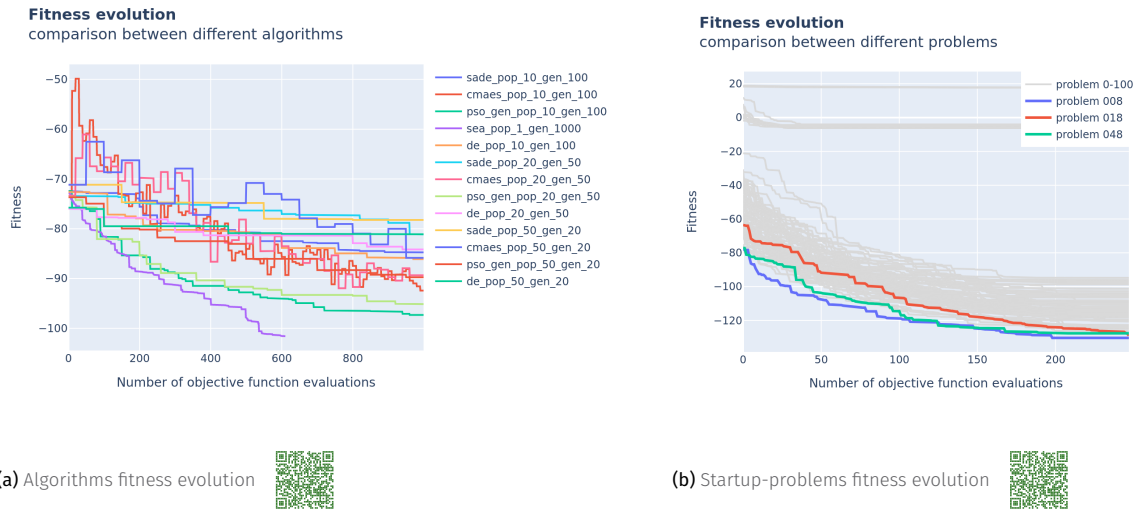


Figure 13.4: Fitness evolution for a particular startup-problem

## 13.6 Optimization results

### 13.6.1 Choosing an algorithm

Once the optimization problem(s) is defined, an algorithm must be chosen that explores the solution space and finds a decision vector that minimizes the objective function.

The solution space has proven to be non-convex, with many local minimums (poor results were obtained when using local-gradient-based algorithms). The size of the decision vector depends on the active periods duration, around 120 elements. In addition, simulation of two days of operation (even when inactive periods are skipped) requires 5-10 seconds of computation time. Algorithm parallelization capabilities are of no use in this case, since many candidate problems will already be evaluated in parallel. The objective is then to find a global large-scale optimization algorithm that can find near-optimal solutions with 200 to 300 objective function evaluations (totaling 2-4 hours of computation time). In order to find the best algorithm, one of the candidate problems is arbitrary chosen and a library of global-evolutionary optimization algorithms is used from the PyGMO open-source Python library, specifically: Differential Evolution (DE), Self-adaptive DE (SADE), (N+1)-ES Simple Evolutionary Algorithm (SAE), Covariance Matrix Adaptation Evolution Strategy (CMA-ES) and Particle Swarm Optimization (PSO). Evolution results are shown in Fig.??, showcasing that for this particular problem the best alternative is the (N+1)-ES Simple Evolutionary Algorithm.

### 13.6.2 Choosing a candidate problem

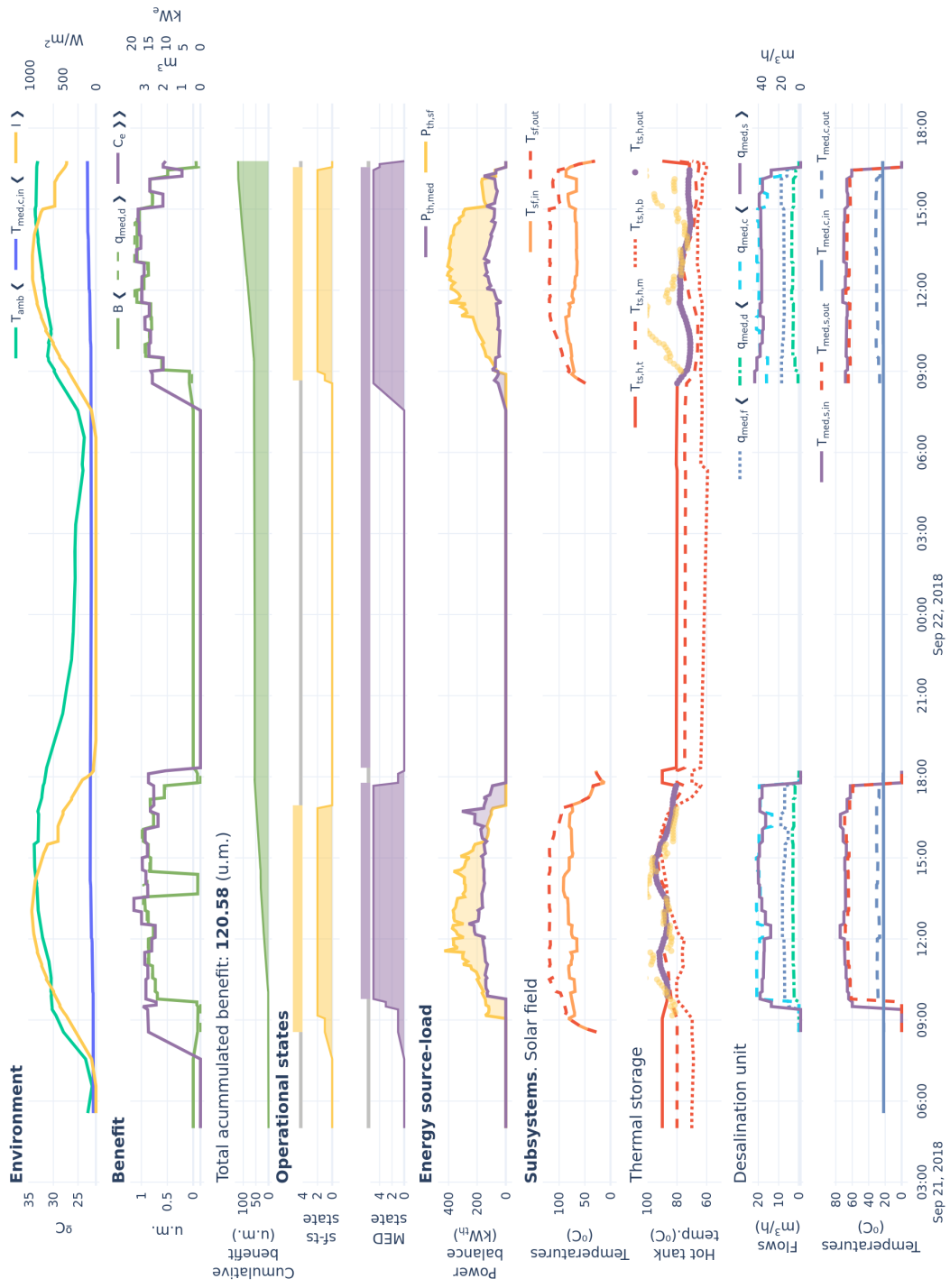
Once an algorithm was chosen, all  $n_{problems}$  were evaluated where the algorithm is only required to choose values for the process variables (continuous). The results of this evaluation are shown in Fig.??, 101 problems were evaluated and visualized is their fitness evolution as a function of objective function evaluations. Problems 8, 18 and 48 resulted in the best fitness after the evolution process and their operation plan can be visualized in Fig. ??.

### 13.6.3 Simulation results

Figure ?? shows results for the simulated system in a total of X days. Where the first two days present favorable - sunny - conditions, followed by a cloudy day, and finishing with a sunny day (Figure ?? - *Environment*).

## Solar MED optimal coupling

Evaluation results



#### 13.6.4 Performance comparison with alternative strategies

baseline operation and just operation optimization



## **CONCLUSIONS AND OUTLOOK**



## Conclusions

### Outlook and future work

#### Optimal water and electricity management in a combined cooling system

**Improved Pareto front computation.** In the current optimization implementation, the Pareto front for each step in the optimization horizon is constructed using a grid search over the decision space. This approach can become computationally expensive, especially as the grid resolution increases. Additionally, the Pareto front must be recalculated from scratch at every step, even though the sequential steps are often very similar—cost parameters remain constant, and only the thermal load and weather conditions change, typically with small variations. A more efficient solution would be to use a multi-objective optimization algorithm such as NSGA-II [[<empty citation>](#)], which can transfer evolved populations between successive evaluations, significantly reducing redundant computations.

<empty citation>

**Better water management** In the current implementation, the primary water source is distributed evenly each day, so the optimization process uses up the entire supply daily. However, a more intelligent daily distribution—essentially, a new optimization problem—could improve water management by allocating different amounts on different days, based on expected weather conditions and predicted generation. This approach would likely be incorporated as a new layer in the hierarchical control structure.<sup>14</sup>

**Techno-economic analysis.** The presented cooling alternatives comparative in this thesis focus on the operation cost of the system, but to get a better picture of the alternatives performance, a techno-economic analysis that includes the capital cost of the system and the expected lifetime of the components should be performed *i.e.* considering all costs associated with the system the plant's lifetime. This is currently being worked on as part of [SOLHycool], where the methodology presented here in terms of operation costs will be integrated in a techno-economic analysis for different case studies.

14: The resulting structure would be: 1. Water allocation, 2. CCS operation optimization, 3. Combined Cooler (CC) regulatory control.

#### Energy management in MED processes driven by variable energy sources

**Alternative configurations for an MED brine concentrator.** Configuraciones alternativas para procesos MED para aplicaciones de concentración de salmueras: geometría variable de efectos, fuentes externas en efectos distintos al primero, acoplamiento con MSF para efectos posteriores.

**Alternative configurations for solar-driven MED.** Configuraciones alternativas para el proceso solar MED (almacenamiento con distintos puntos de carga y descarga, MED con distintos puntos de fuente externa, etc. Incluir diagrama de draw.io con las distintas configuraciones)

The layout configuration of the facility focused on reliability and simplifying operation and maintenance, not strictly on thermodynamic efficiency. The efficiency of the system could be improved:

1. if direct coupling between solar field and thermal storage was used, avoiding the heat exchanger energy transfer associated losses
2. thermal storage allowed charge and discharge from different levels, in order to take advantage of the temperature stratification and avoid fluid mixing

3.

4.

These decisions were made to, on the one hand allow to separate the solar field and thermal storage into two distinct decoupled circuits, providing flexibility, reducing the volume of additives required (only added to the solar field circuit), and operational flexibility (other external loads can be connected to the solar field when the MED is not being operated).

In conclusion this system, although improvable, allows to validate the feasibility of the proposed approach by means of the implementation of a suitable control system, in such a way, that the ideas and techniques presented in this work, could be directly extrapolated to a commercial system just by modifying some of the decision variables to suit the particular implementation.

### Derived scientific contributions

1. Publicaciones en revista
2. Contribuciones a congreso
3. Coloquios doctorales
4. Colaboraciones en proyectos de investigación
5. Estancias de investigación
6. Repositorios de código
7. Repositorios de datos
8. Herramientas interactivas
9. Contribuciones a librerías de código abierto?

## Bibliography

Here are the references in citation order.

- [1] Martin T. Hagan et al. *Neural Network Design*. Martin Hagan, 2014. 800 pp. (cited on pages 10, 11).
- [2] Mark Hudson Beale, Martin T Hagan, and Howard B Demuth. "Neural Network Toolbox." In: *User's Guide, MathWorks* 2 (2010), pp. 77–81 (cited on page 11).
- [3] Lonnie Hamm, B. Wade Brorsen, and Martin T. Hagan. "Comparison of Stochastic Global Optimization Methods to Estimate Neural Network Weights." In: *Neural Processing Letters* 26.3 (Dec. 1, 2007), pp. 145–158. doi: [10.1007/s11063-007-9048-7](https://doi.org/10.1007/s11063-007-9048-7). (Visited on 03/16/2024) (cited on page 11).
- [4] Jiri Nossent, Pieter Elsen, and Willy Bauwens. "Sobol'sensitivity Analysis of a Complex Environmental Model." In: *Environmental Modelling & Software* 26.12 (2011), pp. 1515–1525 (cited on page 15).
- [5] R. Farmani and J.A. Wright. "Self-Adaptive Fitness Formulation for Constrained Optimization." In: *IEEE Transactions on Evolutionary Computation* 7.5 (Oct. 2003), pp. 445–455. doi: [10.1109/TEVC.2003.817236](https://doi.org/10.1109/TEVC.2003.817236). (Visited on 03/31/2025) (cited on page 20).
- [6] Zong Woo Geem, Joong Hoon Kim, and G.V. Loganathan. "A New Heuristic Optimization Algorithm: Harmony Search." In: *SIMULATION* 76.2 (Feb. 1, 2001), pp. 60–68. doi: [10.1177/003754970107600201](https://doi.org/10.1177/003754970107600201). (Visited on 06/16/2025) (cited on page 20).
- [7] Francesco Biscani and Dario Izzo. "A Parallel Global Multiobjective Framework for Optimization: Pagmo." In: *Journal of Open Source Software* 5.53 (2020), p. 2338. doi: [10.21105/joss.02338](https://doi.org/10.21105/joss.02338) (cited on page 20).
- [8] F. Merkel. "Verdunstungskühlung." In: *VDI Zeitschrift Deutscher Ingenieure, Berlin, Alemania* (1925), pp. 123–128 (cited on pages 25, 27).
- [9] C Bourillot. "Hypotheses of Calculation of the Water Flow Rate Evaporated in a Wet Cooling Tower." In: (Aug. 1983) (cited on page 25).
- [10] H. Jaber and R. L. Webb. "Design of Cooling Towers by the Effectiveness-NTU Method." In: *Journal of Heat Transfer* 111.4 (Nov. 1989), pp. 837–843. doi: [10.1115/1.3250794](https://doi.org/10.1115/1.3250794) (cited on page 25).
- [11] M. Poppe and H. Rögner. "Berechnung von Rückkühlwerken." In: *VDI wärmeatlas* (1991), p. Mi 1 (cited on pages 26, 27).
- [12] J.C. Kloppers and D.G. Kröger. "A Critical Investigation into the Heat and Mass Transfer Analysis of Counterflow Wet-Cooling Towers." In: *International Journal of Heat and Mass Transfer* 48.3 (2005), pp. 765–777 (cited on page 26).
- [13] C. G. Cutillas et al. "Energetic, Exergetic and Environmental (3E) Analyses of Different Cooling Technologies (Wet, Dry and Hybrid) in a CSP Thermal Power Plant." In: *Case Studies in Thermal Engineering* 28 (Dec. 1, 2021), p. 101545. doi: [10.1016/j.csite.2021.101545](https://doi.org/10.1016/j.csite.2021.101545). (Visited on 03/27/2024) (cited on page 26).
- [14] M. Hosoz, H. M. Ertunc, and H. Bulgurcu. "Performance Prediction of a Cooling Tower Using Artificial Neural Network." In: *Energy Conversion and Management* 48.4 (Apr. 1, 2007), pp. 1349–1359. doi: [10.1016/j.enconman.2006.06.024](https://doi.org/10.1016/j.enconman.2006.06.024). (Visited on 03/08/2023) (cited on page 26).
- [15] Ming Gao et al. "Artificial Neural Network Model Research on Effects of Cross-Wind to Performance Parameters of Wet Cooling Tower Based on Level Froude Number." In: *Applied Thermal Engineering* 51.1 (Mar. 1, 2013), pp. 1226–1234. doi: [10.1016/j.applthermaleng.2012.06.053](https://doi.org/10.1016/j.applthermaleng.2012.06.053). (Visited on 03/08/2023) (cited on page 26).
- [16] Jialiang Song et al. "A Novel Approach for Energy Efficiency Prediction of Various Natural Draft Wet Cooling Towers Using ANN." In: *Journal of Thermal Science* 30.3 (May 2021), pp. 859–868. doi: [10.1007/s11630-020-1296-0](https://doi.org/10.1007/s11630-020-1296-0). (Visited on 03/04/2023) (cited on page 26).
- [17] P. Navarro et al. "Critical Evaluation of the Thermal Performance Analysis of a New Cooling Tower Prototype." In: *Applied Thermal Engineering* 213 (2022), p. 118719. doi: [10.1016/j.applthermaleng.2022.118719](https://doi.org/10.1016/j.applthermaleng.2022.118719) (cited on pages 26–28).
- [18] Ashrae. "HVAC Systems and Equipment." In: *Chapter 36 Cooling Towers*. 2004 (cited on page 28).
- [19] Chaouki Ghenai et al. "Performance Analysis and Optimization of Hybrid Multi-Effect Distillation Adsorption Desalination System Powered with Solar Thermal Energy for High Salinity Sea Water." In: *Energy* 215 (Jan. 15, 2021), p. 119212. doi: [10.1016/j.energy.2020.119212](https://doi.org/10.1016/j.energy.2020.119212). (Visited on 01/08/2023) (cited on page 43).

- [20] Hyuk Soo Son et al. "Pilot Studies on Synergetic Impacts of Energy Utilization in Hybrid Desalination System: Multi-effect Distillation and Adsorption Cycle (MED-AD)." In: *Desalination* 477 (Mar. 1, 2020), p. 114266. doi: [10.1016/j.desal.2019.114266](https://doi.org/10.1016/j.desal.2019.114266). (Visited on 01/07/2023) (cited on page 43).
- [21] Greg Burgess and Keith Lovegrove. "Solar Thermal Powered Desalination: Membrane versus Distillation Technologies." In: (Jan. 2000) (cited on page 43).
- [22] F. Silva Pinto and R. Cunha Marques. "Desalination Projects Economic Feasibility: A Standardization of Cost Determinants." In: *Renewable and Sustainable Energy Reviews* 78 (Oct. 2017), pp. 904–915. doi: [10.1016/j.rser.2017.05.024](https://doi.org/10.1016/j.rser.2017.05.024). (Visited on 07/27/2023) (cited on page 43).
- [23] Karan H. Mistry et al. "Entropy Generation Analysis of Desalination Technologies." In: *Entropy. An International and Interdisciplinary Journal of Entropy and Information Studies* 13.10 (2011), pp. 1829–1864. doi: [10.3390/e13101829](https://doi.org/10.3390/e13101829) (cited on page 43).
- [24] H. T. El-Dessouky and H. M. Ettouney. *Fundamentals of Salt Water Desalination*. Elsevier, Mar. 20, 2002. 691 pp. (cited on pages 43, 45, 55).
- [25] A. Christ, K. Regenauer-Lieb, and H.T. Chua. "Thermodynamic Optimisation of Multi Effect Distillation Driven by Sensible Heat Sources." In: *Desalination* 336.1 (2014), pp. 160–167. doi: [10.1016/j.desal.2013.12.006](https://doi.org/10.1016/j.desal.2013.12.006) (cited on pages 43, 45).
- [26] John H. Lienhard et al. "Thermodynamics, Exergy, and Energy Efficiency in Desalination Systems." In: *Lienhard via Angie Locknar* (2017). (Visited on 04/04/2022) (cited on pages 43, 44, 49).
- [27] Andrew T. Bouma, Jaichander Swaminathan, and John H. Lienhard V. "Metrics Matter: Accurately Defining Energy Efficiency in Desalination." In: *Journal of Heat Transfer* 142.12 (Oct. 7, 2020). doi: [10.1115/1.4048250](https://doi.org/10.1115/1.4048250). (Visited on 03/22/2023) (cited on pages 43, 45, 49).
- [28] M. A. Darwish, Faisal Al-Juwayhel, and Hassan K. Abdulraheim. "Multi-Effect Boiling Systems from an Energy Viewpoint." In: *Desalination* 194.1 (June 10, 2006), pp. 22–39. doi: [10.1016/j.desal.2005.08.029](https://doi.org/10.1016/j.desal.2005.08.029). (Visited on 06/01/2022) (cited on pages 44, 49).
- [29] Muhammad Wakil Shahzad, Muhammad Burhan, and Kim Choom Ng. "A Standard Primary Energy Approach for Comparing Desalination Processes." In: *npj Clean Water* 2.1 (Jan. 7, 2019), pp. 1–7. doi: [10.1038/s41545-018-0028-4](https://doi.org/10.1038/s41545-018-0028-4). (Visited on 07/23/2024) (cited on page 44).
- [30] Doriano Brogioli, Fabio La Mantia, and Ngai Yin Yip. "Thermodynamic Analysis and Energy Efficiency of Thermal Desalination Processes." In: *Desalination* 428 (Feb. 15, 2018), pp. 29–39. doi: [10.1016/j.desal.2017.11.010](https://doi.org/10.1016/j.desal.2017.11.010). (Visited on 01/05/2023) (cited on pages 44, 55).
- [31] K.S. Spiegler and Y.M. El-Sayed. "El-Sayed, Y.M.: The Energetics of Desalination Processes. Desalination 134, 109–128." In: *Desalination* 134 (Apr. 1, 2001), pp. 109–128. doi: [10.1016/S0011-9164\(01\)00121-7](https://doi.org/10.1016/S0011-9164(01)00121-7) (cited on page 44).
- [32] Mostafa H. Sharqawy, John H. Lienhard V, and Syed M. Zubair. "On Exergy Calculations of Seawater with Applications in Desalination Systems." In: *International Journal of Thermal Sciences* 50.2 (Feb. 1, 2011), pp. 187–196. doi: [10.1016/j.ijthermalsci.2010.09.013](https://doi.org/10.1016/j.ijthermalsci.2010.09.013). (Visited on 03/22/2023) (cited on pages 44, 48).
- [33] Mostafa H. Sharqawy, Syed M. Zubair, and John H. Lienhard. "Formulation of Seawater Flow Exergy Using Accurate Thermodynamic Data." In: *Prof. Lienhard via Angie Locknar* (Nov. 2010). (Visited on 04/13/2023) (cited on page 44).
- [34] Karan H. Mistry and John H. Lienhard V. "Effect of Nonideal Solution Behavior on Desalination of a Sodium Chloride (NaCl) Solution and Comparison to Seawater." In: *Karan Mistry* (Nov. 2012). (Visited on 04/22/2023) (cited on page 44).
- [35] Karan H. Mistry and John H. Lienhard. "Generalized Least Energy of Separation for Desalination and Other Chemical Separation Processes." In: *Entropy. An International and Interdisciplinary Journal of Entropy and Information Studies* 15.6 (2013), pp. 2046–2080. doi: [10.3390/e15062046](https://doi.org/10.3390/e15062046) (cited on page 44).
- [36] Gregory P. Thiel et al. "Energy Consumption in Desalinating Produced Water from Shale Oil and Gas Extraction." In: *Desalination. Energy and Desalination* 366 (June 15, 2015), pp. 94–112. doi: [10.1016/j.desal.2014.12.038](https://doi.org/10.1016/j.desal.2014.12.038). (Visited on 03/06/2023) (cited on pages 44, 47, 49).
- [37] Loreto Valenzuela, Rafael López-Martín, and Eduardo Zarza. "Optical and Thermal Performance of Large-Size Parabolic-Trough Solar Collectors from Outdoor Experiments: A Test Method and a Case Study." In: *Energy* 70 (June 1, 2014), pp. 456–464. doi: [10.1016/j.energy.2014.04.016](https://doi.org/10.1016/j.energy.2014.04.016). (Visited on 07/17/2024) (cited on page 44).
- [38] Christoph Prahl, Christoph Happich, and Jesús Fernández. *Protocol for Characterization of Complete Solar Concentrators Using Photogrammetry or Deflectometry*. WP14 – Task 14.2. DLR, Feb. 2018 (cited on page 44).

- [39] Rocío Bayón and Esther Rojas. "Development of a New Methodology for Validating Thermal Storage Media: Application to Phase Change Materials." In: *International Journal of Energy Research* 43.12 (2019), pp. 6521–6541. doi: [10.1002/er.4589](https://doi.org/10.1002/er.4589). (Visited on 07/17/2024) (cited on page 44).
- [40] Karan H. Mistry and John H. Lienhard. "An Economics-Based Second Law Efficiency." In: *Entropy* 15.7 (7 July 2013), pp. 2736–2765. doi: [10.3390/e15072736](https://doi.org/10.3390/e15072736). (Visited on 03/22/2023) (cited on page 45).
- [41] Alexander Christ et al. "Techno-Economic Analysis of Geothermal Desalination Using Hot Sedimentary Aquifers: A Pre-Feasibility Study for Western Australia." In: *Desalination* 404 (Feb. 17, 2017), pp. 167–181. doi: [10.1016/j.desal.2016.11.009](https://doi.org/10.1016/j.desal.2016.11.009). (Visited on 01/05/2023) (cited on page 45).
- [42] Alexander Christ, Klaus Regenauer-Lieb, and Hui Tong Chua. "Application of the Boosted MED Process for Low-Grade Heat Sources — A Pilot Plant." In: *Desalination. Energy and Desalination* 366 (June 15, 2015), pp. 47–58. doi: [10.1016/j.desal.2014.10.032](https://doi.org/10.1016/j.desal.2014.10.032). (Visited on 01/04/2023) (cited on page 45).
- [43] Alexander Christ, Klaus Regenauer-Lieb, and Hui Tong Chua. "Boosted Multi-Effect Distillation for Sensible Low-Grade Heat Sources: A Comparison with Feed Pre-Heating Multi-Effect Distillation." In: *Desalination. Energy and Desalination* 366 (June 15, 2015), pp. 32–46. doi: [10.1016/j.desal.2014.12.047](https://doi.org/10.1016/j.desal.2014.12.047). (Visited on 01/04/2023) (cited on page 45).
- [44] Edward Jones et al. "The State of Desalination and Brine Production: A Global Outlook." In: *Science of The Total Environment* 657 (Mar. 20, 2019), pp. 1343–1356. doi: [10.1016/j.scitotenv.2018.12.076](https://doi.org/10.1016/j.scitotenv.2018.12.076). (Visited on 06/29/2022) (cited on page 46).
- [45] Patricia Palenzuela, Diego-César Alarcón-Padilla, and Guillermo Zaragoza. *Concentrating Solar Power and Desalination Plants*. Oct. 9, 2015 (cited on pages 46, 50).
- [46] John H. Lienhard V et al. "SOLAR DESALINATION." In: *Annual Review of Heat Transfer* 15 (2012). doi: [10.1146/annurevheattransfer.2012.004659](https://doi.org/10.1146/annurevheattransfer.2012.004659). (Visited on 10/17/2024) (cited on page 47).
- [47] Qian Chen et al. "A Zero Liquid Discharge System Integrating Multi-Effect Distillation and Evaporative Crystallization for Desalination Brine Treatment." In: *Desalination* 502 (Apr. 2021), p. 114928. doi: [10.1016/j.desal.2020.114928](https://doi.org/10.1016/j.desal.2020.114928) (cited on page 48).
- [48] Adrian Bejan. *Advanced Engineering Thermodynamics*. John Wiley & Sons, 2016 (cited on page 48).
- [49] JCGM 100:2008. *GUM 1995 with Minor Corrections. Evaluation of Measurement Data — Guide to the Expression of Uncertainty in Measurement*. Joint Committee for Guides in Metrology, 2008. URL: [https://www.bipm.org/documents/20126/2071204/JCGM\\_101\\_2008\\_E.pdf/325dcaad-c15a-407c-1105-8b7f322d651c](https://www.bipm.org/documents/20126/2071204/JCGM_101_2008_E.pdf/325dcaad-c15a-407c-1105-8b7f322d651c) (cited on page 52).
- [50] Ralph C. Smith. *Uncertainty Quantification: Theory, Implementation, and Applications*. SIAM, Dec. 2, 2013. 400 pp. (cited on page 52).
- [51] nist. "NIST Guidelines for Evaluating and Expressing the Uncertainty of NIST Measurement Results Cover." In: *NIST* (). (Visited on 06/16/2023) (cited on page 53).
- [52] JCGM101:2008. *Evaluation of Measurement Data — Supplement 1 to the "Guide to the Expression of Uncertainty in Measurement"—Propagation of Distributions Using a Monte Carlo Method*. Joint Committee for Guides in Metrology, 2008. URL: [https://www.bipm.org/documents/20126/2071204/JCGM\\_101\\_2008\\_E.pdf/325dcaad-c15a-407c-1105-8b7f322d651c](https://www.bipm.org/documents/20126/2071204/JCGM_101_2008_E.pdf/325dcaad-c15a-407c-1105-8b7f322d651c) (cited on page 53).
- [53] Ulli Wolff. "Monte Carlo Errors with Less Errors." In: *Computer Physics Communications* 176.5 (Mar. 2007), p. 383. doi: [10.1016/j.cpc.2006.12.001](https://doi.org/10.1016/j.cpc.2006.12.001). (Visited on 06/19/2023) (cited on page 53).
- [54] Milan Korbel et al. "Steady State Identification for On-Line Data Reconciliation Based on Wavelet Transform and Filtering." In: *Computers & Chemical Engineering* 63 (Apr. 17, 2014), pp. 206–218. doi: [10.1016/j.compchemeng.2014.02.003](https://doi.org/10.1016/j.compchemeng.2014.02.003). (Visited on 12/14/2022) (cited on page 53).
- [55] Taiwen Jiang et al. "Application of Steady-State Detection Method Based on Wavelet Transform." In: *Computers & Chemical Engineering* 27.4 (Apr. 15, 2003), pp. 569–578. doi: [10.1016/S0098-1354\(02\)00235-1](https://doi.org/10.1016/S0098-1354(02)00235-1). (Visited on 01/03/2023) (cited on page 53).
- [56] Taiwen Jiang, Bingzhen Chen, and Xiaorong He. "Industrial Application of Wavelet Transform to the On-Line Prediction of Side Draw Qualities of Crude Unit." In: *Computers & Chemical Engineering* 24.2 (July 15, 2000), pp. 507–512. doi: [10.1016/S0098-1354\(00\)00520-2](https://doi.org/10.1016/S0098-1354(00)00520-2). (Visited on 12/27/2022) (cited on page 53).
- [57] Karl Johan Åström and Tore Hägglund. *PID Controllers: Theory, Design, and Tuning*. ISA - The Instrumentation, Systems and Automation Society, 1995 (cited on page 54).

- [58] Karan H. Mistry, Mohamed A. Antar, and John H. Lienhard V. "An Improved Model for Multiple Effect Distillation." In: *Desalination and Water Treatment* 51.4–6 (Jan. 1, 2013), pp. 807–821. doi: [10.1080/19443994.2012.703383](https://doi.org/10.1080/19443994.2012.703383). (Visited on 06/01/2022) (cited on page 55).
- [59] John W Ryznar. "A New Index for Determining Amount of Calcium Carbonate Scale Formed by a Water." In: *Journal-American Water Works Association* 36.4 (1944), pp. 472–483 (cited on page 55).
- [60] John H. Lienhard V. "Energy Savings in Desalination Technologies: Reducing Entropy Generation by Transport Processes." In: *Journal of Heat Transfer* 141.7 (May 17, 2019). doi: [10.1115/1.4043571](https://doi.org/10.1115/1.4043571). (Visited on 03/30/2023) (cited on page 62).
- [61] Gary Ampuño et al. "Modeling and Simulation of a Solar Field Based on Flat-Plate Collectors." In: *Solar Energy* 170 (Aug. 1, 2018), pp. 369–378. doi: [10.1016/j.solener.2018.05.076](https://doi.org/10.1016/j.solener.2018.05.076). (Visited on 03/17/2023) (cited on page 63).
- [62] Gary Ampuño et al. "Apparent Delay Analysis for a Flat-Plate Solar Field Model Designed for Control Purposes." In: *Solar Energy* 177 (Jan. 1, 2019), pp. 241–254. doi: [10.1016/j.solener.2018.11.014](https://doi.org/10.1016/j.solener.2018.11.014). (Visited on 03/15/2023) (cited on page 64).
- [63] Julio E. Normey-Rico et al. "A Robust Adaptive Dead-Time Compensator with Application to A Solar Collector Field1." In: *IFAC Proceedings Volumes*. IFAC Workshop on Linear Time Delay Systems (LTDS '98), Grenoble, France, 6-7 July 31.19 (July 1, 1998), pp. 93–98. doi: [10.1016/S1474-6670\(17\)41134-7](https://doi.org/10.1016/S1474-6670(17)41134-7). (Visited on 02/19/2024) (cited on page 64).
- [64] Yunus A. Çengel and Afshin J. Ghajar. *Heat and Mass Transfer: Fundamentals & Applications*. Fifth edition. New York, NY: McGraw Hill Education, 2015. 968 pp. (cited on page 66).
- [65] William Morrow Kays and Alexander Louis London. *Compact Heat Exchangers: A Summary of Basic Heat Transfer and Flow Friction Design Data*. McGraw-Hill, 1958. 180 pp. (cited on page 66).
- [66] Ignacio E. Grossmann. *Advanced Optimization for Process Systems Engineering*. Cambridge Series in Chemical Engineering. Cambridge: Cambridge University Press, 2021 (cited on page 73).
- [67] Rob J. Hyndman and George Athanasopoulos. *Forecasting: Principles and Practice*. 3rd ed. OTexts, 2021 (cited on pages 74, 75).

## Alphabetical Index

preface, ix